QUANTITATIVE VISUALIZATION OF LARGE-VARIATION PHASE OBJECTS

by

Robert Arthur Sprague

Submitted in Partial Fulfillment

of the

Requirements for the Degree

DOCTOR OF PHILOSOPHY

Supervised by Dr. Brian J. Thompson

Institute of Optics

The University of Rochester

Rochester, New York

1971

Vitae

The author was born in Bronxville, N. Y. on February 27, 1945. Following graduation from high school, he went to the University of Rochester where he received his Bachelor of Science degree with Distinction in optics in 1967. During five years starting in 1965, he held summer research positions at Perkin-Elmer, I. B. M., North American Philips Co., and Xerox, working in the areas of interferometry, image formation, coherent optics, and holography.

The author entered graduate school at the University of Rochester in September 1967. His thesis work is concerned with image formation and coherent optics and has been supervised by Dr. Brian J. Thompson. This work has been supported by an N. D. E. A. Fellowship in 1967-68, a University of Rochester Teaching Assistantship in 1968-69 and 1969-70, and a University of Rochester Research Assistantship in 1970-71.

Acknowledgments

The author would like to thank his adviser, Dr. Brian Thompson, for a great amount of technical advice and moral support supplied throughout the course of this thesis.

Many helpful suggestions were also supplied by Richard Becherer, Gary Sommargren, and Lynn Seppala during numerous fruitful discussions.

Thanks are also due to Gary DeBell for his patient endurance of the author's questions and mistakes in the thin films lab.

The printing of the equations, as well as many lonely hours, were endured by the author's wife Lynn.

David McCumber and Alan Knapp are also to be thanked for a lot of last minute drafting and photographic work.

Abstract

Living cells, thermoplastics, bleached photographic emulsions, optical elements, and aerodynamic flow patterns are all phase objects. It is desirable in the study of these objects to have a technique by which they may be imaged as an intensity variation having a direct relationship between the image intensity and the object phase. The technique of phase contrast achieves this result, but is limited in application to objects having phase variations smaller than a small fraction of a wavelength.

This thesis describes a technique which achieves the same result for objects with large phase changes. The phase object is placed in a coherent optical system containing a spatial filter whose transmittance varies as a linear slope plus a constant. The image, which is the derivative of the phase variation biassed by the phase variation itself, is recorded on photographic film with unit gamma and used as the input to a second coherent system. In the second system a filter is used whose transmittance varies as the inverse of spatial frequency, effectively performing an integration. If the constant term is also partially blocked, the modulus of the image amplitude is directly proportional to the object phase, with

no approximation on the magnitude of that phase. If the bias amplitude is fairly large, the image intensity is also proportional to the object phase.

To implement this system, the spatial filters are produced photographically on Kodak 649F Photographic Emulsion. For the differentiation filter, film non-linearities are compensated by using a sliding mask technique. For the integration filter, the film is exposed by the shadow of a knife edge produced with a wide source. Film nonlinearities are compensated by varying the source shape. The image in the differentiation system is recorded on 649F emulsion and developed at unit gamma with D165 developer.

The system is evaluated by using it to image several sample phase objects. The technique is shown analytically and experimentally to produce the desired result for large-variation two-dimensional phase objects. It is shown to be limited in application to phase objects which do not vary too rapidly. This limitation is analyzed in detail and the system is determined to give the correct image if the phase function does not change by more than a wavelength across the total width of the system point spread function.

A number of other possible techniques for achieving the same result are also discussed.

Table of Contents

List of Figures

Chapter I

Introduction

Objects are seen by the human eye because they introduce variations of amplitude and phase onto an illuminating beam of light. If the illumination is totally spatially incoherent, only the absorption of the object will affect its appearance. If the illumination is partially coherent however, phase structure in the object will also affect its image. Objects having only phase structure may be made visible in a partially or fully coherent system by a number of methods. These techniques are valuable in the study of living cells, thermoplastics, bleached photographic emulsions, optical elements, and aerodynamic flow patterns, all of which contain information which exists only as an internal index of refraction variation, a relieved surface structure, or both.

Any coherent optical system whose point spread function is broader than the detailed structure of a phase object will exhibit irradiance variations in its image plane. These variations may be increased by defocussing the system to broaden the point spread function. The image produced, called a shadowgram, is used very extensively in the study of aerodynamic flow patterns. This technique is limited to qualitative interpretation however, because it fails to provide a simple relationship between image intensity and object phase.

Quantitative interpretation of slowly varying phase objects may be made through use of the well developed technique of inter-

ferometry. These objects are examined by splitting a wavefront into a number of parts, allowing one part, the "object wave," to pass through the phase object and adding it to the other "reference wave(s)" in the image plane. The resulting image, called a two-beam or multiple-beam interferogram, appears as a set of fringes crossing the object. Each fringe represents a contour of constant phase in the object. By making photometric traces across the image and considering each fringe as a contour line, very accurate measurements of the object phase can be made.[1,2]

The interferometric technique has recently been augmented by application of holography to the problem,[3, 4, 5, 6, 7] which allows for interferometry of transient events. Holography also introduces the new possibilities of multiple wave length interferometry or single wavelength with multiple index interferometry through successive exposures of the hologram.[8, 9, 10] If the interferometry is done holographically, small phase variations may be amplified by proper use of film nonlinearities.[11, 12, 13] Moire interferometry may also be applied to the problem.[14, 15] In addition, it has been recently shown that by photometrically scanning an out-of-focus interferogram (Fresnel hologram) we may computationally determine the structure of a weakly scattering phase object.[16, 17, 18, 19, 20]

All these interferometric techniques are very valuable in the study of simple phase structures since they lend themselves to precise numerical analysis. However, for objects having large amounts of fine detail such as biological specimens, interpretation

of the fringe patterns is extremely difficult or even impossible. A semi-quantitative visual technique is desired to study this class of objects.

When a phase object is illuminated with a plane wave its Fourier Transform appears in the rear focal plane of the imaging lens. If half of this Fourier Transform is covered with an edge, the appearance of the image will be altered. In the Schlieren technique this edge is an opaque half-plane and the resulting image intensity is proportional to the phase function derivative for small variation phase objects.[21] This technique is particularly aesthetically pleasing if a white light source is used and the half-plane is replaced with a color matrix.[22] If the half-plane is replaced with a half-wave phase step, the image intensity is proportional to the object's Hilbert Transform. This latter technique produces a highly luminous image, but interpretation of this image may be ambiguous.[23] Both these techniques may be implemented for transient phenomena with an intermediate holographic step.[24, 25, 26, 27] In all cases, however, quantitative interpretation of the object thickness is difficult.

The interferometric techniques already described may be applied to phase objects containing a lot of detailed structure by adding the reference on axis. Interference microscopes of this type exist in many possible designs which use either a separate plane wave or the object beam itself shifted laterally to produce the required reference beam.[28, 29]

Interference with a plane wave reference is achieved by

splitting the illumination into two portions. The reference portion either bipasses the object completely or traverses the object and is defocussed before reaching the image plane. If the object wave is added to a coherent background which is phase shifted by δ, the image will be described by

$$i(x,y) = e^{ik\phi(x,y)} + e^{i\delta} = 2e^{\frac{i}{2}(k\phi(x,y)+\delta)} \cos\left[\tfrac{1}{2}(k\phi(x,y)-\delta)\right] \tag{1.1}$$

$$I(x,y) = 4\cos^2\left[\tfrac{1}{2}(k\phi(x,y)-\delta)\right], \tag{1.2}$$

$\phi(x,y)$ = object phase variation

k = wave number of illumination

$i(x,y)$ = image amplitude

$I(x,y)$ = image intensity

This image intensity will change with object phase, having a new zero for every additional wave of phase variation. The object is quite visible, however, with a definite spatial relationship between the image and the object. If the phase is a small fraction of a wavelength and $\delta = \pi$,

$$I(x,y) \simeq 2k^2\phi^2(x,y). \tag{1.3}$$

This case is similar to dark ground illumination and will be discussed in more detail later in this chapter.

Lateral shearing microscopes produce twin images of the object, introducing a lateral shift between them. If the object is spatially localized (i.e. one cell) and the shear is larger than the cell size, operation is in the total shearing mode. Two images are formed, the appearance of each one being the same as in the

interference microscope already discussed. If the shear is small, operation is in the differential shearing mode. This arrangement, also called interference contrast, gives an image related to the object derivative.

The images are sheared by an amount ΔX and it is assumed that the phase $\phi(x,y)$ varies slowly over this distance. $\phi(x+\Delta x, y)$ may be approximated by a Taylor series approximation about the point X as

$$\phi(x+\Delta x, y) \simeq \phi(x,y) + \Delta x \, \phi'_x(x,y). \tag{1.4}$$

where $\phi'_x(x,y)$ is the derivative of $\phi(x,y)$ in the X direction. If one image is shifted in phase by δ with respect to the other,

$$\begin{aligned} i(x,y) &= e^{ik\phi(x+\Delta x, y)} + e^{i(k\phi(x,y)+\delta)} \\ &\simeq e^{ik\phi(x,y)}\left[e^{ik\Delta x \phi'_x(x,y)} + e^{i\delta}\right] \\ &= e^{i\left[k\phi(x,y)+\frac{1}{2}(k\Delta x \phi'_x(x,y)+\delta)\right]} \cdot 2\cos\left[\tfrac{1}{2}(k\Delta x \phi'_x(x,y) - \delta)\right] \end{aligned} \tag{1.5}$$

$$I(x,y) = 4\cos^2\left[\tfrac{1}{2}(k\Delta x \phi'_x(x,y) - \delta)\right]. \tag{1.6}$$

If δ is approximately π, it may be redefined as

$$\delta = \pi - \delta' \tag{1.7}$$

where δ' is small.

$$I(x,y) = 4\cos^2\left[\tfrac{1}{2}\left(k\,\Delta x\,\phi_x'(x,y) + \delta'\right) - \tfrac{\pi}{2}\right]$$

$$= 4\sin^2\left[\tfrac{1}{2}\left(k\,\Delta x\,\phi_x'(x,y) + \delta'\right)\right] \tag{1.8}$$

By proper choice of the instrument parameters, Δx may be made small enough that $k\,\Delta x\,\phi_x'(x,y) + \delta' \ll 2\pi$. The image intensity then becomes

$$I(x,y) \simeq \left[\delta' + k\,\Delta x\,\phi_x'(x,y)\right]^2 \tag{1.9}$$

In addition, if $\delta' \gg k\,\Delta x\,\phi_x'(x,y)$,

$$I(x,y) \simeq \delta'^2 + 2\delta' k\,\Delta x\,\phi_x'(x,y). \tag{1.10}$$

This image intensity is proportional to the derivative of the phase function and the object appears to be raised off the surface and illuminated at an angle. This interpretation makes this technique a very understandable and powerful tool, but can be misleading or ambiguous.

The one technique which does lead to unambiguous interpretation for a certain class of objects is the technique of phase contrast.[30, 31, 32] If the object phase variations are a small fraction of a wavelength, the phase function may be approximated as

$$e^{ik\phi(x,y)} \simeq 1 + ik\phi(x,y). \tag{1.11}$$

When this object is illuminated with a plane wave, its Fourier Transform will appear in the rear focal plane of the imaging lens. If this transform is represented by $F(x')$ where x' is the

spatial coordinate in the transform plane, f is the focal length, and $\tilde{\phi}(x',y')$ is the Fourier Transform of $\phi(x,y)$,

$$F(x',y') = \iint e^{ik\phi(x,y)} e^{i\frac{kxx'}{f}} dx\, e^{i\frac{kyy'}{f}} dy$$

$$\simeq \delta(x')\delta(y') + ik\tilde{\phi}(x',y'). \tag{1.11}$$

A small partially absorbing spot having a quarter wave phase shift is placed on axis in this plane at the position of the transform delta function. This weights the transform to give

$$F(x',y') = i[C\delta(x')\delta(y') + k\tilde{\phi}(x',y')]. \tag{1.12}$$

Neglecting multiplicative constants, the final image amplitude is then

$$i(x,y) = C + k\phi(x,y). \tag{1.13}$$

If $C=0$ (totally absorbing spot) operation is in the dark ground mode and the intensity is given by

$$I(x,y) = \phi^2(x,y). \tag{1.14}$$

This is the same result produced in the interference microscope for small phase objects and although it is very high contrast, interpretation is ambiguous because there is no way to distinguish between positive and negative ϕ. If C is fairly large so that

$$C \gg k\phi(x,y),$$
$$I(x,y) \simeq C^2 + 2Ck\phi(x,y). \tag{1.15}$$

The phase object has thus been imaged as an intensity variation

with a linear relationship between object phase and image intensity. Interpretation of this image is now unambiguous.

This technique is widely used and very effective but it only works properly if phase variations in the object do not exceed a small fraction of a wavelength. As a rule of thumb, this means $\phi(x,y) \leq \lambda/20$. This condition can be met for a relieved surface object by immersion in a near index matching oil. If the phase variation occurs as internal index variation however, as it does for biological objects, index matching to this extent is impossible.

The purpose of this thesis is to suggest several ways in which large-variation phase objects can be viewed unambiguously in a manner analogous to phase contrast. One technique is investigated at length and results shown.

Chapter II

System Analysis

Simplified Analysis

The idea of differentiating and integrating to obtain an image irradiance proportional to phase for large-variation phase objects was first conceived by Develis and Reynolds[33]. Their system was never implemented experimentally however, because it is limited in resolution. The idea requires that the object be multiplied by a grating and that two spectral orders of the grating be passed by the system. This requirement not only cuts the effective system resolution in half but also makes excessive demands on the grating quality needed for microscopic work. Their analysis was also limited to one-dimensional objects. This thesis describes a similar technique which removes these resolution limitations and allows for experimental application to actual two-dimensional phase objects.

The object amplitude distribution has the representation $f_1(X_1) = e^{ik\phi(x_1)}$. When this object is illuminated with a plane wave, its Fourier Transform appears in the rear focal plane of the imaging lens. A photographic transparency (spatial filter) whose amplitude transmittance is $t(X_2) = \alpha (X_0 - X_2)$ is placed in this plane. (α = constant, X_2 = transverse coordinate in the focal plane, X_0 = constant) This filter function effectively multiplies the Fourier Transform. When an image is formed in the X_3 plane, it is thus similar to the derivative of the object biassed by the object itself. This image amplitude distribution

is

$$f_3(x_3) = \left(\frac{x_0}{f} + \phi'(-x_3) \right) e^{ik\phi(-x_3)}, \qquad (2.1)$$

where $\phi'(x_3)$ is the derivative of $\phi(x_3)$.

When this image is recorded on photographic film and developed for the right amount of time with the correct developer, the resulting film intensity transmittance will be proportional to the exposing intensity. If $T_f(x_3)$ is the film intensity transmittance,

$$T_f(x_3) = \left| \frac{x_0}{f} + \phi'(-x_3) \right|^2. \qquad (2.2)$$

This film is immersed in an index matching oil bath, so its amplitude transmittance will be proportional to the square root of the intensity transmittance. If x_0/f is chosen to make $x_0/f + \phi(-x_3)$ a positive definite function, this square root will be

$$t_f(x_3) = \frac{x_0}{f} + \phi'(-x_3). \qquad (2.3)$$

This photographic transparency may be used as the input to a second coherent optical system. In this system, a filter is used to operate on the transform which has the following amplitude transmittance :

$$t(x_4) = \frac{D}{x_4} \qquad x_4 > 0 \qquad D = \text{constant}$$

$$= iB \qquad x_4 = 0. \qquad B = \text{constant} \qquad (2.4)$$

This filter multiplies the Fourier transform so that the image

relates to the integral of the object,

$$f_5(X_5) = \frac{CX_0}{f} + \phi(X_5). \quad C = \text{constant} \tag{2.5}$$

If CX_0/f is considerably larger than $\phi(X_5)$, the intensity in this plane will then be

$$I(X_5) \simeq \frac{C^2 X_0^2}{f} + \frac{2CX_0}{f}\phi(X_5). \tag{2.6}$$

This image intensity is linearly proportional to the object phase with no approximations made as to the magnitude of that phase.

This analysis was one-dimensional, which is of no real interest. A two-dimensional phase function $\phi(X_1, Y_1)$ may be written as $\phi(X_1, Y_1) = \phi_a(X_1, Y_1) + \phi_b(Y_1)$. $\phi_b(Y_1)$ is that additive portion of the phase function which varies only in the Y_1 direction and $\phi_a(X_1, Y_1)$ is defined as the remaining portion of the phase variation. $\phi_b(Y_1)$ will consist of edges, linear slopes, or gratings oriented in the Y_1 direction. If a one-dimensional spatial filter is used to differentiate this two-dimensional phase object, the portion $\phi_b(Y_1)$ will differentiate to zero and can not be recovered. The object is $f_1(X_1, Y_1) = e^{ik[\phi_a(X_1, Y_1) + \phi_b(Y_1)]}$.

Its image in the differentiation system is

$$f_3(X_3, Y_3) = \left(\frac{X_0}{f} + \phi_{aX}'(-X_3, -Y_3)\right) e^{ik[\phi_a(-X_3, -Y_3) + \phi_b(-Y_3)]}. \tag{2.7}$$

($\phi_{aX}'(X, Y)$ is defined as the derviative of $\phi_a(X, Y)$ taken in the X direction.) When this image is recorded on photographic

film and integrated in the X direction in the second optical system, the final image amplitude is

$$f_5(x_5, y_5) = C + \phi_a(x_5, y_5). \tag{2.8}$$

The two dimensional phase function is thus imaged correctly except for that portion $\phi_b(y)$ which varies only in the y direction.

The effect of this information loss on image appearance depends upon the particular object structure. Irregular objects, such as biological specimens, contain very few straight edges or linear slopes, so the image appearance will be good. The experimenter may choose the direction of the X_1 -axis by rotating the differentiation filter until the differentiation does not discriminate against any object detail. If the object contains edges in all directions, a better solution is to use the complex spatial filter

$$t(x_2, y_2) = \hat{i}\, x_2 + \hat{j}\, y_2, \tag{2.9}$$

where $\hat{i}$ and $\hat{j}$ are unit vectors in the x_2 and y_2 directions respectively. (This filter can be produced through holographic recording of the filter using opposed polarizations.) If the two derivatives produced are separated with an analyzer, integrated in their respective directions, and the images are recombined with opposing polarizations, some degree of detail will be restored.[34] If $\phi(x_1, y_1) = \phi_a(x_1, y_1) + \phi_b(y_1) + \phi_c(x_1)$, the final image intensity will be

$$I_5(x_5, y_5) = C + 2\phi_a(x_5, y_5) + \phi_b(y_5) + \phi_c(x_5) \tag{2.10}$$

where $\phi_b(y)$ and $\phi_c(x)$ are those additive portions of the phase function which vary only in the y or x directions respectively.

This section was a brief review of the basic idea for visualization of large-variation phase objects. The theoretical and experimental details of this system are analyzed in the sections that follow.

Detailed Analysis

The object amplitude distribution is represented by the functional form $f_1(x_1, y_1) = e^{ik\phi(x_1, y_1)}$. To simplify the analysis, it may be assumed that $f_1(x_1, y_1) = 0$ for the region $|x_1| \geq F, \quad |y_1| \geq F$, where $F < A$. The following definitions will be used:

(x_1, y_1) = Object plane coordinates

(x_2, y_2) = Fourier Transform coordinates in differentiation system

(x_3, y_3) = Image coordinates for differentiation = object coordinates for integration

α, x_0 = Constants

(x_4, y_4) = Fourier Transform coordinates for integration

(x_5, y_5) = Image coordinates for integration

A = Aperture half width

k = Wave number

f = Focal length .

The filter placed in the first transform plane is $t_2(x_2, y_2)$ and is defined by

$$t_2(x_2, y_2) = \alpha (x_0 - x_2). \tag{2.11}$$

This is a standard differentiation filter to which a bias level has been added. If the system consists of a standard two lens unit magnification system, each succeeding focal plane will be the transform plane for the one before it. A transparency placed in a focal plane multiplies the amplitude distribution in its plane so that the effective object Fourier Transform is

$$t_2(x_2,y_2)f_2(x_2,y_2) = \alpha(x_0-x_2)\int_{-F}^{F}dx_1\int_{-F}^{F}dy_1\, f_1(x_1,y_1)\, e^{i\frac{k}{f}(x_1x_2+y_1y_2)} \quad . \tag{2.12}$$

The image amplitude is the inverse Fourier Transform of this filtered function. Since the lens is a finite aperture of half-width A,

$$f_3(x_3,y_3) = \int_{-A}^{A}dx_2\int_{-A}^{A}dy_2\, e^{\frac{ik}{f}(x_2x_3+y_2y_3)}\,\alpha(x_0-x_2)\int_{-F}^{F}dx_1\int_{-F}^{F}dy_1\, e^{i\frac{k}{f}(x_1x_2+y_1y_2)}\, f_1(x_1,y_1). \tag{2.12}$$

The limits on the second integral in this image expression are finite, so the order of integration may be changed.

$$f_3(x_3,y_3) = \int_{-F}^{F}dx_1\int_{-F}^{F}dy_1 f_1(x_1,y_1)\int_{-A}^{A}dx_2\int_{-A}^{A}dy_2\,\alpha(x_0-x_2)\, e^{i\frac{k}{f}\left[(x_1+x_3)x_2+(y_1+y_3)y_2\right]} \tag{2.13}$$

To facilitate the integration, the following quantities are defined:

$$I_0(x_1,x_3) = \int_{-A}^{A}dx_2\, e^{i\frac{k}{f}(x_1+x_3)x_2} = 2A\,\mathrm{sinc}\left[\frac{k}{f}(x_1+x_3)A\right] \tag{2.14}$$

$$I_1(x_1,x_3) = \int_{-A}^{A}dx_2\,(x_0-x_2)\, e^{i\frac{k}{f}(x_1+x_3)x_2} \quad . \tag{2.15}$$

The first quantity may be differentiated and substituted to evaluate

the second.

$$\frac{d}{dx_1} I_0(x_1, x_3) = \frac{ik}{f} \int_{-A}^{A} dx_2 \, x_2 \, e^{i\frac{k}{f}(x_1+x_3)x_2} \tag{2.16}$$

$$I_1(x_1, x_3) = -\frac{f}{ik} \frac{d}{dx_1} I_0(x_1, x_3) + x_0 I_0(x_1, x_3) \tag{2.17}$$

$$f_3(x_3, y_3) = \alpha \int_{-F}^{F} dy_1 \, I_0(y_1, y_3) \int_{-F}^{F} dx_1 f_1(x_1, y_1) \left[x_0 I_0(x_1, x_3) - \frac{f}{ik} \frac{d}{dx_1} I_0(x_1, x_3) \right] \tag{2.18}$$

The second part of this integral may be integrated by parts.

$$u = f_1(x_1, y_1) \qquad dv = d I_0(x_1, x_3)/dx_1$$
$$du = f_{1x}'(x_1, y_1)\, dx_1 \qquad v = I_0(x_1, x_3)$$

$$f_3(x_3, y_3) = \alpha \int_{-F}^{F} dy_1 I_0(y_1, y_3) \left[x_0 \int_{-F}^{F} f_1(x_1, y_1) I_0(x_1, x_3) dx_1 - \frac{f}{ik} \left(f_1(x_1, y_1) I_0(x_1, x_3) \Big|_{-F}^{F} - \int_{-F}^{F} f_{1x}'(x_1, x_3) I_0(x_1, x_3) dx_1 \right) \right] \tag{2.19}$$

For image points near the optic axis ($|x_3| < F$), the middle two terms of this expression are insignificant so that

$$f_3(x_3, y_3) = 4A^2 \alpha \int_{-F}^{F} dy_1 \, \mathrm{sinc}\left[\frac{k}{f}(y_1 + y_3)A\right] \int_{-F}^{F} dx_1 \left[x_0 f(x_1, y_1) + \frac{f}{ik} f_{1x}'(x_1, y_1) \right] \mathrm{sinc}\left[\frac{k}{f}(x_1 + x_3)A\right]. \tag{2.20}$$

If the object is a pure phase object, the final image amplitude then becomes

$$f_3(x_3, y_3) = 4A^2 \alpha f \int_{-F}^{F} dy_1 \, \mathrm{sinc}\left[\frac{k}{f}(y_1 + y_3)A\right] \int_{-F}^{F} \left(\frac{x_0}{f} + \phi_x'(x_1, y_1) \right) e^{ik\phi(x_1, y_1)} \mathrm{sinc}\left[\frac{k}{f}(x_1 + x_3)A\right] dx_1 \tag{2.21}$$

The transform filter function, which is a sum of two terms, thus produces two corresponding image terms: one related to the object and one to its derivative. Both image terms are convolved with the point spread function of the finite aperture. Since the object amplitude distribution contains phase variations, the effect of its convolution with this broad point spread function is not intuitively interpretable for its effect on the image appearance. This effect will be studied in detail in the section on limitations of optical differentiation where it is shown that the image appearance is indeed approximately correct if the object phase does not vary too rapidly across the total width of the point spread function.

For the present analysis, the assumption will be made that the aperture is infinite. The image amplitude is then given by

$$f_3(x_3, y_3) = C\left[\frac{x_0}{f} + \phi_x'(-x_3, -y_3)\right] e^{ik\phi(-x_3, -y_3)}, \tag{2.22}$$

where C is a constant. The intensity in this plane will be the square modulus of this amplitude.

$$I_3(x_3, y_3) = f_3^*(x_3, y_3)\, f_3(x_3, y_3)$$

$$I_3(x_3, y_3) = C^2 \left|\frac{x_0}{f} + \phi_x'(-x_3, -y_3)\right|^2 \tag{2.23}$$

Since $\phi(-x_3, -y_3)$ is a real function, $\phi_x'(-x_3, -y_3)$ is also a real function, so that

$$I_3(x_3, y_3) = C^2 \left(\frac{x_0}{f} + \phi_x'(-x_3, -y_3)\right)^2. \tag{2.24}$$

Although photographic film is a nonlinear recording material, a graph of density vs. log exposure for a given emulsion will contain a straight line portion. If the slope of this portion is γ_1 for the negative process and γ_2 for the subsequent positive process, and if the exposure is always made on the linear portions of the respective curves, the intensity transmittance of the positive will be given by

$$T_f(x_3, y_3) = \left[C^2 \left(\frac{x_0}{f} + \phi_x'(-x_3, -y_3) \right)^2 \right]^{\gamma_1 \gamma_2}. \qquad (2.25)$$

The exposure may be kept within the limited exposure range characteristic of the linear portion of the D vs. Log E curve because the image is of sufficiently low contrast. This is true because the maximum value of the phase function derivative is limited by the finite resolution of the system. (See the section on limitations of optical differentiation.)

If $\gamma_1 \gamma_2$ is chosen to be equal to one and the transparency produced is immersed in an index-matching oil, its amplitude transmittance is proportional to the square root of the intensity transmittance. Since x_0/f has already been stated to be larger than $\phi_x'(-x_3, -y_3)$, the function $\frac{x_0}{f} + \phi_x'(-x_3, -y_3)$ is positive definite. The square root of its square is thus the function itself:

$$t_f(x_3, y_3) = C \left[\frac{x_0}{f} + \phi_x'(-x_3, -y_3) \right].$$

This transparency is used as the object in another coherent optical system which forms an image of the integral of the input.

An ideal integration filter is the function $t(X_4) = \frac{D}{X_4}$. Unfortunately, this function has a singularity at the origin so it can not be produced in practise. Instead, the realizable filter function

$$t(X_4, Y_4) = iB \qquad |X_4| < D$$
$$= D/X_4 \qquad |X_4| \geq D \tag{2.27}$$

may be used. This is a transparency whose intensity transmittance varies as $1/X_4^2$ plus a 180° phase shifter placed over half the Fourier Transform.

The image amplitude produced is given by

$$f_5(X_5, Y_5) = C\int_{-A}^{A} dX_4 \int_{-A}^{A} dY_4\, e^{i\frac{k}{f}(X_5X_4 + Y_5Y_4)}\, t(X_4, Y_4) \int_{-F}^{F} dX_3 \int_{-F}^{F} dY_3\, e^{i\frac{k}{f}(X_4X_3 + Y_4Y_3)} \left[\frac{X_0}{f} + \phi_x'(-X_3, -Y_3)\right]. \tag{2.28}$$

Since both integrals are finite, the order of integration may be altered and the Y_4 integral calculated. If the functional form of $t(X_4, Y_4)$ is also substituted, this equation reduces to

$$f_5(X_5, Y_5) = 2AC \int_{-F}^{F} dY_3\, \mathrm{sinc}\left[\frac{k}{f}(Y_3 + Y_5)A\right] \int_{-F}^{F} dX_3 \left[\frac{X_0}{f} + \phi_x'(-X_3, -Y_3)\right] \cdot$$
$$\cdot \left[D\int_{-A}^{-D} \frac{e^{i\frac{k}{f}(X_5 + X_3)X_4}}{X_4} dX_4 + iB\int_{-D}^{D} e^{i\frac{k}{f}(X_5 + X_3)X_4} dX_4 + D\int_{D}^{A} \frac{e^{i\frac{k}{f}(X_5 + X_3)X_4}}{X_4} dX_4\right].$$

$$f_5(X_5, Y_5) = 2AC \int_{-F}^{F} dY_3\, \mathrm{sinc}\left(\frac{k}{f}A(Y_3 + Y_5)\right) \int_{-F}^{F} dX_3 \left(\frac{X_0}{f} + \phi_x'(-X_3, -Y_3)\right) \cdot$$
$$\cdot \left[2iD\int_{D}^{A} dX_4\, \frac{\sin\left(\frac{k}{f}X_4(X_5 + X_3)\right)}{X_4} + iB\int_{-D}^{D} \frac{e^{i\frac{k}{f}X_4(X_5 + X_3)}}{dX_4}\right]. \tag{2.29}$$

This image amplitude is a sum of four parts. These parts

arise from the imaging of two object terms (a constant and a phase function derivative) by two aperture terms (a truncated integration function and a low-pass spatial filter). The integrals in these expressions are calculated in Appendix I. The results give rise to some interesting criteria for the choice of system parameters.

Term # 1

$$\begin{aligned}\text{Term \#1} = \frac{2iDX_o}{f}\Bigg[& F\left(Si\left(\tfrac{kA}{f}(X_5+F)\right) - Si\left(\tfrac{kD}{f}(X_5+F)\right)\right. \\ & \left. + Si\left(\tfrac{kA}{f}(X_5-F)\right) - Si\left(\tfrac{kD}{f}(X_5-F)\right)\right) \\ & + \frac{f}{kA}\left(\cos\left(\tfrac{kA}{f}(X_5+F)\right) - \cos\left(\tfrac{kA}{f}(X_5-F)\right)\right) \\ & - \frac{f}{kD}\left(\cos\left(\tfrac{kD}{f}(X_5+F)\right) - \cos\left(\tfrac{kD}{f}(X_5-F)\right)\right) \\ & + X_5\left(Si\left(\tfrac{kA}{f}(X_5+F)\right) - Si\left(\tfrac{kA}{f}(X_5-F)\right)\right. \\ & \left. - Si\left(\tfrac{kD}{f}(X_5+F)\right) + Si\left(\tfrac{kD}{f}(X_5-F)\right)\right)\Bigg] \end{aligned} \tag{2.30}$$

This term is very small. It represents integration of the constant X_o object term by the truncated integration filter. It is present because the finite resolution of the system causes the X_o term to be Fourier Transformed not to a delta function but to a broader function which somewhat overlaps the region $|X_4| < D$. The contribution of this term to the image is small for certain values of the system parameters which may be determined in the following way. For locations well separated from the edge of the image field, the sine integrals may be approximated by their

assymptotic expansion

$$Si(z) = \frac{\pi}{2} - \frac{1}{z}\left(1 - \frac{2!}{z^2} + \frac{4!}{z^4} + \ldots\right)\cos(z) - \frac{1}{z^2}\left(1 - \frac{3!}{z^2} + \frac{5!}{z^4} + \ldots\right)\sin(z) \qquad (2.31)$$

If only the first term in $1/z$ is retained,

$$\text{Term \# 1} = 0. \qquad (2.32)$$

The condition for this approximation was $1/z \ll 1$,

or alternatively

$$\frac{kA}{f}(X_5 \pm F) \gg 1$$

$$\frac{kD}{f}(X_5 \pm F) \gg 1 \qquad (2.33)$$

The second condition, which is the most critical, is a condition on the field of view for a given D. Alternatively, it sets the minimum limit on the size of D, if the width of the field of view is allowed to go to zero, i.e. let $X_5 = 0$,

$$D \gg \frac{f}{kF}. \qquad (2.34)$$

Even if this condition is not completely satisfied, additional terms in the expansion are of the order $(1/z)^2$, where $1/z$ is small. A condition of this sort is not unreasonable, as it sets a minimum limit on the size of the bias level block. This width must be larger than the point spread function characteristic of the Fourier Transform plane.

Term # 2

$$\text{Term } \#2 = 2iD\Big[\frac{k}{f}\int_{-F}^{F}\phi(-x_3,-y_3)\left(A\,\mathrm{sinc}\tfrac{k}{f}(x_5+x_3)A - D\,\mathrm{sinc}\tfrac{k}{f}(x_5+x_3)D\right)dx_3$$
$$-\phi(-F,-y_3)\left\{Si\left(\tfrac{k}{f}(x_5+F)A\right)-Si\left(\tfrac{k}{f}(x_5+F)D\right)\right\}$$
$$+\phi(F,-y_3)\left\{Si\left(\tfrac{k}{f}(x_5-F)A\right)-Si\left(\tfrac{k}{f}(x_5-F)D\right)\right\}\Big] \qquad (2.35)$$

This term represents imaging of the phase function derivative by the truncated integration filter. It consists of a high-pass filtered image of the phase function itself plus two terms which make contributions at the edge of the image field near $x_5 = \pm F$. The effect of the high-pass filtering on the image appearance will depend upon the amount of low spatial frequency information in the function $\phi(x)$. This point is discussed more fully in the section on the limitations of coherent integration. It is apparent however, that for broad-band objects it is important that $D \ll A$. The terms which appear at the edge of the image field may be made small through the same choice of D determined for Term # 1.

Term # 3

$$\text{Term } \#3 = 2iBD\int_{-F}^{F}\phi_x'(-x_3,-y_3)\ \mathrm{sinc}\left(\tfrac{k}{f}(x_5+x_3)D\right)dx_3 \qquad (2.36)$$

This term has a negligible value. It represents imaging of the phase function derivative by the low pass filter

$$t(X_4) = iB \qquad X_4 \leq D$$
$$= 0 \qquad X_4 > D \tag{2.37}$$

Its value does depend to some extent on the amount of low spatial frequency content in the derivative. However, since B is a small fraction and since this image is spread by convolution with a broad point spread function, the contribution of Term # 3 will be small.

Term # 4

$$\text{Term } \#4 = \frac{2iBX_o}{k}\left[Si\left(\frac{k}{f}(X_5+F)D\right) - Si\left(\frac{k}{f}(X_5-F)D\right)\right] \tag{2.38}$$

This term provides the constant bias level to the image. It represents imaging of the constant X_o term of the object through the partially absorbing aperture of width 2D. The value of Term # 4 will be constant for the same choice of D determined for Term # 1, $D >> \frac{f}{kF}$.

$$\text{Term } \#4 = \frac{2\pi B X_o i}{k} \tag{2.39}$$

In this case, the criterion intuitively states that the aperture $|X_4| \leq D$ should be large enough so that the bias component of the image is not affected appreciably by diffraction of the delta function transform at the edges of this aperture.

With all the negligible image terms thrown away, the image amplitude of interest becomes

$$f_5(X_5,y_5) = 4iAC\int_{-F}^{F} dy_3\, \text{sinc}\left[\frac{k}{f}(y_3+y_5)A\right]\left\{\frac{\pi BX_o}{k} + \frac{kDA}{f}\int_{-F}^{F}\phi(-X_3,-y_3)\,\text{sinc}\left[\frac{k}{f}(X_3+X_5)A\right]dX_3\right\}. \tag{2.40}$$

This image represents the phase function itself, convolved with

the point spread function of a finite aperture and added to a constant bias level. If BX_o is chosen to be large, the intensity in this image will also be proportional to the phase function. This requires that the image field is restricted to a small region near the axis and that the value of D is chosen to satisfy

$$\frac{f}{kF} << D << A. \tag{2.41}$$

The assumption has also been made that the object contains little low frequency information. The failure of this approximation will be discussed at greater length in the section on limitations of coherent integration.

Limitations of Coherent Differentiation

The point spread function of a system is defined as the Fourier Transform of the aperture distribution. If this aperture distribution is the filter function $t(x',y') = \alpha (X_o - X')$, the point spread function (see Appendix II) is given by

$$A_d(x,y) = 4A\alpha \operatorname{sinc}\left(\frac{kyA}{f}\right)\left[\frac{X_o}{A}\operatorname{sinc}\left(\frac{kxA}{f}\right) + i\left(\operatorname{cosinc}\left(\frac{kAx}{f}\right) - \frac{\sin\left(\frac{kAx}{f}\right)}{\left(\frac{kAx}{f}\right)^2}\right)\right], \tag{2.42}$$

where

$A_d(x,y)$ = point spread function of differentiation system

f = focal length of lenses

k = wave number of illumination

A = aperture half width

This function has two parts. The first corresponds to the X_o term of the aperture function and is a typical diffraction

limited point spread function for a square aperture. The second part corresponds to the linear sloped term of the aperture function and is the part which causes differentiation. This latter term is graphed in Fig. 2.1 and is a two-lobed function; the two lobes have opposite signs and are separated by approximately the width of the unfiltered point spread function. Since the point spread function describes the image of a single point object, and since the total object consists of an array of point sources, it is apparent that differentiation is achieved by forming two images of the object slightly displaced from each other with opposite signs. This is hardly surprising as it is analogous to the shearing interferometer described in the introduction. The shearing interferometer, however, is a differencing instrument which produces a derivative only if the object phase varies slowly across the region of shear. It is important to study the extent to which this analogy can be extended to determine the limitations, if any, of coherent differentiation. The analogy will be perhaps limited because of the finite width of each lobe of the point spread function. The two images are not only separated, but each is convolved with its individual point spread function. In the shearing interferometer, the shear separation and the width of the imaging point spread function are independent quantities. In coherent differentiation, they are intimately related to each other through the finite numerical aperture of the system.

The limitations produced by this effect are best examined by considering the image of a sloped phase edge. This edge is defined by the function in Fig. 2.2.

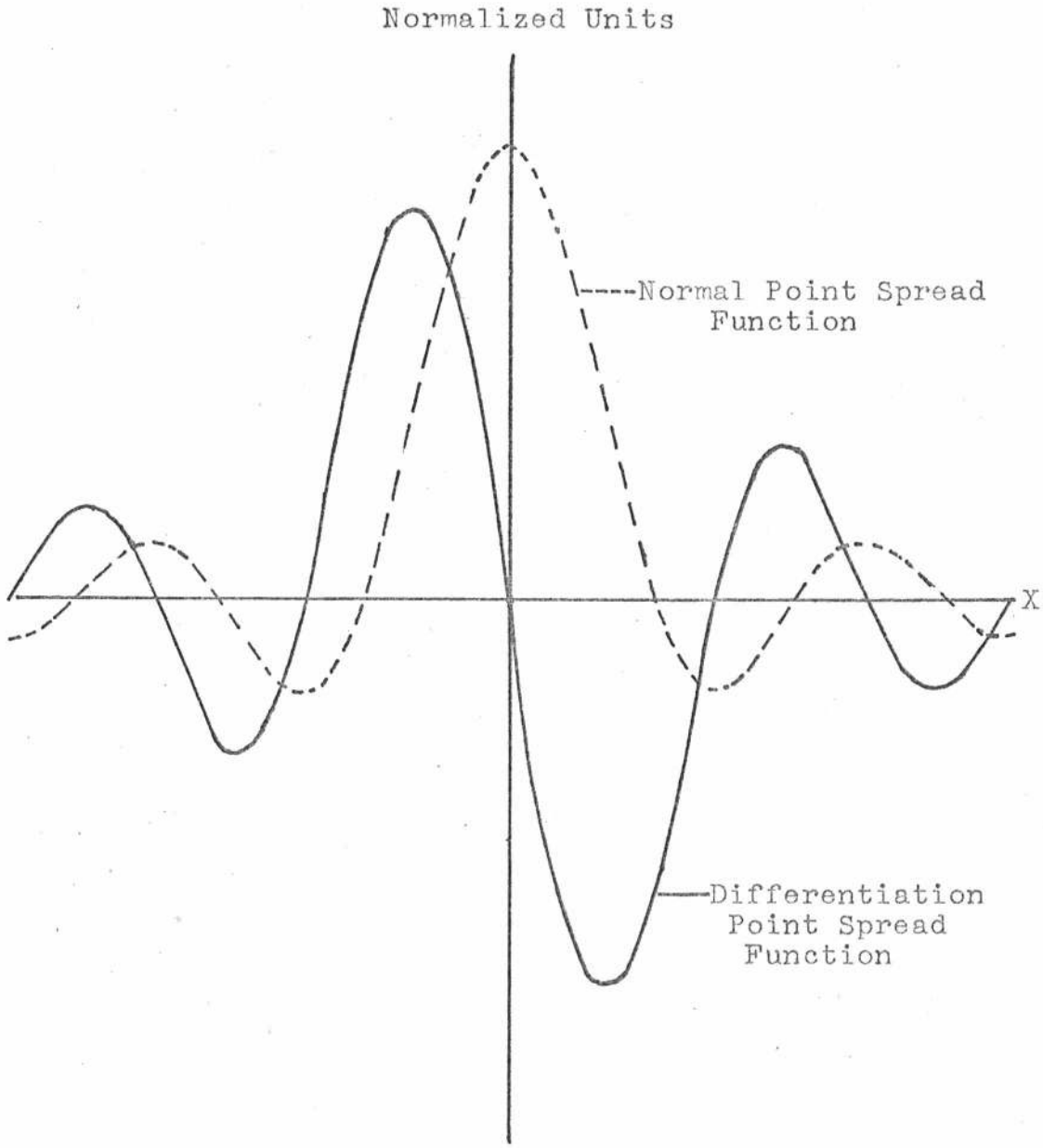

Figure 2.1

Point Spread Function of Differentiation System

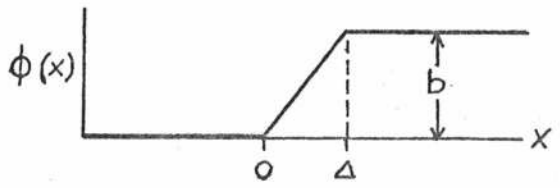

$$\phi(x) = 0 \quad x < 0$$
$$= \frac{bx}{\Delta} \quad 0 \le x \le \Delta$$
$$= b \quad x > \Delta$$

Figure 2.2 - Sloped Phase Edge Function

Δ is the width of the phase edge and b is its height. When this phase object is imaged with the differentiation system, the image amplitude produced is determined by convolving the differentiation point spread function with the object itself. This calculation is done in Appendix III. The result is the image amplitude

$$f_3(x_3) = \frac{\alpha x_0 f}{k}\left(\pi + 2\,Si\left[\frac{kAx_3}{f}\right]\right) + \frac{\alpha x_0 f}{k} e^{ikb}\left(\pi - 2\,Si\left[\frac{kA(x_3+\Delta)}{f}\right]\right)$$
$$- i\alpha\left[\frac{fx_0}{k} + \frac{bf^2}{\Delta k}\right] e^{-i\frac{kbx_3}{\Delta}}\left[Ci\left[k\left(\frac{b}{\Delta}+\frac{A}{f}\right)(x_3+\Delta)\right] - Ci\left[k\left(\frac{b}{\Delta}-\frac{A}{f}\right)(x_3+\Delta)\right]\right.$$
$$- Ci\left[k\left(\frac{b}{\Delta}+\frac{A}{f}\right)x_3\right] + Ci\left[k\left(\frac{b}{\Delta}-\frac{A}{f}\right)x_3\right] + i\left\{Si\left[k\left(\frac{b}{\Delta}+\frac{A}{f}\right)(x_3+\Delta)\right]\right.$$
$$\left.\left. - Si\left[k\left(\frac{b}{\Delta}-\frac{A}{f}\right)(x_3+\Delta)\right] - Si\left[k\left(\frac{b}{\Delta}+\frac{A}{f}\right)x_3\right] + Si\left[k\left(\frac{b}{\Delta}-\frac{A}{f}\right)x_3\right]\right\}\right]. \tag{2.42}$$

The intensity in this image is recorded on film with $\gamma = 1$ and used as the input to the integration system. The amplitude transmittance of the film will be proportional to $|f_3(x_3)|$. This function is drawn in Figure 2.3 for several different values of the edge slope b/Δ. For small slopes, the image appears to be a slightly blurred derivative of the edge. For larger values of b/Δ, the image is distorted by a large component in the spatial

location of the edge which subtracts from the bias level. This component arises primarily from failure of the phase function to be imaged as a pure phase variation by the X_0 portion of the differentiation spatial filter.

To evaluate the limit this error term places on coherent differentiation, it is important to note that the function $|f_3(X_3)|$ is integrated in the second optical system. The important evaluative criterion is thus an integral across the edge position. Since the graphed curves were calculated for a fixed Δ, the proper integral should also increase linearly with the edge slope b/Δ. This integral value is drawn in Fig. 2.4 as a function of b/Δ. An approximately linear relationship between the integral and the edge slope is seen to exist for $-.75\, A/f \leq b/\Delta \leq .75\, A/f$. Although the exact value of these limits may vary for different edge widths, examination of the functional form of $f_3(X_3)$ shows that the value of the argument $b/\Delta - A/f$ is critical in the appearance of the image. As a rule of thumb, only if $A/f > b/\Delta$ will the image appearance be similar to that of the ideal derivative. This criterion sets a limit on the edge sharpness that may be properly differentiated, but not on the actual height or width of the phase variation. This condition is similar to the limitation of the shearing interferometer, but the criterion is considerably more relaxed than would be expected from a direct analogy.

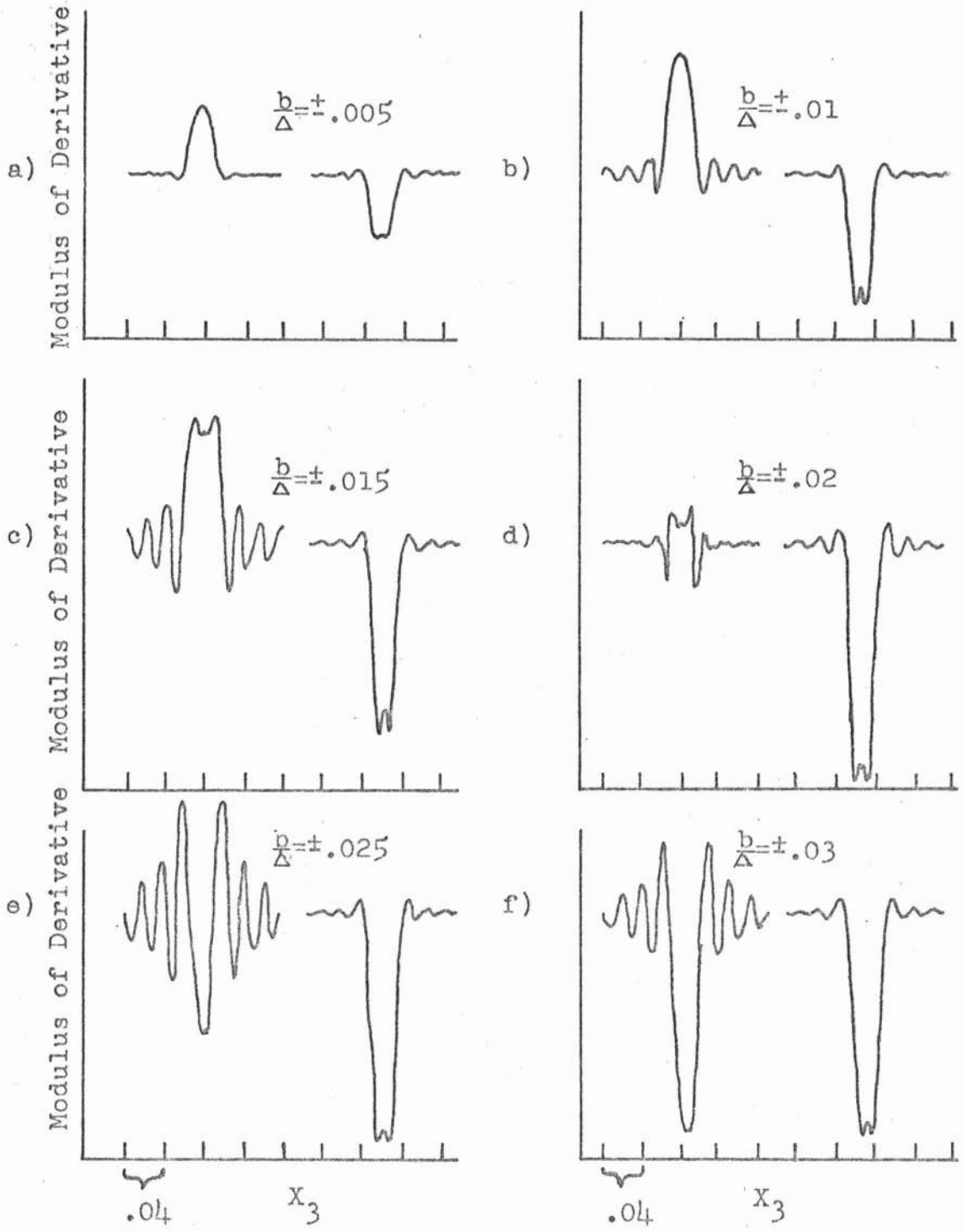

Figure 2.3

Derivative of Sloped Phase Edge

(Δ = .04, X_o = 3, A/f = .02)

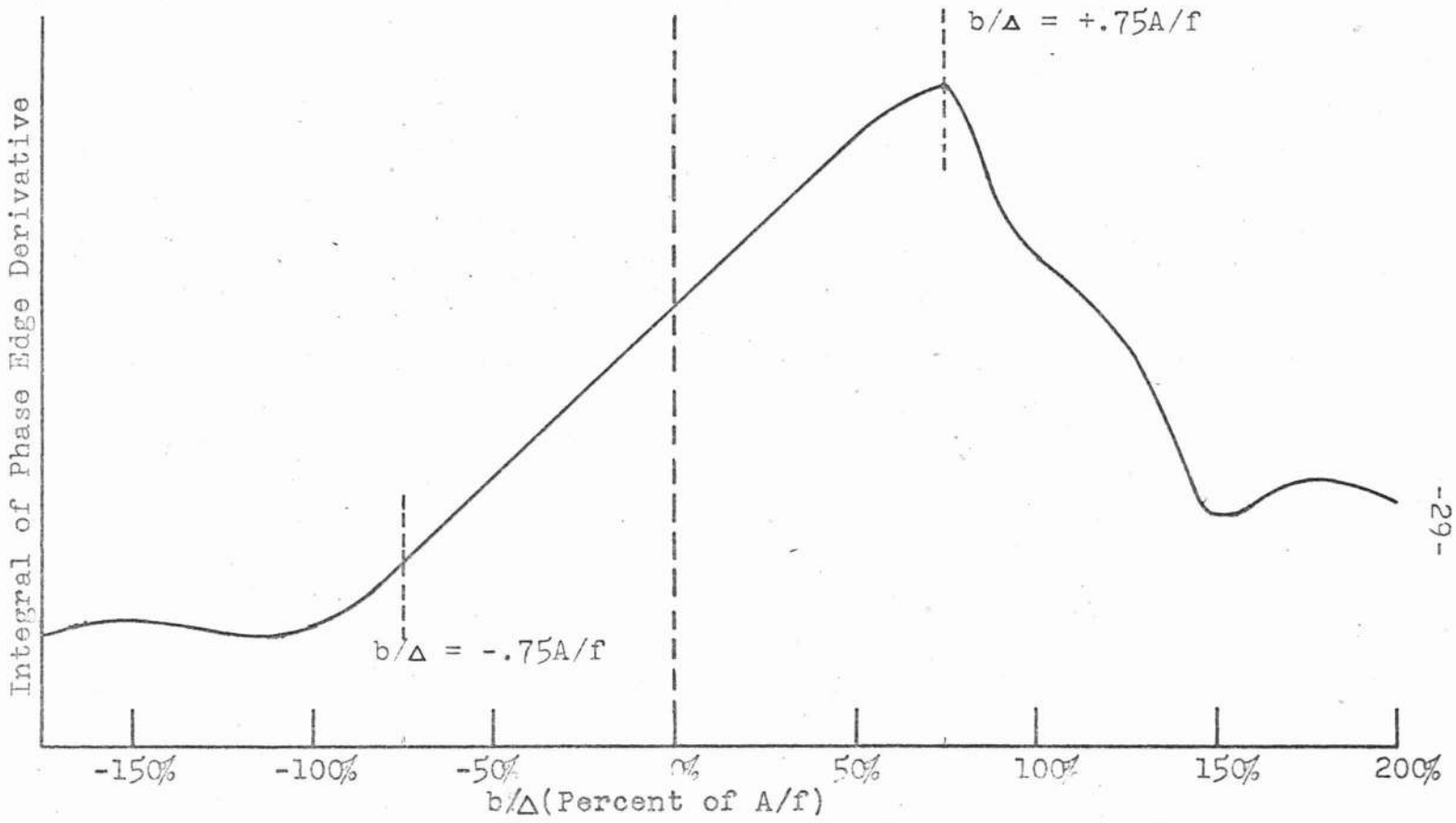

Figure 2.4

Integral of Phase Edge Derivative As A Function of Edge Slope

(Calculated for A/f = .02, Δ = .04)

The significance of this criterion is understood by noting that $(\Delta X)_D = f\lambda/A$, where $(\Delta X)_D$ is the total width of the point spread function for a clear-aperture diffraction-limited system. The evaluative criterion thus becomes

$$\frac{b}{\lambda} < \left(\frac{\Delta}{(\Delta X)_D}\right). \tag{2.43}$$

This condition now states that the number of wavelengths phase variation across the width of the point spread function must not exceed one. This criterion is intuitively comprehensible because wavelength ambiguity beyond the resolution limit of a system is always a problem. What is needed for this system is a method to band limit the phase function (for a given phase height) before allowing it to enter the differentiation system. Unfortunately, this is difficult to do because of the nonlinear relation between image phase and object phase. Due to this limitation, optical differentiation applied to biological phase objects may be limited in importance. Further study is needed to determine the relevance of this condition for actual specimens.

This system will also be limted by absorption in the object. If this absorption is described by the function $a(X_1)$, the object, rather than being pure phase is given by

$$f_1(X_1) = a(X_1)\, e^{ik\phi(X_1)}. \tag{2.44}$$

Imaging of this function in the differentiation system will result

in the image amplitude

$$f_3(X_3) = \left[X_0 + f\,\phi'(-X_3) - \frac{i\,a'(-X_3)}{a(-X_3)}\right] a(-X_3)\, e^{ik\phi(-X_3)}. \tag{2.45}$$

If this image is recorded photographically with $\gamma = +1$, the resulting film amplitude transmittance will be

$$t_f(X_3) = \sqrt{f_3(X_3) f_3^*(X_3)} = \left[\left(X_0 + f\,\phi'(-X_3)\right)^2 + \left(\frac{a'(-X_3)}{a(-X_3)}\right)^2\right]^{\frac{1}{2}} \left[\left(a(-X_3)\right)^2\right]^{\frac{1}{2}}. \tag{2.46}$$

If $a(X)$ is a slowly varying function, then $a'(-X_3)/a(-X_3) \ll 1$ and

$$t_f(X_3) \simeq \left[X_0 + f\,\phi'(-X_3)\right] \left[\left(a(-X_3)\right)^2\right]^{\frac{1}{2}}. \tag{2.47}$$

$\left[(a(X))^2\right]^{\frac{1}{2}}$ may be recorded separately in the optical system with no spatial filter present and used to divide out the error term. However, this division technique is still limited in application to slowly varying absorption functions.

Limitations of Coherent Integration

It has previously been stated that the limitations of coherent integration due to truncation of the integration filter depend upon the amount of the low spatial frequency information present in the object. This low spatial frequency information is transmitted by the truncated portion of the filter and is not integrated. Although the effect of this object low frequency loss on the image appearance is not intuitively obvious, it is well to note that system may be considered in reverse. The situation is identical to perfect integration with a high pass filter. The image will thus appear to be somewhat edge sharpened.

The effect of this information loss on the image is perhaps best understood by investigating the point spread function of the integration filter. If the non-truncated filter is considered, its point spread function is a perfect half wave phase step. Convolution of this function with any object gives the integral of that object. If the truncated integration filter is now considered, its point spread function is given by (see Appendix IV)

$$A_{It}(X,Y) = 4iAD\,\mathrm{sinc}\left(\frac{kAy}{f}\right)\left[Si\left(\frac{kAx}{f}\right) - Si\left(\frac{kDx}{f}\right)\right]. \quad (2.48)$$

Figure 2.5 is a plot of this function. The truncation is seen to cause the point spread function to taper off to zero for large X. This tapering off will cause a lack of correlation in the image for integration over two points with wide separation. Two points which are close together with respect to the width of the point spread function will see this function as a step. Points further apart will show less correlation and an apparent adjacency effect.

This apparent adjacency effect is easily demonstrated by considering the integral of the derivative of a bar. If the bar has a width of $2F$ and a height G, its one dimensional derivative consists of two delta functions. The object for the integration system is thus given by

$$f_3(X_3) = G\left[\delta(X_3+F) - \delta(X_3-F)\right]. \quad (2.49)$$

The image of this function determined by convolving it with the

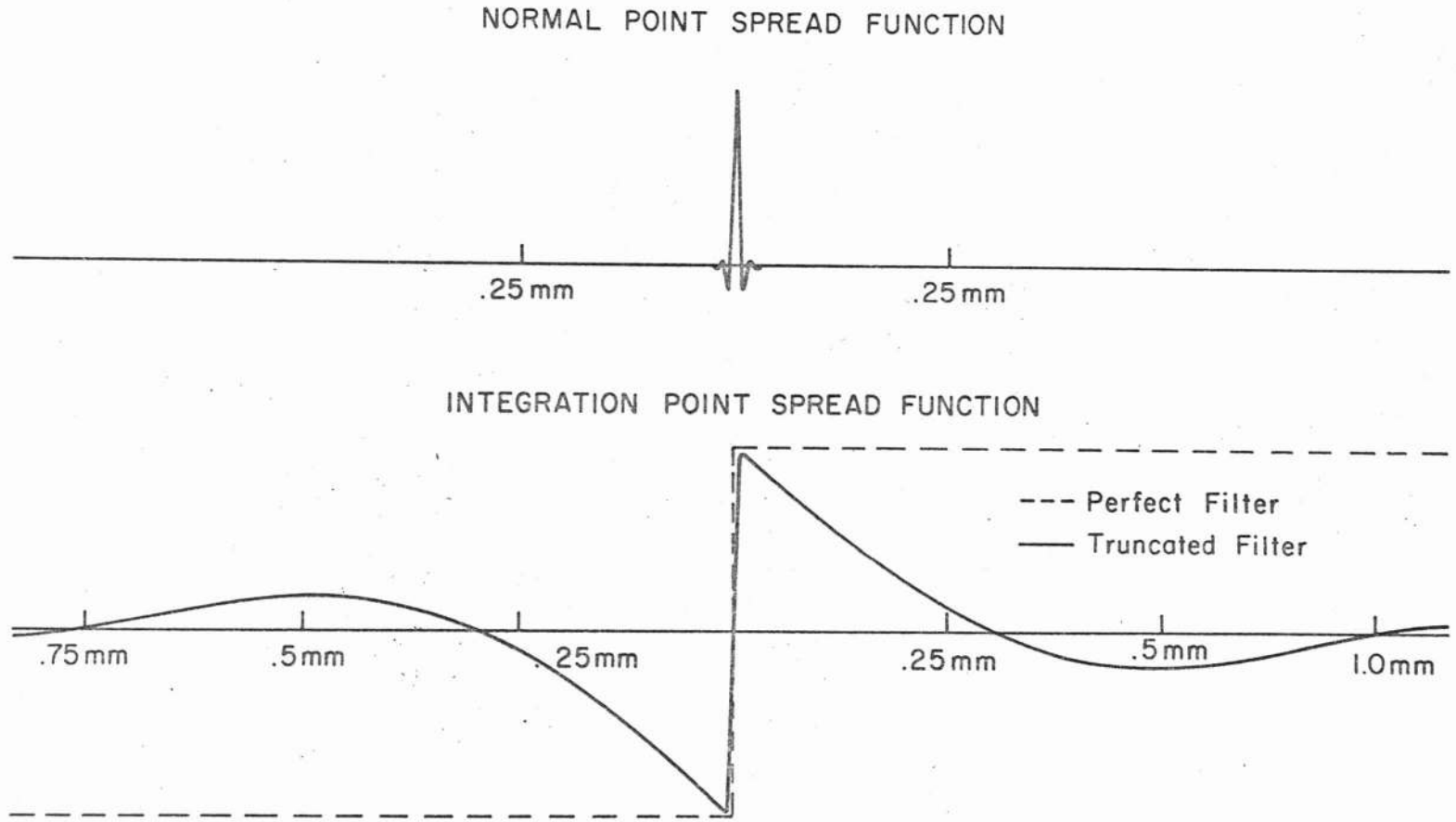
NORMAL POINT SPREAD FUNCTION
.25 mm
.25 mm
INTEGRATION POINT SPREAD FUNCTION
--- Perfect Filter
—— Truncated Filter
.75 mm
.5 mm
.25 mm
.25 mm
.5 mm
1.0 mm

Figure 2.5

integration point spread function has the form

$$f_5(x_5) = G\left[\mathrm{Si}\left[\frac{kA(x_5+F)}{f}\right] - \mathrm{Si}\left[\frac{kD(x_5+F)}{f}\right] - \mathrm{Si}\left[\frac{kA(x_5-F)}{f}\right] + \mathrm{Si}\left[\frac{kD(x_5-F)}{f}\right]\right]. \quad (2.50)$$

This image is drawn in Fig. 2.6 for several values of F. For a width F much narrower than the width of the point spread function, the image reproduces the bar quite accurately. For large F a distinct adjacency effect is observed with a drop in the center of the bar.

It may be noted that the truncation width D of the integration filter is determined only by the experimental apparatus. If limited image field is acceptable, D may be made small enough so that the width of the point spread function covers the entire image field. In this case, the integration will appear good with no edge sharpening.

Objects having amplitude absorption or phase edges which are too sharp will not be differentiated properly, giving rise to incorrect image terms. The effect of these terms is now seen to be unfortunate because of the broad width and assymetry of the point spread function of the integration filter. Any extraneous derivative terms will be blurred across the entire image field, producing a considerable amount of image noise. If there are a large number of these extraneous image terms, the actual signal may become unrecognizable. This point will be investigated in greater detail experimentally.

In conclusion, the truncated integration filter does work properly, but with a loss of low frequency information. For some

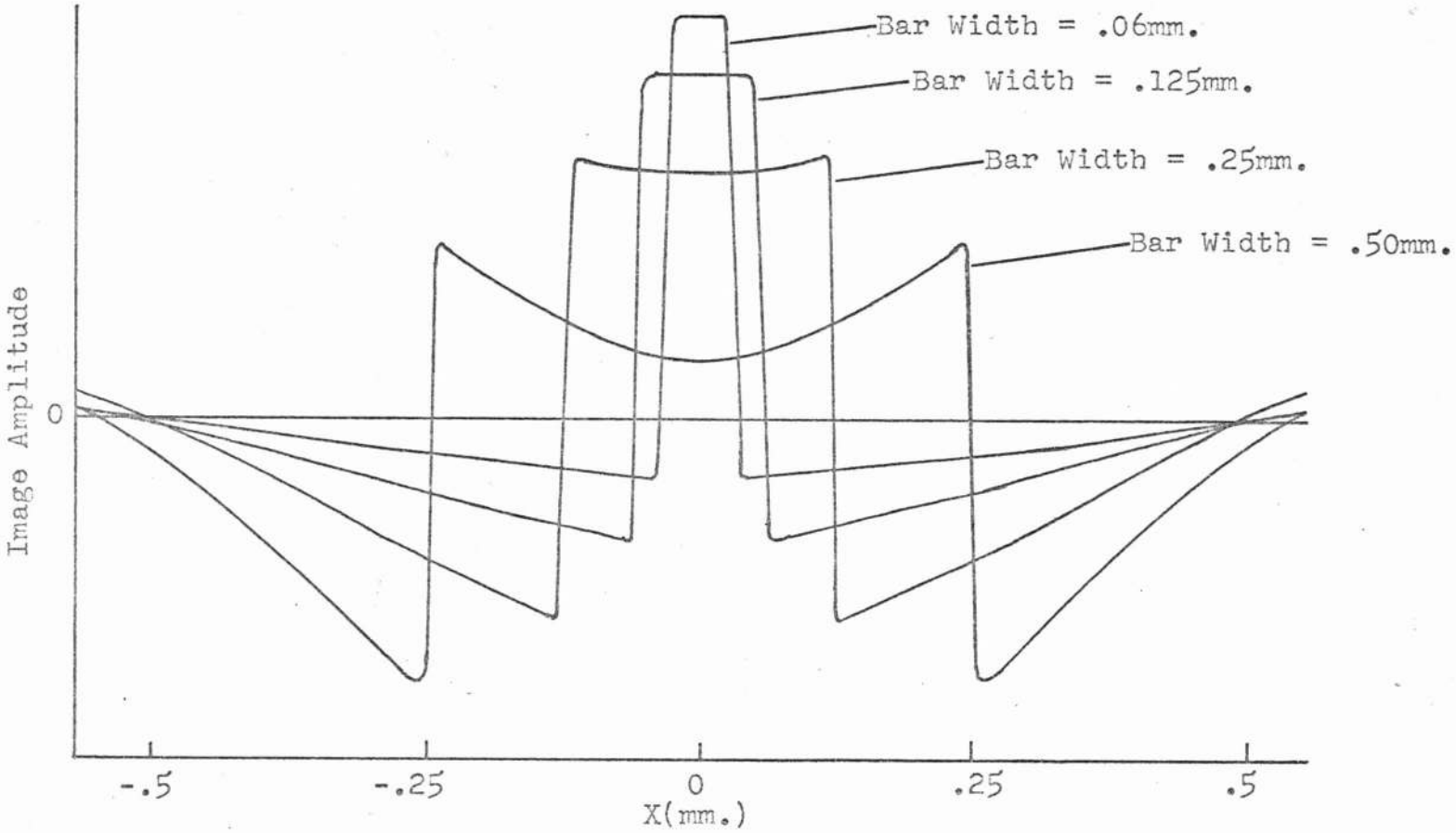

Figure 2.6

Theoretical Image of Integral of Phase Object Derivative

Formed With Truncated Integration Filter--Phase Bar Input

objects this discrimination may even be desirable if the informational content consists of fine detail. This is particularly true for sample phase objects, such as biological specimens which are mounted on microscope slides that are not optically flat. The discrimination is also desirable in the readout of thermoplastic recordings which may be mounted on a backing which contains thickness variations.

Choice of Filter Parameters

Differentiation Filter

The aperture transmittance function for the differentiation system is defined by $t(x_2) = \alpha (x_0 - x_2)$. The selection of the arbitrary constants α and x_0 is described in the following paragraphs.

The filter bias parameter x_0 is needed to insure that the modulus of the image amplitude is a positive definite function. x_0 must be large enough so that the bias image term is always larger than the maximum negative portion of the object derivative. This value may be determined by investigating the image of the sloped edge. This image amplitude, Equation 2.42, may be written as

$$f_3(x_3) = \alpha g(x_3)\, e^{-i\frac{kbx_3}{\Delta}} \tag{2.51}$$

where

$$\begin{aligned} \mathrm{Re}[g(x_3)] = &\left(\frac{f x_0}{k} + \frac{bf^2}{k\Delta}\right) \left\{ \mathrm{Si}\left[k\left(\frac{b}{\Delta} + \frac{A}{f}\right)(x_3 + \Delta)\right] \right. \\ &\left. - \mathrm{Si}\left[k\left(\frac{b}{\Delta} - \frac{A}{f}\right)(x_3 + \Delta)\right] - \mathrm{Si}\left[k\left(\frac{b}{\Delta} + \frac{A}{f}\right)x_3\right] + \mathrm{Si}\left[k\left(\frac{b}{\Delta} - \frac{A}{f}\right)x_3\right] \right\} \\ &+ \frac{x_0 f}{k}\left(\pi + 2\,\mathrm{Si}\left(\frac{kAx_3}{f}\right)\right)\cos\frac{kbx_3}{\Delta} + \frac{x_0 f}{k}\left(\pi - 2\,\mathrm{Si}\left(\frac{kA(x_3+\Delta)}{f}\right)\right)\cos\left(\frac{kbx_3}{\Delta} + kb\right) \end{aligned} \tag{2.52}$$

and

$$\mathrm{Im}[g(X_3)] = -\left(\frac{fX_0}{k} + \frac{bf^2}{\Delta k}\right)\left\{Ci\left[k\left(\frac{b}{\Delta}+\frac{A}{f}\right)(X_3+\Delta)\right] - Ci\left[k\left(\frac{b}{\Delta}-\frac{A}{f}\right)(X_3+\Delta)\right] - Ci\left[k\left(\frac{b}{\Delta}+\frac{A}{f}\right)X_3\right] + Ci\left[k\left(\frac{b}{\Delta}-\frac{A}{f}\right)X_3\right]\right\}$$
$$+\frac{X_0 f}{k}\left(\pi + 2Si\left(\frac{kAX_3}{f}\right)\right)\sin\frac{kbX_3}{\Delta} + \frac{X_0 f}{k}\left(\pi - 2Si\left(\frac{kA(X_3+\Delta)}{f}\right)\right)\sin\left(\frac{kbX_3}{\Delta}+kb\right)^2 \qquad (2.53)$$

The intensity in this image is given by the square modulus of the image amplitude, $I_3(X_3) = \left(\mathrm{Re}[g(X_3)]\right)^2 + \left(\mathrm{Im}[g(X_3)]\right)^2$. In the limiting case where $A \to \infty$, $\mathrm{Im}[g(X_3)]$ becomes zero in the spatial region of the edge derivative $-\Delta \leq X_3 \leq 0$ . . In the same region, the real part becomes

$$\mathrm{Re}[g(X_3)] = 2\pi\left[\frac{fX_0}{k} + \frac{bf^2}{k\Delta}\right]. \qquad (2.54)$$

To make this a positive definite function, X_0 must be chosen to satisfy $fX_0/k \geq bf^2/k\Delta$ to account for negative b/Δ .

If A is non-infinite, $\mathrm{Im}[g(X_3)]$ becomes non-zero. For edges which are differentiated properly however, $\mathrm{Re}[g(X_3)] >> \mathrm{Im}[g(X_3)]$ in the region of the edge derivative so that

$$\begin{aligned}|f_3(X_3)| &= \left[\left(\mathrm{Re}[g(X_3)]\right)^2 + \left(\mathrm{Im}[g(X_3)]\right)^2\right]^{\frac{1}{2}} \\ &= \left[\left(\mathrm{Re}[g(X_3)]\right)^2\right]^{\frac{1}{2}}\left[1 + \left(\frac{\mathrm{Im}[g(X_3)]}{\mathrm{Re}[g(X_3)]}\right)^2\right]^{\frac{1}{2}} \\ &\simeq \left[\left(\mathrm{Re}[g(X_3)]\right)^2\right]^{\frac{1}{2}}.\end{aligned} \qquad (2.55)$$

The required condition is still that $\mathrm{Re}[g(X_3)]$ be positive definite so that $|f_3(X_3)| \simeq \mathrm{Re}[g(X_3)]$. If Δ is considerably larger than the width of the point spread function,

the last two terms in $Re[g(x_3)]$ will be negligible near the center of the edge derivative and may be neglected. Additional effects caused by these terms will be spurious and need not be recorded properly. The condition on X_0 then becomes

$$\left(\frac{fX_0}{k}+\frac{bf^2}{k\Delta}\right)\left(Si\left[k\left(\frac{b}{\Delta}+\frac{A}{f}\right)(x_3+\Delta)\right]-Si\left[k\left(\frac{b}{\Delta}-\frac{A}{f}\right)(x_3+\Delta)\right]-Si\left[k\left(\frac{b}{\Delta}+\frac{A}{f}\right)x_3\right]+Si\left[k\left(\frac{b}{\Delta}-\frac{A}{f}\right)x_3\right]\right)\geq 0. \quad (2.56)$$

$-\Delta < x_3 < 0$

Since for edges of interest $A/f > b/\Delta$, Equation 2.56 is satisfied for all X_3 in this region by the supplementary condition

$$\frac{fX_0}{k}+\frac{bf^2}{k\Delta}\geq 0 \quad , \quad X_0 \geq \frac{bf}{\Delta} \quad . \quad (2.57)$$

The maximum b/Δ which may be properly differentiated has been shown to be $b/\Delta = .75\,A/f$, so that Equation 2.57 finally reduces to

$$X_0 \geq .75A.$$

A standard differentiation filter has the amplitude transmittance $t(x_2)=x_2$. The limitation on the value of X_0 simply states that the origin of this standard differentiation filter must be laterally displaced by an amount approximately equal to the half width of the aperture. This criterion is particularly convenient experimentally because it allows for a differentiation filter having no negative transmittance values.

Once a value for X_0 has been selected, the constant α must be chosen to allow the desired transmittance values to fall in a region which is realizable photographically. Although the filter transmittance may be rendered negative by the use of a

half wave phase plate, it is simpler to use a positive filter function. To achieve this end, if the maximum and minimum film transmittance values are t_{max} and t_{min} respectively, these values will appear at the positions $X_2 = -A, +A$. These film limitations define two simultaneous equations for X_o and α :

$$1)\ t(-A) = t_{max} = \alpha (X_o + A) \tag{2.58}$$

$$2)\ t(A) = t_{min} = \alpha (X_o - A). \tag{2.59}$$

α and X_o must satisfy these equations as well as the additional condition $X_o \geq .75A$. Solving the second equation for X_o , $X_o = (t_{min}/\alpha) + A$. Since this value of X_o satisfies the additional condition $X_o \geq .75A$ for any α , α may be chosen from $t_{max} - t_{min} = 2\alpha A$,

$$\alpha = \frac{t_{max} - t_{min}}{2A} . \tag{2.60}$$

Integration Filter

The aperture amplitude transmittance function for the integration system is defined by

$$t(X_4) = \begin{cases} i\,B & X_4 < D \\ \dfrac{D}{X_4} & X_4 \geq D \end{cases} \tag{2.61}$$

Once a value for D has been selected, the maximum width of the integrating portion of this filter will be limited by the film dynamic range. The limits of the filter extent are determined by

$$t_{max} = \frac{D}{X_{4min}} \Rightarrow \qquad X_{4min} = \frac{D}{t_{max}} \tag{2.62}$$

$$t_{min} = \frac{D}{X_{4max}} \Rightarrow \qquad X_{4max} = \frac{D}{t_{min}} \, . \tag{2.63}$$

Because of these limitations, the dynamic range in frequency response is given by

$$\frac{\omega_{max}}{\omega_{min}} = \frac{X_{4max}}{X_{4min}} = \frac{t_{max}}{t_{min}} \, , \tag{2.64}$$

where ω represents spatial frequency. The absolute range of this band-limited response will depend on the focal lengths and wavelength of illumination for a particular system, but its dynamic range limits are set by the transmittance range of the filter material.

Chapter III

Experimental Implementation

The system which has been described has been implemented experimentally. This work forms the major portion of this thesis and is now described in detail. Discussion has been divided into several sections, each of which describes one phase of the experimental work.

Phase Target Production

Several different types of phase objects were used as the input to this system. The first sample objects were phase resolution targets which were convenient for studying the spatial frequency response of the system. They were manufactured by exposing a photographic plate to the image of an air force bar target, developing the latent image, and then bleaching out the silver with photographic bleach. Because the emulsion shrinkage is affected by byproducts of development, this left the emulsion with a relieved surface contour related to the original exposure. The bleaching process also gives rise to internal index of refraction variations, but these can be minimized through use of a surface relief bleach.

To study differentiation of phase edges of varying slopes and heights, several different targets were prepared. Variation in bar height was achieved by changing the exposure. Variation in edge slope was achieved by imaging the original

absorption bar target onto the emulsion through a small aperture. By altering the size of this aperture, the resolution limit of the system could be controlled, changing the edge sharpness. The apparatus used is schematically illustrated in Figure 3.1.

Kodak 649F Photographic Emulsion was used to make the phase targets. It was processed as follows:

Develop HRP 1:2	5 min.
Wash	10 min.
R10 Bleach	2 min.
Wash	4 min.
Kodak Rapid Fix	8 min.
Wash	15 min.
Dry in still air	

The photographic bleach R10 is made by mixing 1 part Sol. A, 1 part Sol. B, and 10 parts water, where

Solution A-- 500 ml. water
20 gm. ammonium bichromate
14 ml. concentrated sulfuric acid
water to make 1 liter

Solution B-- 45 gm. sodium chloride
water to make 1 liter.[35]

Several different phase objects were produced in this manner. The phase height was varied from a small fraction of a wavelength through about two and one-half wavelengths by changing the exposure time, and the range of resolution limits was 30 to 120 lines/mm. This bleach gives almost completely

PHASE TARGET EXPOSURE APPARATUS

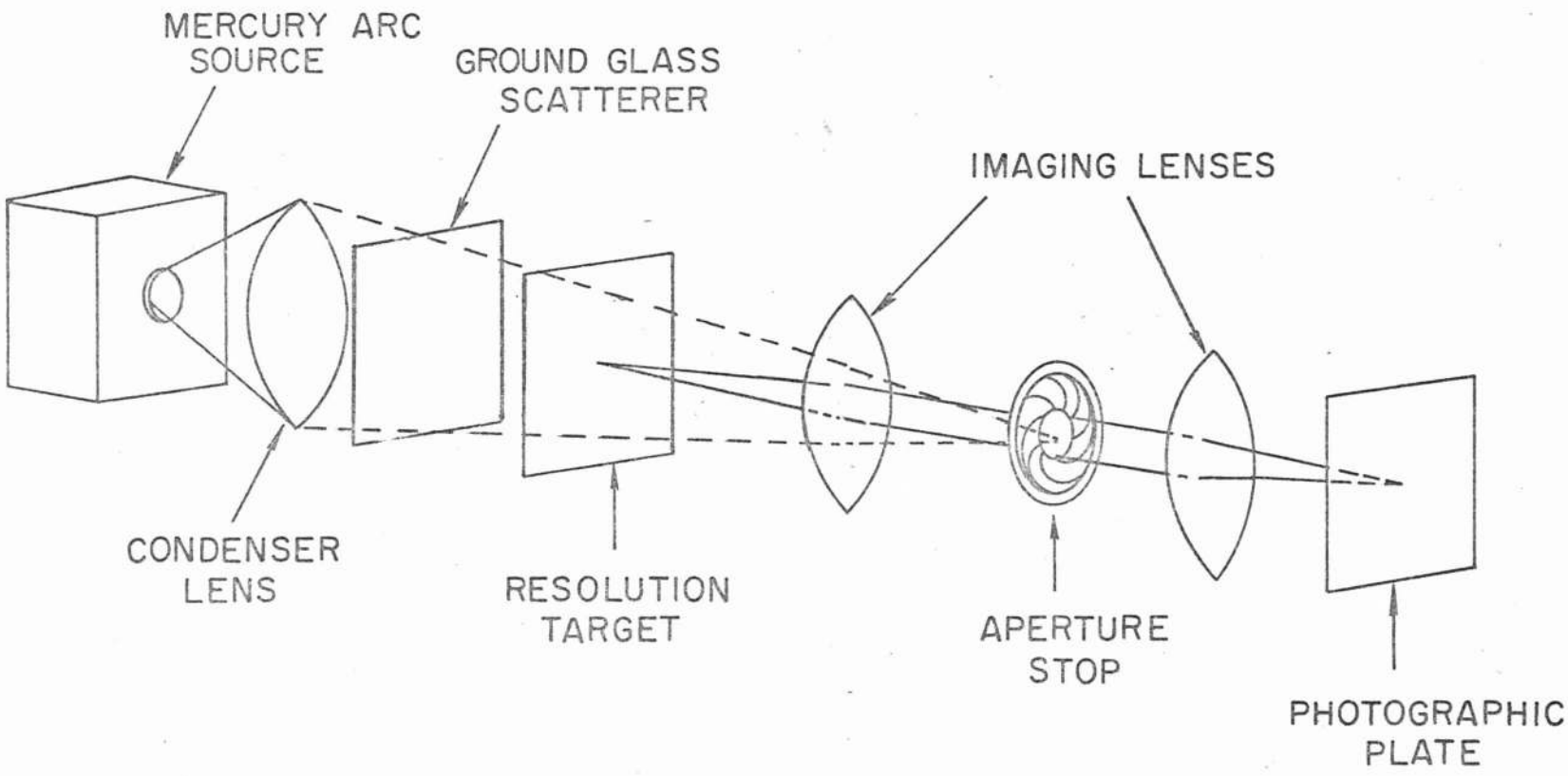

Figure 3.1

transparent targets ($\Delta D < .02$) for exposures with equivalent densities of less that 2.0. For equivalent densities above this level, a slight residual absorption image remains.

A set of phase steps of increasing height was used as a sample object to check the system for range of grey-steps. The target was produced by contact printing a ronchi ruling exposed through a continuous tone density wedge. Because of a slight separation between the ronchi ruling and the photographic emulsion, edge sharpness was limited. When the film was developed and bleached, in the manner already described, it contained a continuous range of phase steps from half a wavelength through two and one half wavelengths in height.

A third type of target was desired which exhibited a continuous range of phase from zero through a few wavelengths. Although the two types of targets already described satisfy this criterion, their phase varies so rapidly over this range that the phase functions are essentially binary. Photographic bleaching was found to be unsuitable for producing a continuous range phase target because of the poor low spatial frequency response of the bleaching process. Instead, targets were produced in the following manner. A thin layer of Duco Cement was smeared across a clear glass plate with a microscope slide and allowed to dry until it was just barely hard. At this time a small artificial pearl (being the cheapest and most easily obtainable small sphere) was pressed lightly into the surface. This left

a small round phase depression having a slightly raised lip. The depth of this phase crater could be altered by using a different size sphere or changing the amount of applied force. Although the same technique was tried with other transparent materials, Duco Cement was the only one which left smooth depressions without surface cracking.

Spatial Filter Production--Photographic Part

Both spatial filters which are used in this system contain one dimensional variations in amplitude transmittance as a function of spatial coordinate. These transmittance variations were produced photographically with apparatus which compensates in exposure for film nonlinearities. Two techniques were used to do this, each one having certain advantages and limitations.

The differentiation filter was produced using a sliding mask technique. The experimental apparatus, which is schematically illustrated in Figure 3.2 contains a uniform slide assembly driven by a synchronous motor attached to a lead screw. An opaque mask having a clear area in the center is mounted on this slide assembly and scanned in front of a photographic plate. When the entire apparatus is illuminated from the right with a plane wave, a given position on the film will receive exposure for a time proportional to the width of the clear area of the mask in front of it. By first using a stepped mask of known width, a callibration plate may be obtained.

APPARATUS FOR SPATIAL FILTER PRODUCTION (I)

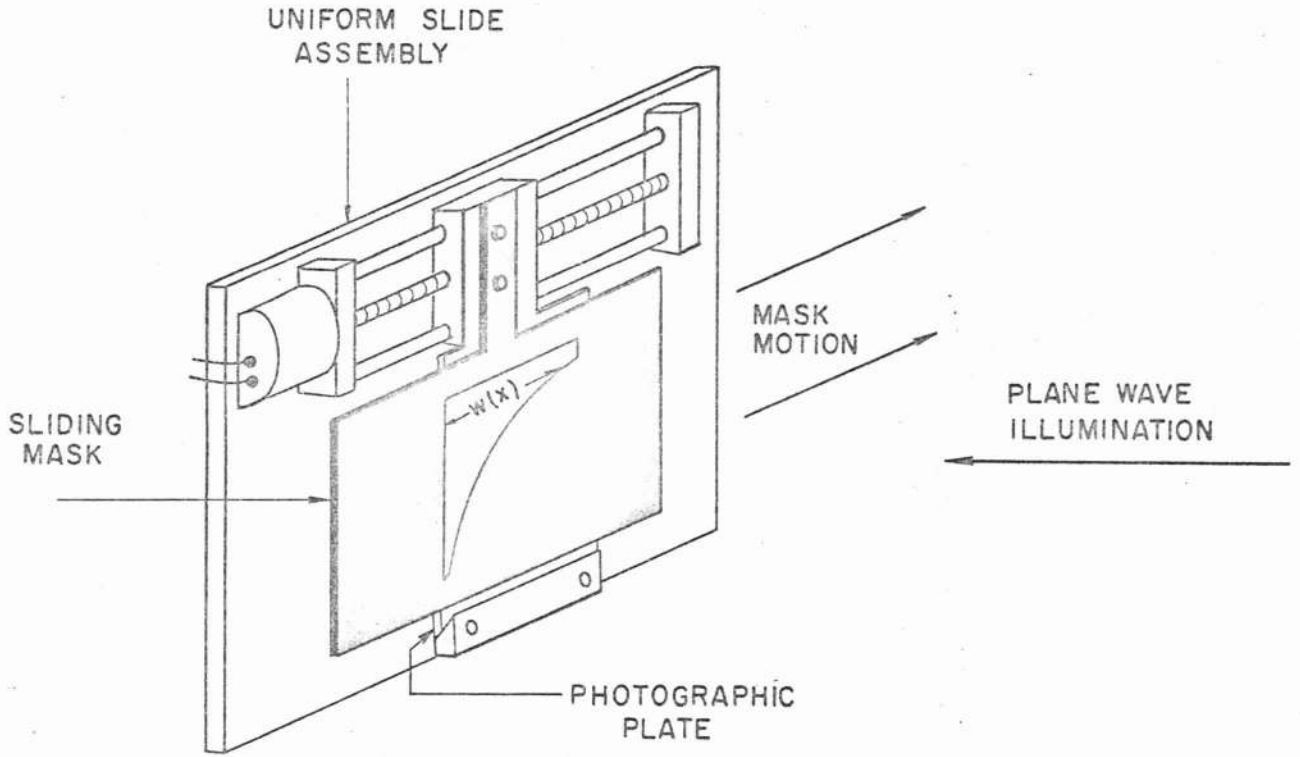

$$E(x) = A\, w(x)$$

Figure 3.2

When this plate is processed and scanned with a microdensitometer, a curve of density vs. mask width is obtained. Since the desired density function is known, the required mask function may be determined. This function is plotted on a large piece of chart paper, the region it encloses is cut out, this is turned over and mounted on a piece of black cardboard, and the pattern is photographically reduced to the proper size.

Although this technique for mask production is accurate and simple, great care must be taken to insure mask cleanliness and uniform density in the clear area. Dust on the mask will cause streaks in the plate exposure and a non-uniform clear area will produce an incorrect exposure.

The actual differentiation filters were recorded on Kodak 649F Emulsion and tray processed in the following manner:

Develop HRP 1:4	1 min.
Wash	15 sec.
Stop	30 sec.
Wash	15 sec.
Rapid Fix	2 min.
Wash	11 min.
50% Methyl Alcohol. 50% Water	5 min.
75% Methyl Alcohol, 25% Water	5 min.
100% Methyl Alcohol	5 min.
Dry in still air	

The mercury arc source was checked for intensity level before and after each exposure to insure exposure intensity repeatability. To insure constant development conditions, the developer was immersed in a temperature controlled bath and continuously agitated. A low contrast developer was used (HRP 1:4) as this created less density sensitivity to temperature, development time, exposure time, mask width variation, and source intensity. The enhanced film nonlinearities caused by working at low contrast were no problem because they were compensated by the shape of the mask width function.

The two differentiation filters used were measured on a Joyce-Loebel Microdensitometer. The density traces obtained are shown in Figures 3.3a and 3.3b and the amplitude transmittance functions which may be determined from this data are in Figure 3.4. These two filters cover a density range of .1 to 2.25 and an amplitude transmittance range of 8% to 90%. This variation is across a distance of 6 mm. for one filter and 12 mm. for the other which in this system corresponds to $\pm$ 30 lines/mm. and $\pm$ 60 lines/mm..

The sliding mask technique is a good one because the determination of the required mask function is extremely simple and not susceptible to error. If the mask width function is $\omega(X)$, the exposure function it produces is given by

$$E(X) = A \cdot \omega(X) \qquad A = \text{constant} \tag{3.1}$$

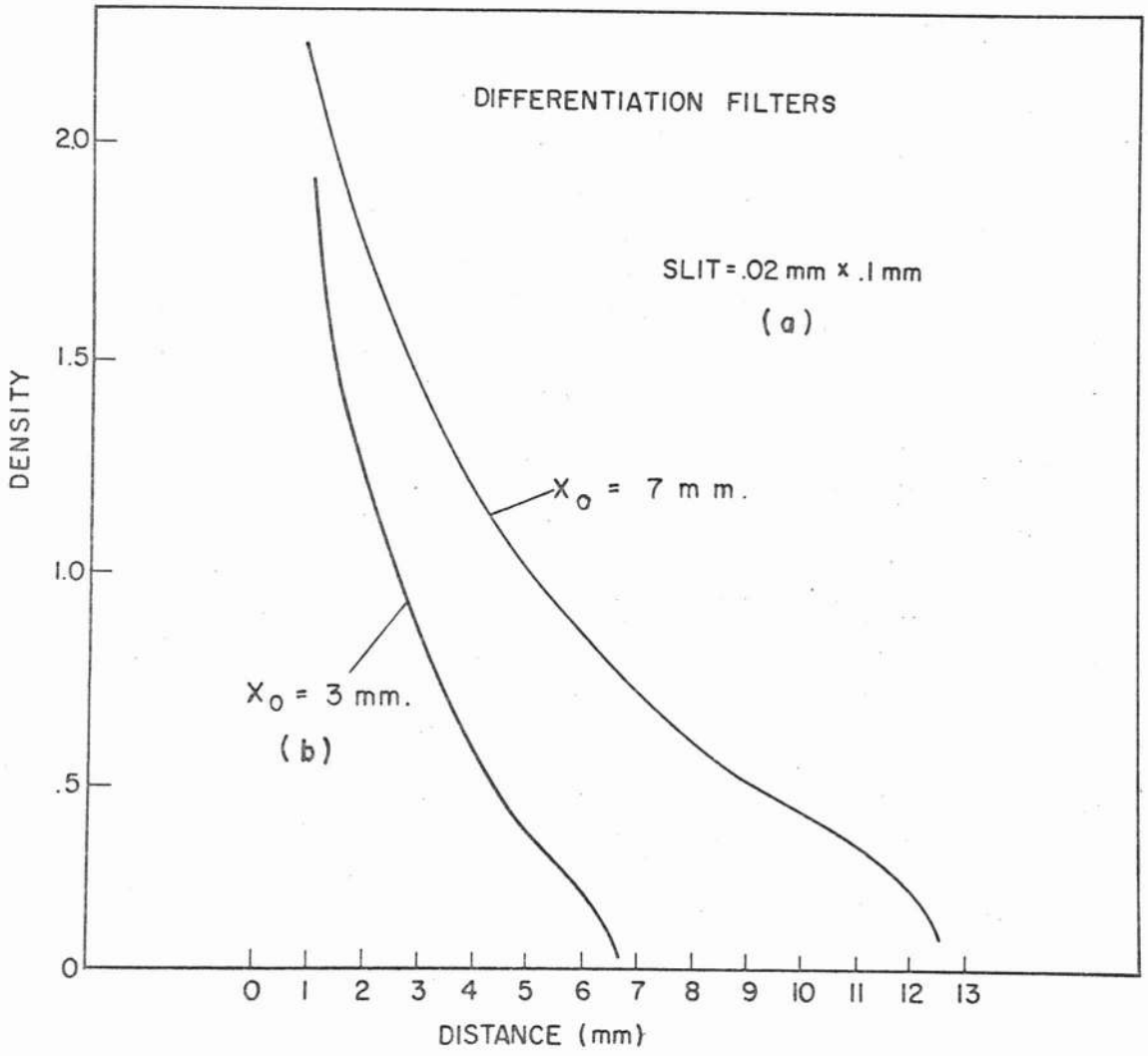
DIFFERENTIATION FILTERS
SLIT = .02 mm x .1 mm
(a)
X_o = 7 m m.
X_o = 3 mm.
(b)
DENSITY
2.0
1.5
1.0
.5
0
0 1 2 3 4 5 6 7 8 9 10 11 12 13
DISTANCE (mm)

Figure 3.3

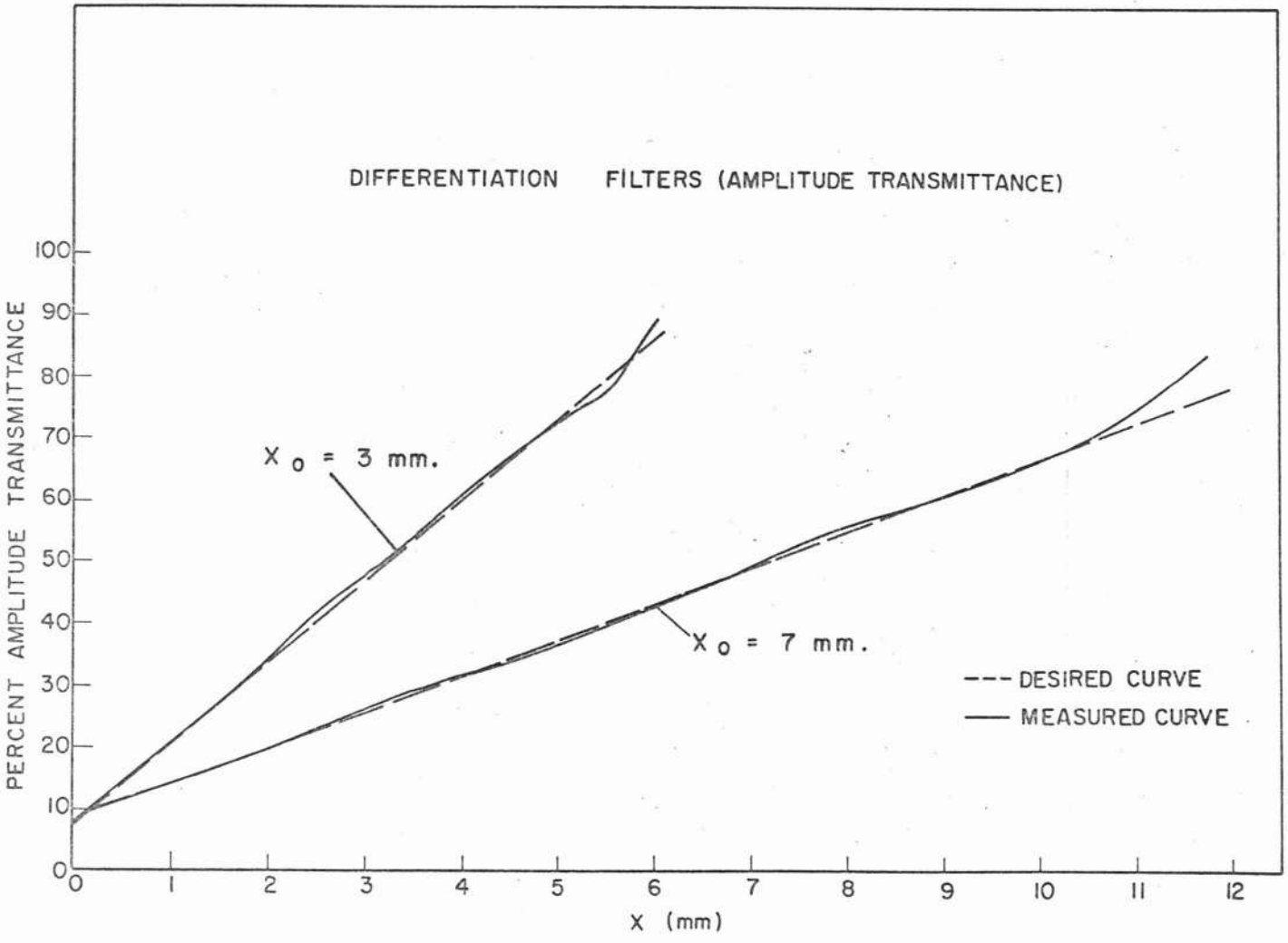
DIFFERENTIATION FILTERS (AMPLITUDE TRANSMITTANCE)
PERCENT AMPLITUDE TRANSMITTANCE
X (mm)
X_o = 3 mm.
X_o = 7 mm.
--- DESIRED CURVE
—— MEASURED CURVE
0
10
20
30
40
50
60
70
80
90
100
0
1
2
3
4
5
6
7
8
9
10
11
12

Figure 3.4

This technique has the additional advantage that the exposure at any X position is independent of the exposure at the rest of the X values. Because of this, mask width errors are not additive but merely form a slight error function in transmittance which oscillates about the proper curve.

Unfortunately, this system is limited in its ability to produce exposure functions which vary rapidly with X. This limitation is due to imperfect horizontal slide motion. Any wobble of the mask as it traverses the system will blur any rapidly varying portion of the exposure. Also, alignment of the mask along the line of motion is very critical. This alignment was achieved by observing a straight line portion of the mask through a mounted microscope containing a filer eyepiece. The mask was rotated until the vertical position of the line remained constant as the mask traversed the system. With this alignment, resolution in exposure variations was limited to several fractions of a millimeter.

The sliding mask system has the additional limitation of limited dynamic range in exposure. Since it is desirable to develop with low contrast, a wide range of desired density values requires a large dynamic range in exposure. Since the exposure is proportional to the mask width, this dynamic range will be the same as that available in variation of this width. The system is fundamentally limited in this dimension by diffraction at the mask edges. If the mask width is much smaller than a fraction of a millimeter, diffraction will destroy any rapidly varying exposure distribution. The dynamic range of exposure

mask width for this system was about two orders of magnitude as .5 mm. $<\omega(x)<$ 50 mm..

The required integration transmittance function is $t(x) = D/x$. This spatial filter transmittance varies very rapidly with X over a wide range of density values, so it can not be produced with the sliding mask technique. The original instigation for another technique is an article by Kent.[36] In this article he suggests that by using a broad source in a thin film evaporation chamber, a mounted substrate, and a knife edge placed somehwere between the two, a linear absorption wedge of aluminum can be evaporated on the substrate. This result is obtained because the evaporation shadow of the knife edge created by the broad source is cast on the substrate. The analogy of this effect can be created optically. Furthermore, there is an additional parameter which may also be varied, which is the width of the source.

The operation of this system is described by the diagrams in Figure 3.5. The shadow of a vertical knife edge produced by a point source is a step function, slightly blurred by diffraction off the knife edge. If this point source is broadened to a line source in the horizontal coordinate, the new shadow function will be a linear graded step, as shown in the second diagram of Figure 3.5. This graded step will have a transition region from zero to uniform illumination whose width is proportional to the projection of the line source

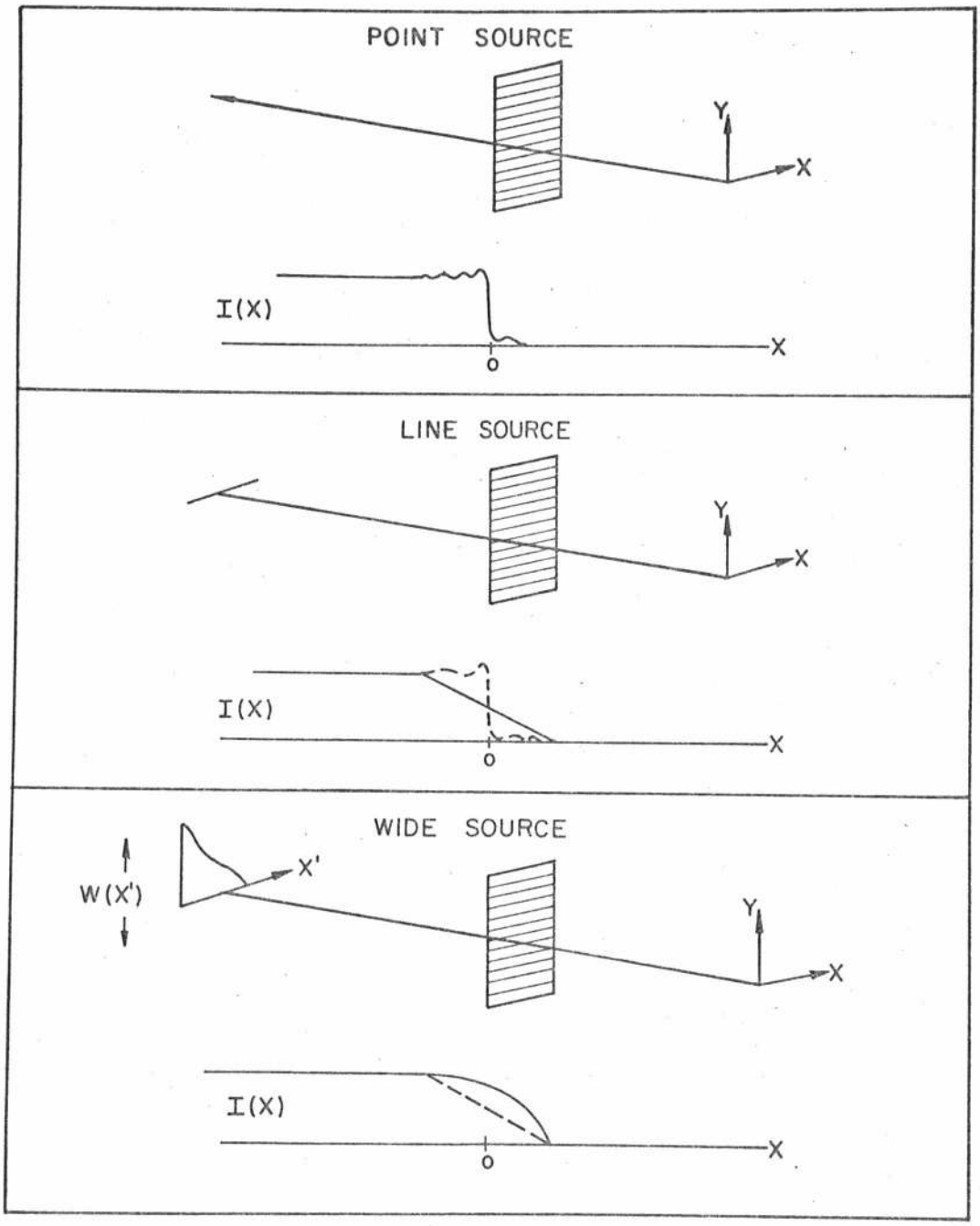

Figure 3.5

Explanation of Knife Edge Shadowing Technique

in the shadow plane. If the source is now broadened in the vertical direction by a width function W(x), (or analogously, if its intensity is caused to vary as W(x)), the horizontal width of the intensity transition region will not be affected, but the shape of the intensity function in this region will change. By varying the shape of the source width function, the shape of this intensity curve may be formed to any desired monotonic function. In particular, if

$A(x')$ = Knife edge diffraction pattern

$W(x')$ = Source width function

$E(x)$ = Exposure function

a = Distance from source to knife edge

b = Distance from knife edge to exposure plane,

the exposure function will be given by

$$E(x) = \int_{-\infty}^{\infty} W(x')\, A\left(-x - \frac{bx'}{a}\right) dx'. \tag{3.2}$$

By making a standard step wedge exposure and knowing the desired film transmittance function, the required exposure function may be determined. To a reasonable degree of approximation, Equation 3.2 may then be inverted to find $W(x')$ for this $E(x)$, taking into account the diffraction pattern $A(x')$. However, note that

$$\frac{dE(x)}{dx} = -\int_{-\infty}^{\infty} W(x')\, A'\left(-x - \frac{bx'}{a}\right) dx'. \tag{3.3}$$

This expression is similar to the convolution equation which determines the image intensity in an incoherent optical system. A resolution limit is thus set on the rapidity with which the exposure function can change. This limit, which is determined by the width of $A'(x')$, is analagous to the incoherent image resolution limit. Since the width of $A'(x')$ is the edge width produced by diffraction off the vertical edge, inversion of the original equation to find $W(x')$ cannot be expected to give significantly better results than a geometrical ray trace approach to the problem, which is much simpler computationally.

One simple addition to this ray trace approach may be made however, by examining the diffraction pattern $A(x')$ graphed in Figure 3.6. It is seen from Figure 3.6 that a good approximation to $A(x')$ is a linear graded edge of width δ. δ is determined from

$$\delta = \sqrt{\frac{b\lambda(a+b)}{2a}} \quad .$$

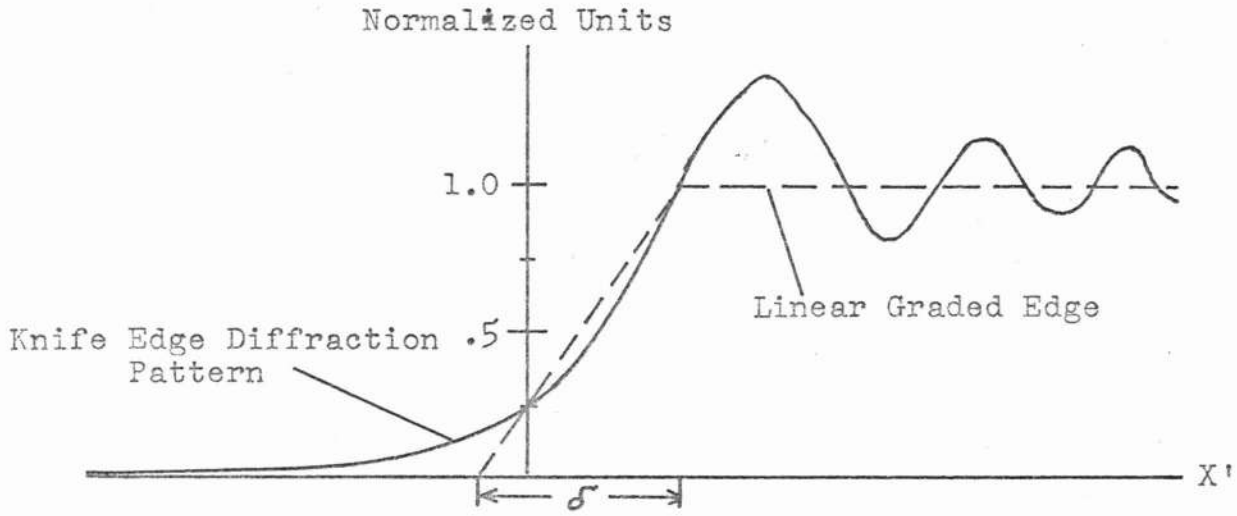

Figure 3.6

Knife Edge Diffraction Pattern

It is also apparent from Figure 3.6 that the major effect of diffraction has been to shift the effective edge position, defined by the half intensity point, in the plus X direction by $\delta/4$. When only this correction term is considered,

$$W(x') = \frac{dE(x'')}{dx''}\bigg|_{x''=-\frac{a}{b}(x'+\frac{\delta}{4})} . \qquad (3.4)$$

This expression may be used to determine $W(x')$, remembering that $E(x)$ will be limited by diffraction.

The actual experimental setup is schematically illustrated in Figure 3.7. A double source is used with a double knife edge to produce the required symmetrical exposure function. A light shield is placed on axis between the two halves of the source to prevent exposure overlap. The effective source is made of ground glass illuminated with a light source and a condenser. To determine the actual physical parameters of this system, the condenser aperture is first measured to find the maximum possible source size. Since the desired horizontal extent of the exposure region is known, this measurement determines the maximum possible effective demagnification of the source, which is given by b/a. A trial plate position is then chosen and a scanning photomultiplier is placed in this position. Since choice of this position effectively determines $b+a$, and b/a has already been determined, individual values for a and b can be calculated and the

APPARATUS FOR SPATIAL FILTER PRODUCTION (2)

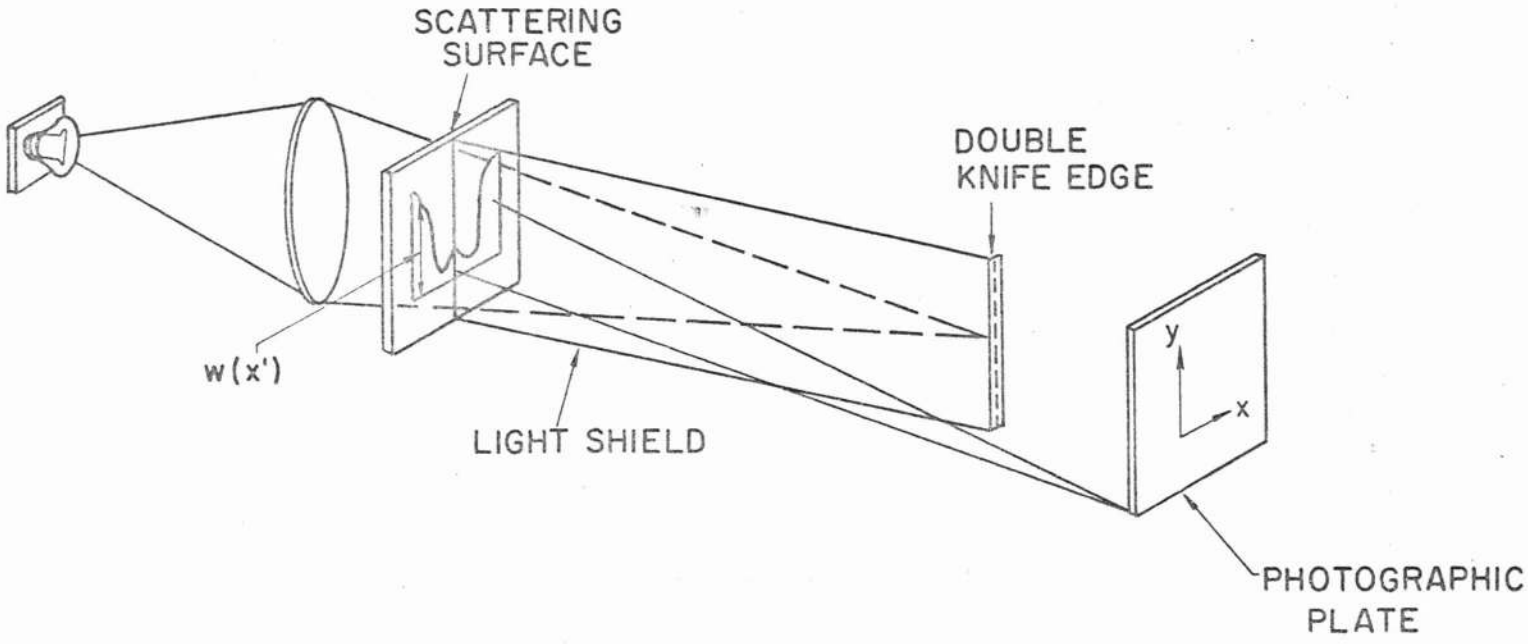

$$E(x) = B\int^{x} w(x')\,dx'$$

Figure 3.7

appropriate position for the knife edge determined. The actual source is then moved until it images at this position, and a full aperture scattering mask is placed in the condenser aperture with no knife edge in the system. The intensity in the plate plane is then scanned to determine its profile. It is required that this intensity profile be uniform across the desired exposure region to within a certain criterion which must be determined. If the intensity variation is greater than this criterion the plate is moved farther away, the source refocussed, and the measurement repeated.

The actual choice of a criterion for the constancy of the intensity is a compromise. To make it very small requires that $a+b$ be chosen large, causing the diffraction blur δ to also be quite large. If

$$c = a+b$$

ΔX = Width of desired exposure region

A = Condenser aperture width,

then $\Delta X = bA/a$. The diffraction limit is determined from

$$\delta = \sqrt{\frac{b\lambda(a+b)}{2a}} = \sqrt{\frac{\lambda c\, \Delta X}{2A}} \quad . \tag{3.5}$$

As might be expected, this diffraction limit is set by the required field extent, the aperture width, and the separation of the source and exposing region. Since the condenser width A is predetermined by the available aperture, there is a

tradeoff between field extent, diffraction blur, and constancy of intensity. The limiting criterion chosen for this experiment was $\Delta I / I = \pm 5\%$. The developer and emulsion used results in γ of about 1.5, giving rise to $\Delta D = .075$ for this criterion. The film processing is not repeatable to significantly greater accuracy than this, and since fine exposure detail is desired, this choice of criterion is a reasonable limit.

With a and b chosen by this procedure, a photographic plate is mounted in the X plane and covered with a step tablet. This plate is exposed with the same source. The actual processing used is the following:

Develop D-165 1:3	4 min.
Wash	15 sec.
Stop	30 sec.
Wash	15 sec.
Rapid Fix	2 min.
Wash	10 min.
50% Methyl Alcohol, 50% Water	2 min.
75% Methyl Alcohol, 25% Water	2 min.
100% Methyl Alcohol	2 min.

The resulting density is measured with a densitometer to provide callibration. Since the desired film transmittance function is known, the needed exposure function can then be determined. This function is drawn on a large piece of chart paper and graphically differentiated to determine the required

mask width function $W(x')$. This function $W(x')$ is then drawn on a piece of ground glass and the exterior areas are covered with black tape. This mask is then inserted in the condenser aperture and the double knife edge placed in its appropriate position.

A trial exposure is then made, measuring the source intensity from the side with a permanently mounted light meter. After development, the density produced is measured at a position far enough off axis to be in the uniform illumination region of the exposure, i.e. outside the geometrical shadow region. The required density in this region is determined by the distance off the axis at which the region begins. The exposure time is then readjusted (keeping the source intensity constant) and successive exposures made until the desired density is achieved. The parameters of the actual system used are

Mask half width = 39.5 mm.

Mask height = 80 mm.

a = 35 cm.

b = 5 cm.

Knife edge separation = 5.0 mm.

δ = .125 mm.

The exposure function produced in this system was scanned with a photomultiplier and found to be accurate to within a few percent. The actual spatial filter produced was scanned with

a Joyce-Loebel Microdensitometer to give the density trace of Figure 3.8. The conversion of this curve to amplitude transmittance is shown in Figure 3.9.

This exposure technique has been shown to produce very accurate and noiseless exposure functions which vary quite rapidly as a function of X . It's limits are set by the physical size of the condenser aperture, although fine resolution in detail may be obtained by sacrificing field extent, or vice-versa. This technique has the disadvantage compared to the sliding mask technique that data evaluation in the determination of $W(X')$ is much more difficult and susceptible to error.

Spatial Filter Production--Thin Film Coating

The differentiation filter function which is used contains only positive transmittance values. Because of this, the entire differentiation filter can be produced photographically by the methods already described.

The integration filter is another story. Its transmittance function has the form

$$t(X_4) = i B \qquad |X_4| < D$$
$$= \frac{D}{X_4} \qquad |X_4| \geq D \tag{3.6}$$

This function is negative for X_4 less than -D and has a phase shift i in the region $|X_4| < D$. To produce these phase portions of the filter, a thin film coating was formed on an optical flat. This optical flat was mounted in the appa-

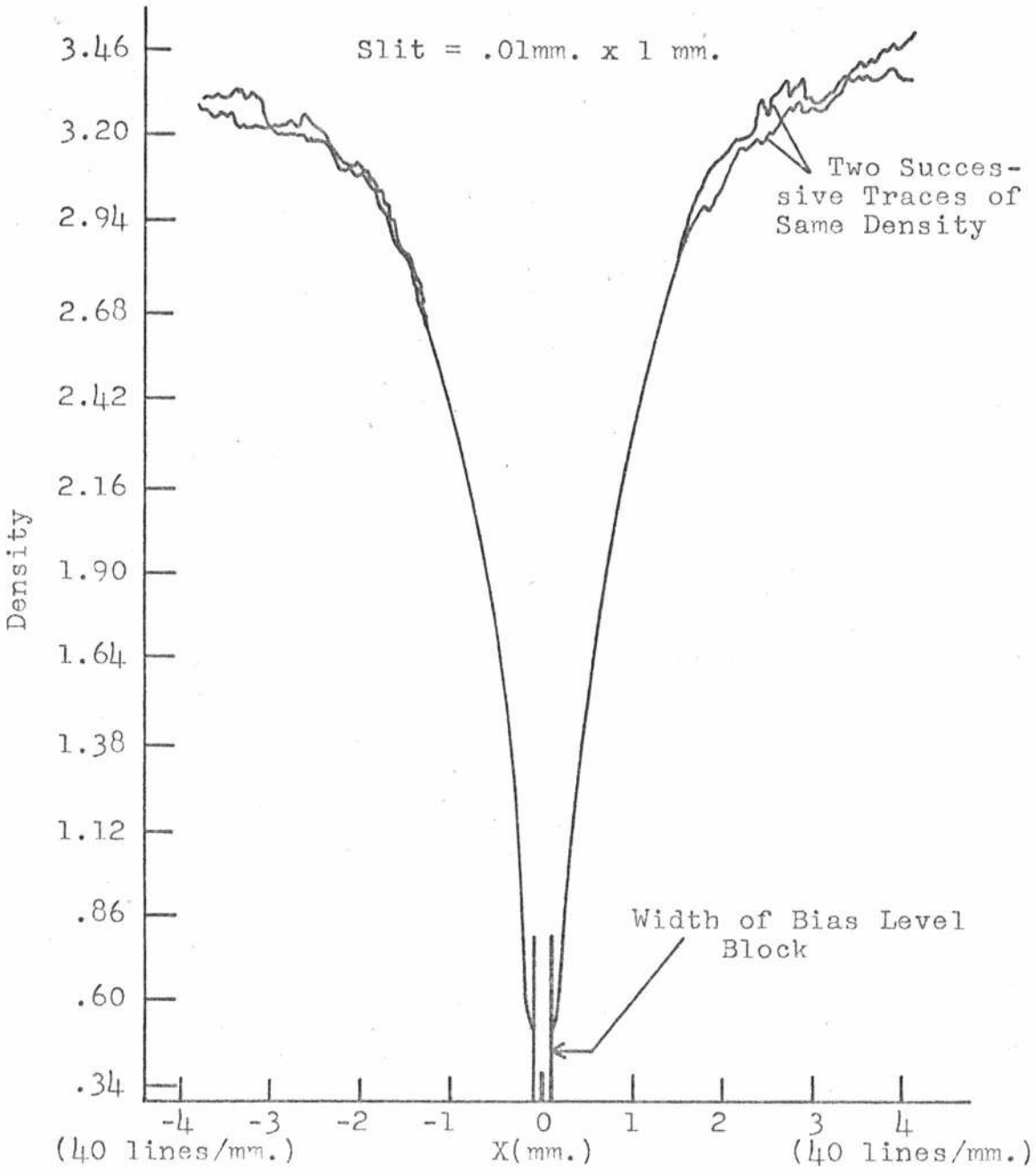

Figure 3.8

Integration Filter

Densitometer Trace

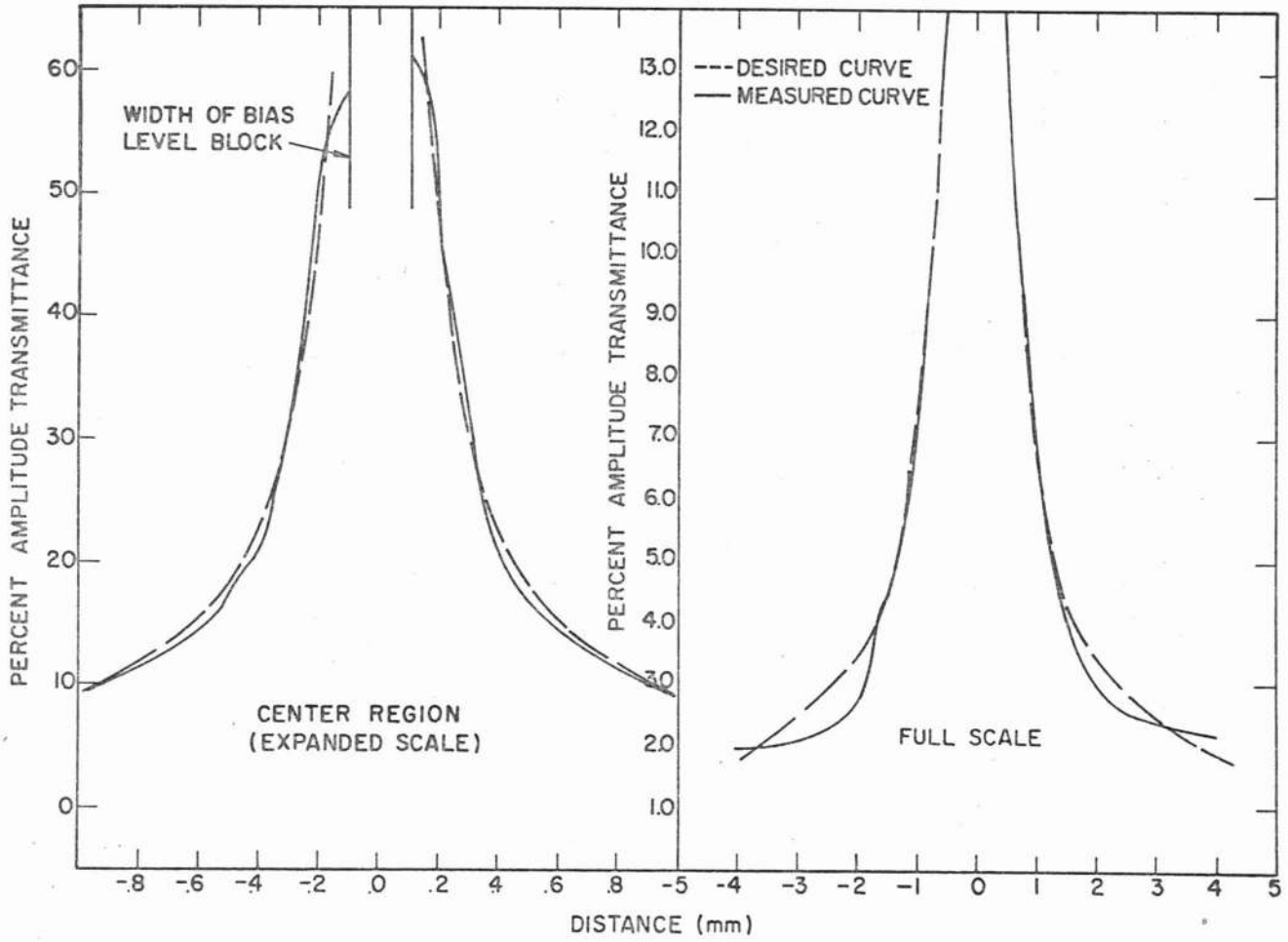

Figure 3.9

Integration Filter

Percent Amplitude Transmittance

ratus illustrated in Figure 3.10. This apparatus contains two screw clamps which hold the flat securely to the base. Two razor blades are attached by screws to the inner edge of each of these clamps. When the razor blade mounting screws are tightened, the razor edges are forced against the glass to form a pressure fit. The edges were adjusted by trial and error to be parallel to within $\pm$ .02mm. and separated by .2mm., as was determined using a microscope equipped with a filar eyepiece.

With the optical flat mounted in this position, the entire apparatus was inverted and suspended from the roof of the evaporation chamber. Aluminum was then evaporated to form a coating along the narrow space between the razor edges. This coating was formed by suspending several small aluminum strips from a spiral heating coil to form a long source. This source was oriented parallel to the razor edges and an aluminum foil edge was placed part way between the source and the substrate so that a shadowing effect was obtained in evaporating the aluminum onto the glass. This technique produced a line of aluminum which varied in absorption from nearly zero at one end to almost completely opaque at the other. The purpose of this was to provide a variable absorption for the center region $|X_4| < D$, as the optimum value for B is different for different objects.

With this coating complete, the apparatus was removed

THIN FILM COATING APPARATUS

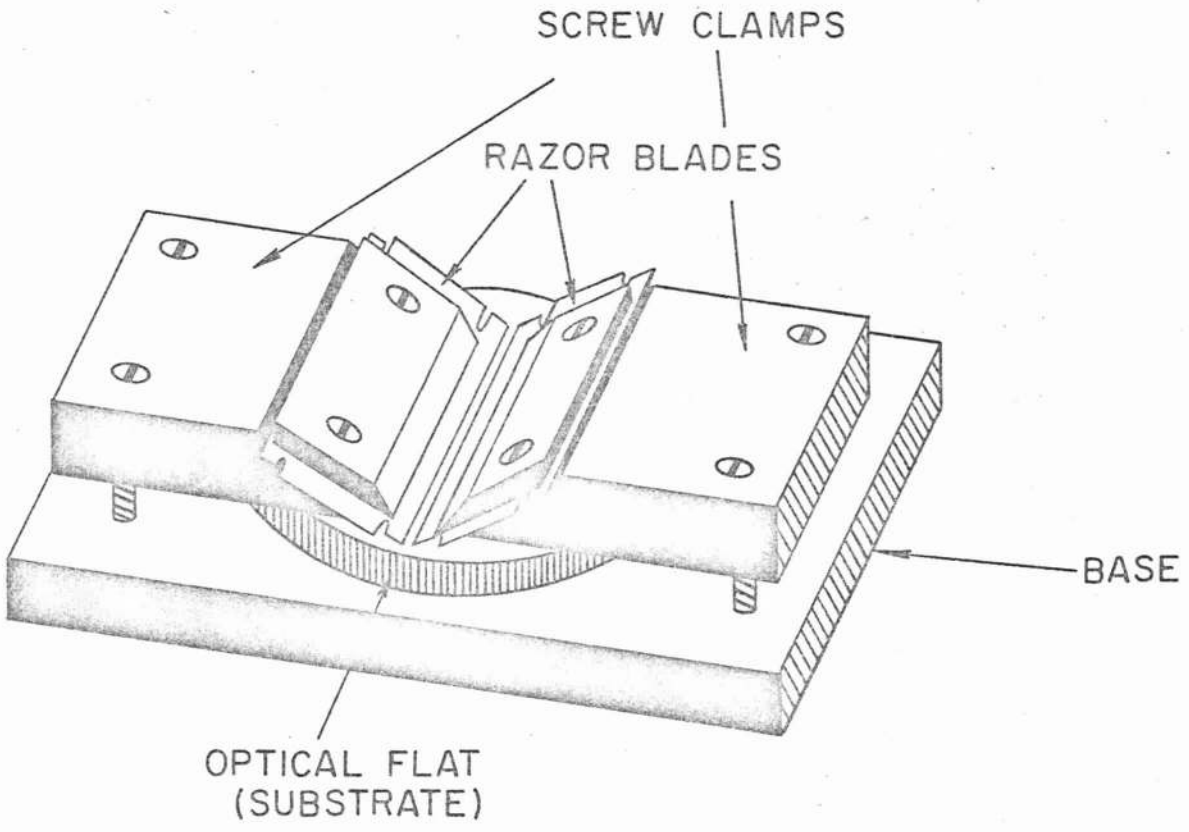

Figure 3.10

from the chamber and one of the clamps was removed to expose half the substrate. Care was taken to be sure the substrate was not moved during this process, so that the other razor still remained exactly aligned with the aluminum strip. The entire apparatus was then replaced in the chamber and a coating of thorium fluoride was evaporated on the exposed half of the substrate. Since the purpose of this coating is to provide a phase difference of 180° between the light transmitted by one side of the flat and that transmitted by the other side, the requirement on its thickness is

$$(n-1)\,t = \frac{\lambda}{2},$$

where n = Index of coating

t = Thickness of coating.

The optical thickness of this coating, which was monitored throughout the evaporation process, is thus given by

$$nt = \frac{n\lambda}{2(n-1)} \tag{3.7}$$

The following coating materials were tried and the results described.

Magnesium Fluoride-- $n = 1.38$, $nt = 1.82\lambda$

This is a desirable coating material because it is hard and non-grainy. Unfortunately, because of the low index of refraction the required coating was so thick that the film surface became crazed (rough) after evaporation. Although extreme care was made to provide slow cooling of the coating by allowing it to

cool overnight in a vacuum, satisfactory results were not obtained.

Zinc Sulfide-- $n = 2.34$ $nt = .87\lambda$

This coating material was seen to scatter a considerable amount of laser light when placed in the system, so it was determined to be unsatisfactory. This coating also deteriorated in time because of absorption of water vapor from the air.

Thorium Fluoride-- $n = 1.55$ $nt = 1.41\lambda$

This coating material was satisfactory. Because its index closely matches that of glass however, it was necessary to monitor the coating on a separate quartz substrate. The surface was smooth and hard, and the scattering was less than that of zinc sulfide.

Although the desired transmittance of the aluminum strip is $t = iB$, no efforts were made to evaporate a quarter wave phase shifting strip. The phase shift i was instead provided by the natural phase shift at the interfaces of the aluminum layer. Since aluminum is an absorbing material, its index of refraction is complex so that interface phase shifts occur. A cross section of the thin film layer in the center of the substrate is drawn in Figure 3.11 .

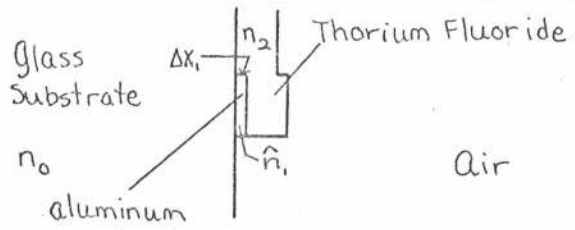

Figure 3.11- Thin Film Cross Section

To determine the transmission coeffiecient in the center region of the flat, multiple reflections in the aluminum layer may be neglected because of absorption. The effect of multiple reflections in the thorium fluoride layer is also negligible because the percent reflectance at the thorium fluoride--air interface is small. The transmission coefficient may thus be approximated by

$$t_a = -t_1 t_2 e^{i\frac{2\pi}{\lambda} n_1 \Delta X_1} \tag{3.8}$$

The t_1 and t_2 defined for these equations are the Fresnel Coefficients for transmission at the interfaces given by

$$t_1 = \frac{2n_0}{\hat{n}_1 + n_0} \qquad t_2 = \frac{2\hat{n}_1}{\hat{n}_1 + n_2} \tag{3.9}$$

The index of aluminum at 6328A is approximately

$\hat{n}_1 = 1.2 + i6.98.$

$$t_a = -t_1 t_2 e^{i\frac{2\pi}{\lambda}\Delta X_1 (1.2)} e^{-\frac{2\pi}{\lambda}\Delta X_1 (6.98)} \tag{3.10}$$

The overall amplitude transmittance of the aluminum strip does not drop below 5%, so it is safe to require that

$$\frac{2\pi}{\lambda}\Delta X_1 \cdot 6.98 < 3 \;, \quad \Delta X_1 < .07\lambda \;. \tag{3.11}$$

Since this is a small fraction of a wavelength, it is furthermore reasonable to assume that the contribution of the exponential term to the phase shift is negligible, the entire phase

shift arising from constant interface values. If the definitions of the Fresnel Coefficients are substituted in t_a and the exponential is neglected, the final transmittance coefficient is given by

$$t_a = -\left\{\left[n_r\left((n_r+n_0)(n_r+n_2)-n_i^2\right)+n_i\left((n_r+n_0)n_i+(n_r+n_2)n_i\right)\right] + i n_i\left[-n_r(n_r+n_0)-n_r(n_r+n_2)+(n_r+n_0)(n_r+n_2)-n_i^2\right]\right\} \Big/ \left[\left((n_r+n_0)(n_r+n_2)-n_i^2\right)^2+\left((n_r+n_0)n_i+(n_r+n_2)n_i\right)^2\right]. \quad (3.12)$$

Since

$$n_0 = 1.5,\ n_2 = 1.5,\ n_r = 1.2,\ n_i = 6.98,$$
$$t_a = -C[213 + i\,334]. \qquad C = \text{constant} \quad (3.13)$$

The complex transmittance in the center region of the film is thus given by

$$t_a = t_r + i\,t_i, \quad (3.14)$$

where $t_r = 213C$ and $t_i = 334C$. This is to be compared with the desired transmittance $t_a = iB$. The object for the integration system is $f_3(x_3) = x_0/f + \phi'(-x_3)$. The action of an ideal integration filter on this object will give the image

$$f_5(x_5) = \phi(x_5) + \frac{x_0 B}{f}.$$

Since the actual transmittance in the center region has a real portion, the effect of the real part on the image may be determined by substituting $B = t_i - i t_r$ to give

$$f_5(x_5) = \phi(x_5) + \frac{x_0 t_i}{f} - i\frac{x_0 t_r}{f} \tag{3.16}$$

The intensity in this image is

$$I(x_5) = \left(\phi(x_5) + \frac{x_0 t_i}{f}\right)^2 + \left(\frac{x_0 t_r}{f}\right)^2. \tag{3.17}$$

This real portion of the transmittance is seen to merely add a constant level to the intensity. This addition causes some reduction in contrast, without affecting the appearance of the image.

Development with $\gamma = 1$

649F Photographic Emulsion was used to record the phase function derivative. This fine grain film was used because it is much less noisy in a coherent system than other films. Unfortunately, this emulsion is normally developed with high contrast, i.e. for gammas between 5 and 10.

Satisfactory results were obtained at $\gamma = 1$ however, with D165.[37] This is a special Kodak developer whose formula is given by

Kodak Elon Developing Agent	6 grams
Sodium Sulfite, dessicated	25 grams
Sodium Carbonate, monohydrated	41.3 grams
Potassium Bromide	1 gram
Water to make	1000 cc.

This developer is designed specifically to give low gamma with high resolution plates. A sample D vs. Log E curve obtained with this developer is reproduced in Figure 3.12. This curve contains a relatively straight linear portion over a density range of at least 2.2. To achieve this specific gamma, development was checked by making a separate step wedge exposure on each plate. The required development time was about two minutes, but varied with different boxes of plates and different developer batches.

Noise Removal

Coherent optical systems tend to produce images which are very noisy. Dust particles, scratches on the lenses, and grease films all scatter light, and since all this light appears in the image as diffraction patterns, the image appearance may be poor. This problem is especially bad in this system because the image produced by the differentiation system is used as the object for a second system. Because of this, all diffraction patterns and image noise in the first system will be integrated in the final result. This integration not only produces considerable image noise due to the large width of the integration point spread function, but it also produces patterns in the second system which are unrecognizable as noise. The eye can no longer evaluate this light specifically as arising from scattering. Noise in the integration system is also a bad problem because a bias level block is used. Since most of the

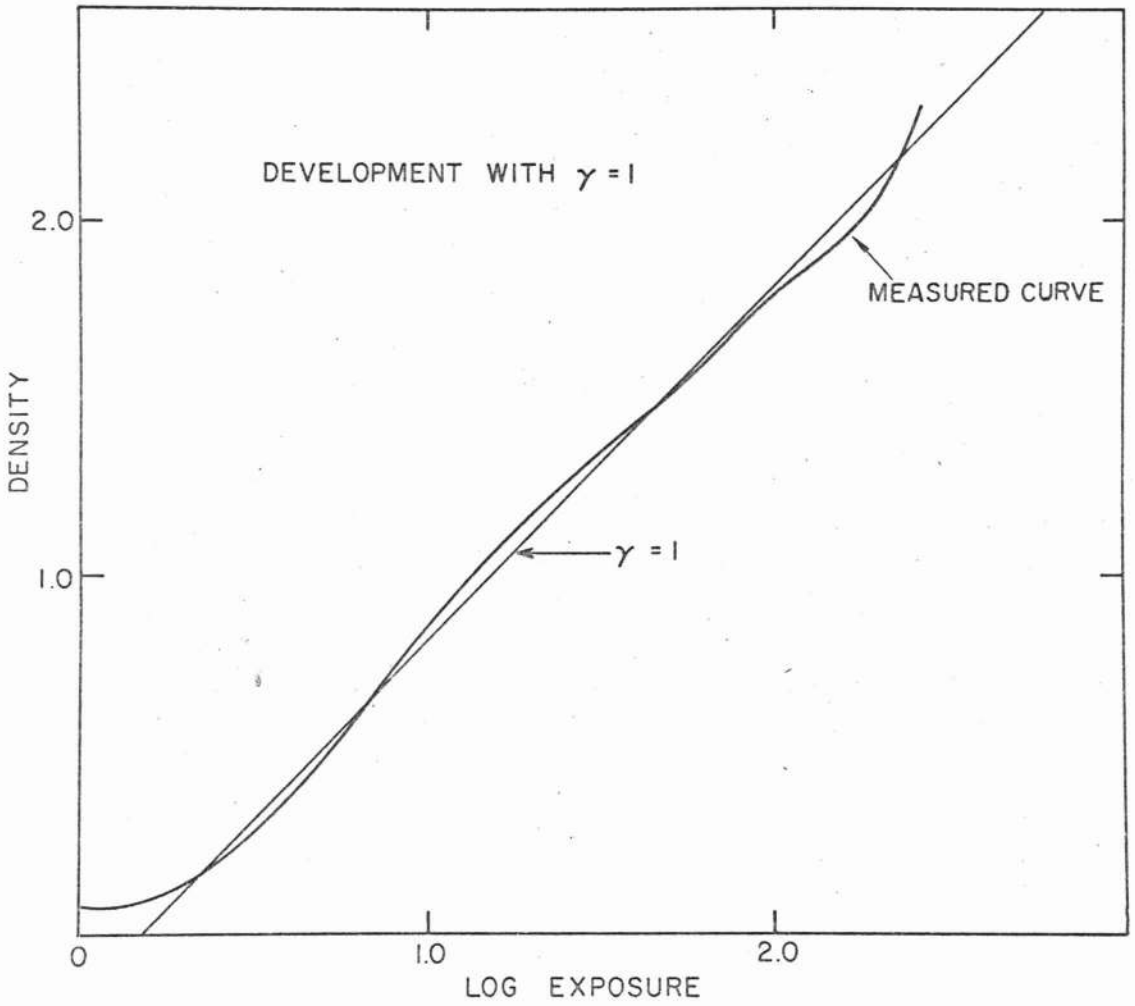
DEVELOPMENT WITH γ = 1
MEASURED CURVE
γ = 1
DENSITY
2.0
1.0
0
1.0
2.0
LOG EXPOSURE

Figure 3.12

background light is removed from the system by this aluminum strip, the noise becomes very high contrast and especially important. Special care was taken in this system to remove the noise by cleaning the lens surfaces as well as possible. Laser mirror cleaning techniques worked particularly well.

Two noise removal techniques are used to remove the remaining image noise. Noise in the differentiation system is removed by placing a moving scatterer near the focus of the collimator. This scatterer adds a slight amount of partial coherence to the system so that noise in the image is placed in motion. When observing this moving noise with a time averaging detector, it will disappear if the averaging time is sufficiently long. The setup is shown in Figure 3.13.

One effect of this partial coherence is to somewhat blur the Fourier Transform. The new light distribution in the transform plane is a convolution of the actual Fourier Transform with the image of the source in that plane. Because the differentiation spatial filter is slowly varying as a function of X however, this blurring of the transform will not significantly degrade the system performance. A very useful scatterer is a piece of antiglare glass. This scatterer provides enough partial coherence to remove the noise without scattering a significant amount of light out of the system, as would a ground glass screen.

Unfortunately, the rotating scatter can not be used in the integration system because the transmittance function of the integration filter varies very rapidly with X . Because of this, any blurring of the Fourier Transform is disastrous. Instead, a technique suggested by Thomas[38] is used. This technique involves placing an optical flat in the diverging beam between the pinhole and the collimating lens. This flat is originally oriented in a plane parallel to that of the lenses. When it is tilted about a transverse axis, the illuminating beam remains a plane wave, but is shifted in angular orientation in a vertical plane. If this tilting is continuous throughout the observation time, the light in the system moves around moving the noise with it, but the image remains stationary. On a time average, this noise disappears. The use of this technique is possible because the spatial filter is one dimensional; when the Fourier Transform is displaced vertically, it sees the same filter function from any position on a vertical axis. The setup is shown in Figure 3.14 on page 81.

One other technique for noise removal in the integration system involves the position and orientation of the blocking aluminum strip. Since this strip removes most of the light from the system, significantly better results are obtained when this light is removed in the first filter plane. With this position of the aluminum block, the major portion of the incident beam strikes a minimum number of dust particles. Although an

absorbing strip is desired ideally, the aluminum strip actually used reflects most of the light it blocks. Because of this, an unexpected source of noise was discovered to result from back scattering off the lens in front of the aluminum strip. The blocked light is reflected right back into the lens where it reflects off surfaces or scatters off dust back into the system where it finally appears as noise. To alleviate this problem, the optical flat containing the aluminum strip was tilted 5^{o} about a vertical axis. The light reflected into the first lens could then be removed with an absorbing card without obstructing the imaging properties of the system. This tilt will introduce third order off axis aberrations into the system only if the small angle approximations do not hold. Since the tilt was small, this condition is valid. The tilt also slightly changes the actual phase shift for negative frequencies to

$$\phi_{actual} = \frac{\lambda}{2\cos\theta'} = 1.01\left(\frac{\lambda}{2}\right),$$

a shift which is insignificant.

Another possible technique to remove the back scattered light is to place the object in the lower half of the object field. If the top half of the first lens is covered with an absorbing screen, the reflection off the aluminum strip will fall in this region and be absorbed. Although this technique is satisfactory, it was felt that the aberrations introduced by moving the object farther off axis were greater than those introduced by tilting the optical flat.

Index Matching Oil Bath

To remove the phase portion of the photographically recorded spatial filters, the plates are immersed in an index matching oil bath. This involves placing them between two optical flats and filling the space between the surfaces with an oil whose index matches that of the emulsion. The choice of the proper index of the oil must be a compromise. This is because the developed emulsion does not have a perfectly constant index and because the glass plate, whose index is different from that of the emulsion, contains thickness variations. A good compromise in index is given by the oil dibutylphthalate, n = 1.490. Xylene and toluene may also be used, but these oils may be harmful to the emulsion, causing it to strip from the backing. Dibutylphthalate was found to not harm the emulsion even when the plate was immersed for several months.

The actual bath used consists of two optical flats held to opposite sides of the photographic plate by capillary action. This arrangement is not as convenient as an off-the-shelf bath in which the plate is simply immersed in a box of oil. However, it is felt that this setup is thinner (to provide less spherical aberration) and less susceptible to phase gradients caused by motion of the fluid in the cell.

The procedure for assembling the oil bath is simple. First, the optical flats and the photographically recorded filter are carefully cleaned. One of the flats is then placed in

half the oil bath mount on a horizontal plane. Three drops of dibutylphthalate are placed on the flat and the photographic plate is slowly lowered into it. One edge of the glass should contact first, the rest of the plate then being lowered until it contacts the oil. The oil is then allowed to spread by itself to fill the space between the surfaces. The other flat is placed in position in an identical manner and the other half of the oil bath mount is screwed in place. Alignment is maintained by the tight contact formed between the plate and the flats by capillary action. To disassemble the oil bath, this capillary bond is reduced by placing several drops of fluid around the edge of the contacting region. One flat is then removed by sliding it off the side and the dibutylphthalate is removed by soaking the parts in benzene.

System Alignment

A diagram of the differentiation system is reproduced in Figure 3.13. This setup, which makes use of Bell and Howell Aerial Reconnaissance lenses, was mounted on a Technical Operations five meter bench. The system is aligned by first centering the beam along the bench axis and then using this beam to center each element of the system. Each element is then focussed in succession by looking through it with a telescope at the light distribution in its front focal plane. The telescope is focussed at night on a distant red light source. With the system completely aligned, the rotating scatterer is finally placed at the focus of the collimating lens and moved toward the object until the image noise disappears.

OPTICAL DIFFERENTIATION

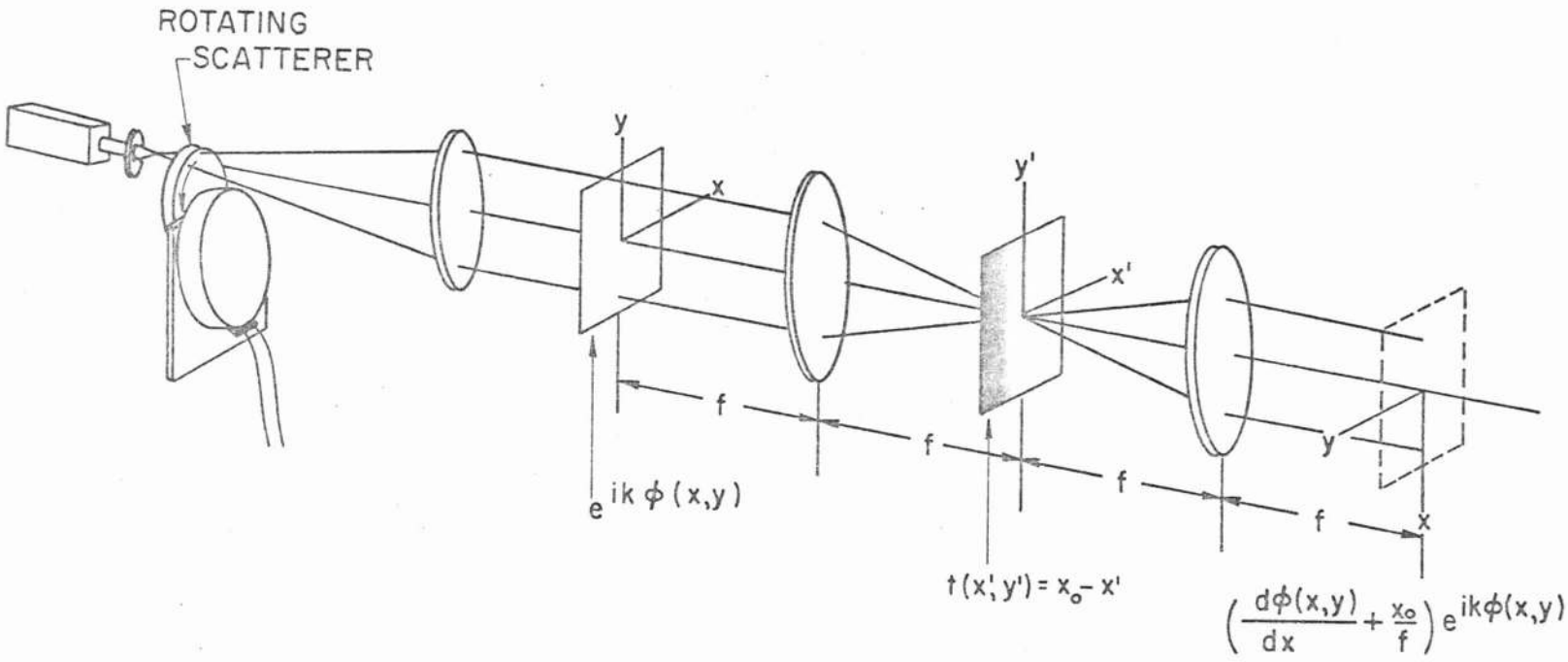

Figure 3.13

There is a compromise which must be made in using the Aerial Reconnaissance lenses for this purpose. These lenses are corrected for infinite conjugate operation. Because of this, when the short conjugate side is placed toward the object, good imaging results, but the Fourier Transform is convolved with a somewhat broadened point spread function. This lack of resolution in the Fourier Transform plane appears as a limiting of image field. This is the space-bandwidth product well known in lens design. For good resolution in the transform plane the lenses are oriented in the other direction, but the result is a limited Fourier Transform field causing limited resolution in the image. The choice of orientation is thus different for the differentiation and integration systems. For optical differentiation, the spatial filter varies slowly with X so that resolution in the transform plane is less important. The short conjugates are thus placed toward the object and image planes, providing maximum resolution. The integration filter, however, consists of a very rapidly varying transmittance function. To achieve proper filtering, good resolution is needed in the Fourier Transform plane, so the lens orientations are reversed from those used for differentiation.

A diagram of the integration system is reproduced in Figure 3.14. Most of the light in this system is blocked out in the first Fourier Transform plane, so by far the largest noise contribution comes from the first lens. For this reason

OPTICAL INTEGRATION

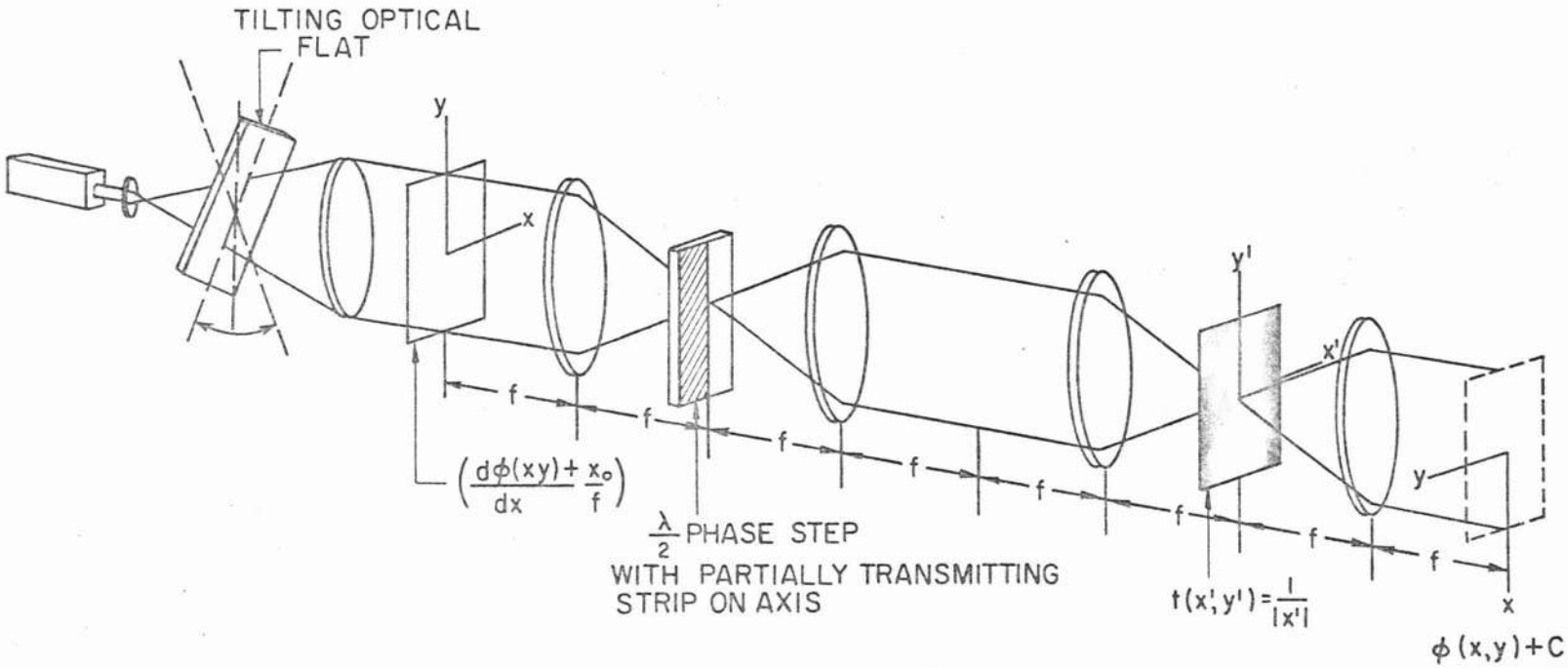

Figure 3.14

each of the four lenses is inspected visually for cleanliness, and the best one chosen as the first element of this system. With that choice determined, the rest of the system is aligned and focussed. The exact focal position of the partially transmitting aluminum strip is very important because this strip is quite narrow. It is first placed approximately in the transform plane and centered. The diffraction pattern produced by this strip consists of two separated bands of light. As the strip is moved into focus, these bands become further separated and eventually reach the edge of the field and disappear. The strip is moved along the bench axis until these bands are separated by a given measured amount and its position on the bench is recorded. The strip is then moved through focus until the same band separation is achieved. This position is also recorded and the aluminum strip positioned midway between these two measurements.

A black card is then taped over the first lens, just far enought in to pick up the reflected beam. The rest of the system is then focussed using the telescope. Finally, by observing the 1/1X1 filter, the image of the aluminum strip, and the object Fourier Transform through the last lens with the telescope, the three are aligned in rotation and lateral displacement.

By translating the aluminum strip in the vertical

direction, its variation in transmission along this axis is used to select a certain value for B . The proper choice is determined by examining the image appearance. With the filter raised, the strip is highly transmitting so the image contrast is low. As it is translated in the negative y direction, image contrast becomes better and better until a certain point is reached at which the image becomes unrecognizable. At this point the biassing is insufficient so that negative image amplitude terms are present. The filter is then moved up slightly until the image appearance becomes good. This is the choice of B which gives maximum contrast.

Chapter IV

Data Evaluation

The entire system which has been described was evaluated by using it to read out several input phase objects. The resulting images were compared with the actual object phase variations and the results are described below.

Phase Resolution Targets

The phase resolution targets were produced with R-10 bleach: a surface relief bleach which produces negligible internal index of refraction variations in the emulsion.[35] Because of this pure relief structure, the surface contour of the targets is related to the phase on transmission by $\Phi_{transmission} = (n-1)\ \Phi_{relief}$, where Φ_{relief} is the physical contour height of the surface. This is convenient because the surface height can be measured in reflection using an interference attachment to a microscope.

The standard interference attachment which was used is schematically illustrated in Figure 4.1. It consists of a small Twyman-Green Interferometer which mounts in place of the microscope objective. This apparatus contains a beam splitter and one reference mirror, the object being the test surface. When this surface is viewed through the eyepiece, interference fringes will be seen superimposed on the object, their tilt and spacing being adjusted by the orientation of the reference mirror. For a simple one-dimensional object such as a bar,

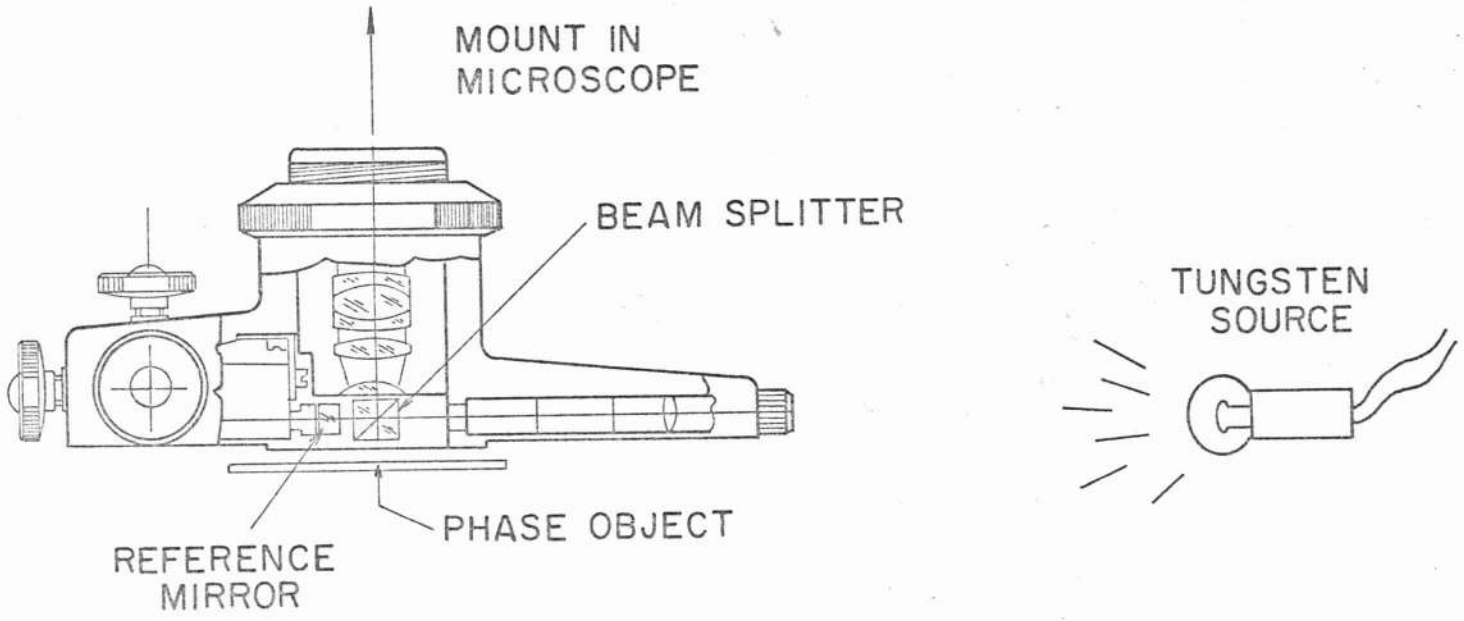

Figure 4.1

Interference Attachment for Microscope

the shape of fringes oriented perpendicular to the bar describes the actual contour of that bar. The interferometer was used with a white light tungsten lamp source to prevent fringe-counting ambiguity, and the pictures obtained are reproduced in Figure 4.2 and Figure 4.3. These pictures represent contours of one bar in each resolution group for two different phase targets.

To evaluate the interferometer measurement, the picture (Figure 4.2d) is first enlarged (in a drafting enlarger) and a trace is taken across one fringe. This trace, which is shown in Figure 4.4 represents a cross-sectional view of the surface of the phase target. Marks are also made in Figure 4.4 in a vertical direction, one for each successive fringe. The separation of these marks represents the characteristic distance on the picture representative of a one wave length phase shift in the test beam. A set of parallel lines (see Figure 4.4) are drawn across the contour in the direction of the fringe orientation with a spacing equal to that of the wavelength marks. If all points where one line crosses the fringe trace are recorded, they represent positions on the contour having a given phase height. A graph of the contour height in wavelengths may thus be determined. This graph is shown as the the solid line in Figure 4.10. (Note that this procedure is merely a simple way of callibrating the actual physical height of the test surface whose shape is described by the fringe

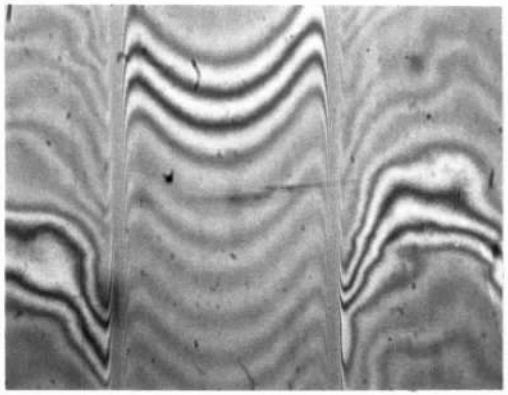

a) Bar Group 0 - 2

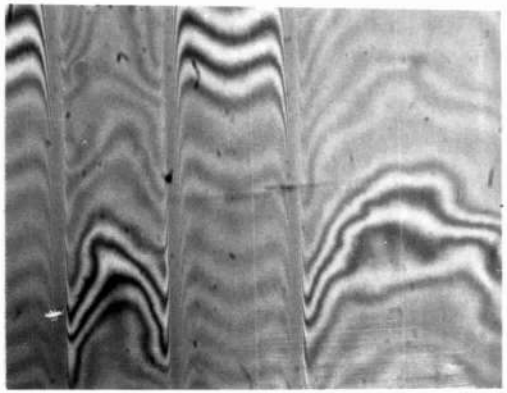

b) Bar Group 1 - 1

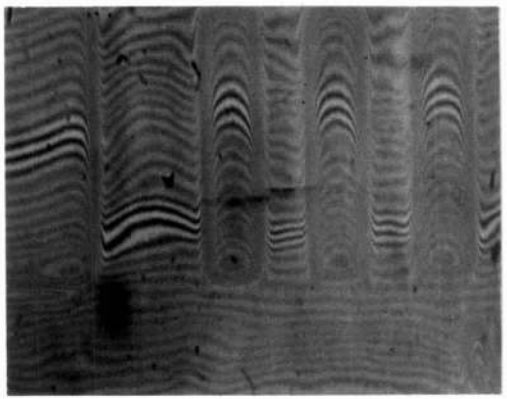

c) Bar Group 2 - 2

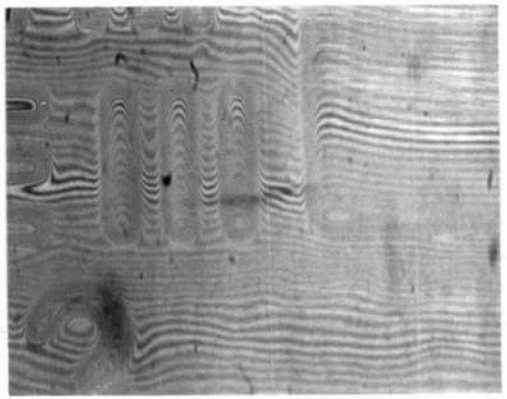

d) Bar Group 3 - 1

Figure 4.2

Interferometer Fringe Patterns

Phase Resolution Target #1

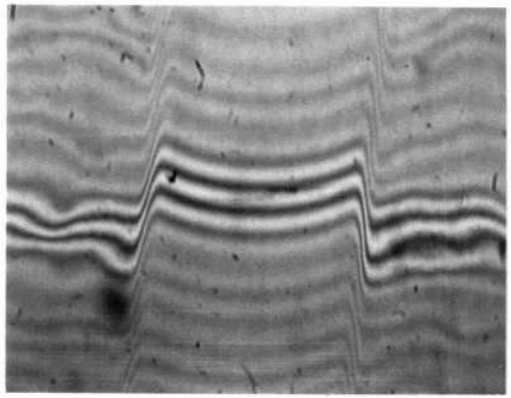

a) Bar Group 0-2

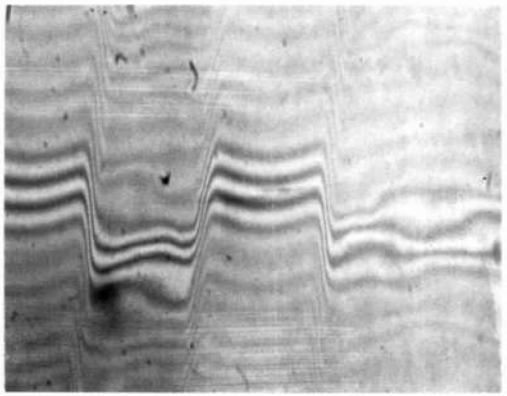

b) Bar Group 1-1

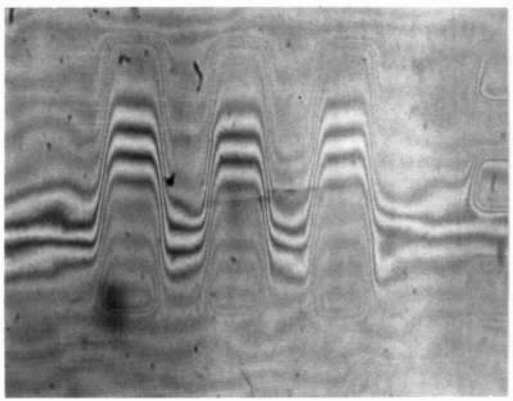

c) Bar Group 2-2

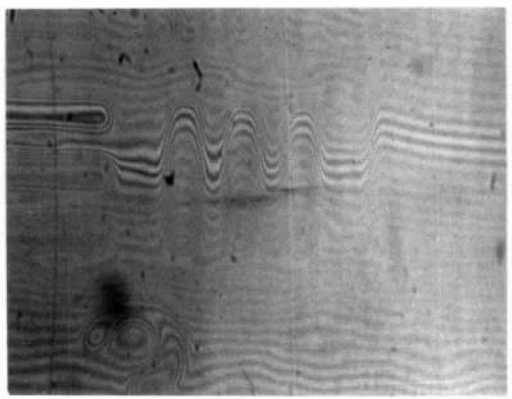

d) Bar Group 3-1

Figure 4.3

Interferometer Fringe Patterns

Phase Resolution Target #2

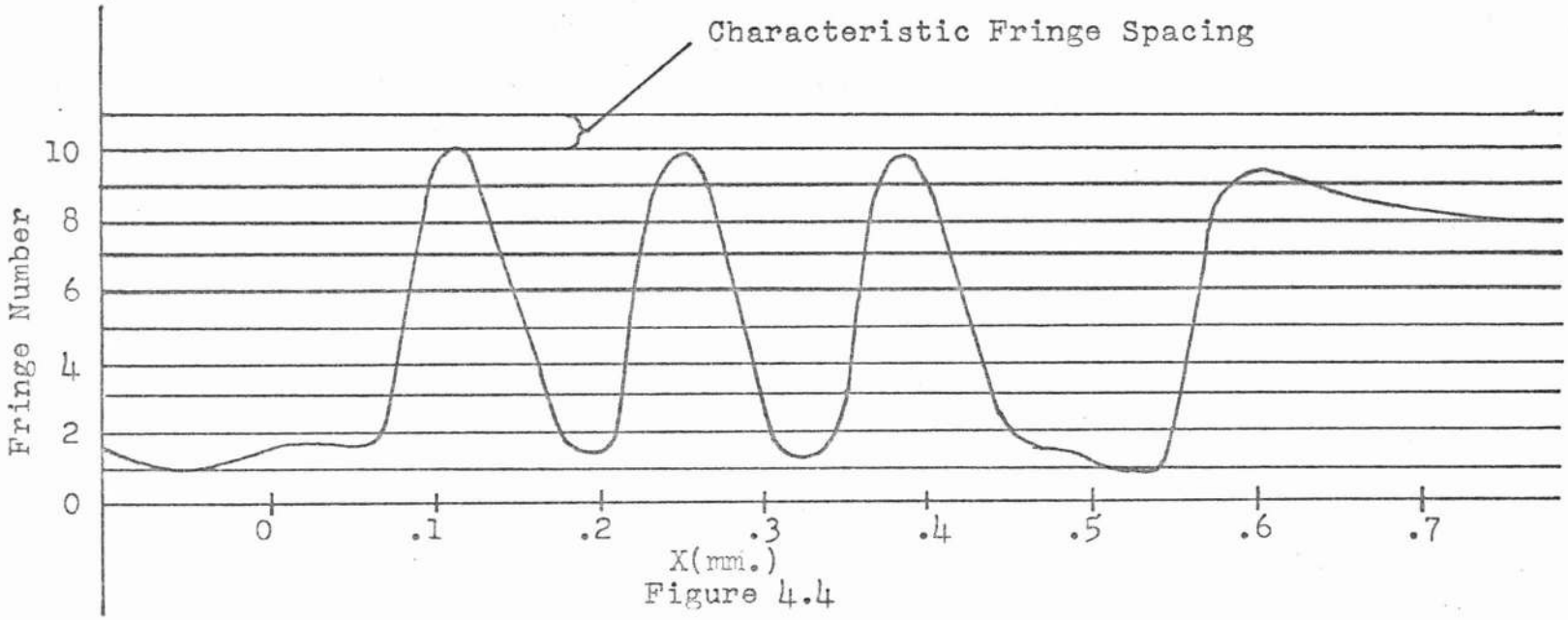

Figure 4.4

Interferometer Fringe Trace

Phase Resolution Target #1

Bar Group 3-1

trace.) The phase in transmission is determined from

$$\Phi_{transmission} = \left(\frac{n-1}{2}\right)(\#\text{of fringes}) = .3(\#\text{of fringes}). \qquad (4.1)$$

With the phase determined in this manner, the entire phase imaging system was evaluated by comparing this phase with the image amplitude in the integration system. The image amplitude was determined by recording a photograph of the image along with a step wedge exposure on the same emulsion. When the density wedge produced by this stepped exposure was scanned with a microdensitometer, a callibration D vs. log E curve for the film could be determined. This callibration curve was used to relate density traces of the image photograph to the actual image amplitude.

Photographic recordings taken in the image planes of the differentiation and integration systems are reproduced in Figure 4.5 and Figure 4.6. These recordings were made on 649F photographic emulsion and developed for four minutes in D-165. (Figure 4.6 is actually a positive enlargement of the negative formed on 649F) A densitometer trace taken from the set of bars 3-1 in Figure 4.6 is exhibited in Figure 4.7. The three separate traces in this figure were taken with different locations of the scanning slit along the bars. This figure is a plot of photographic density vs. distance across the plate. A step wedge was also exposed on the same plate by a light box equipped with a red filter. Figure 4.8 is a trace of the

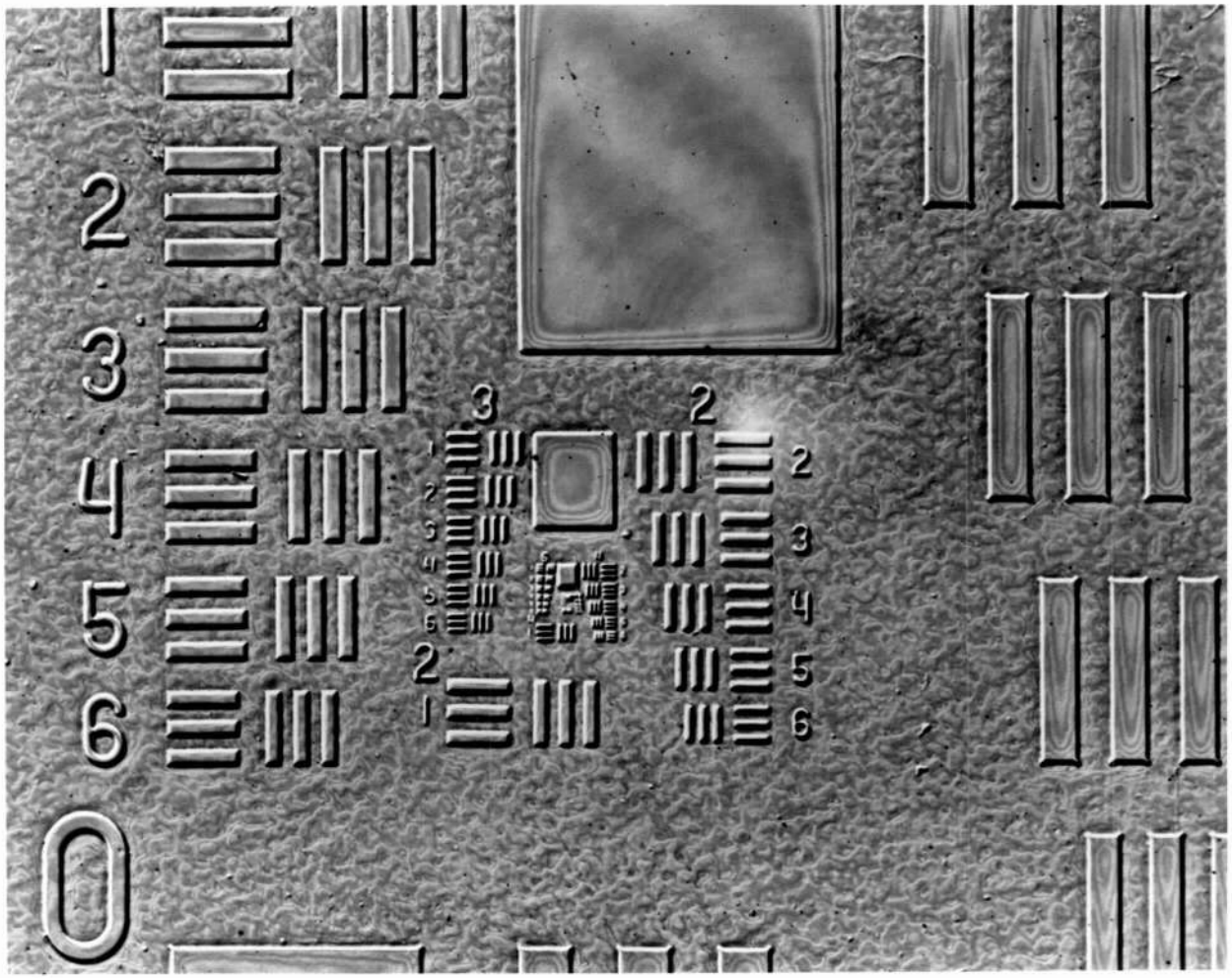

Figure 4.5

Phase Object Derivative

Phase Resolution Target #1

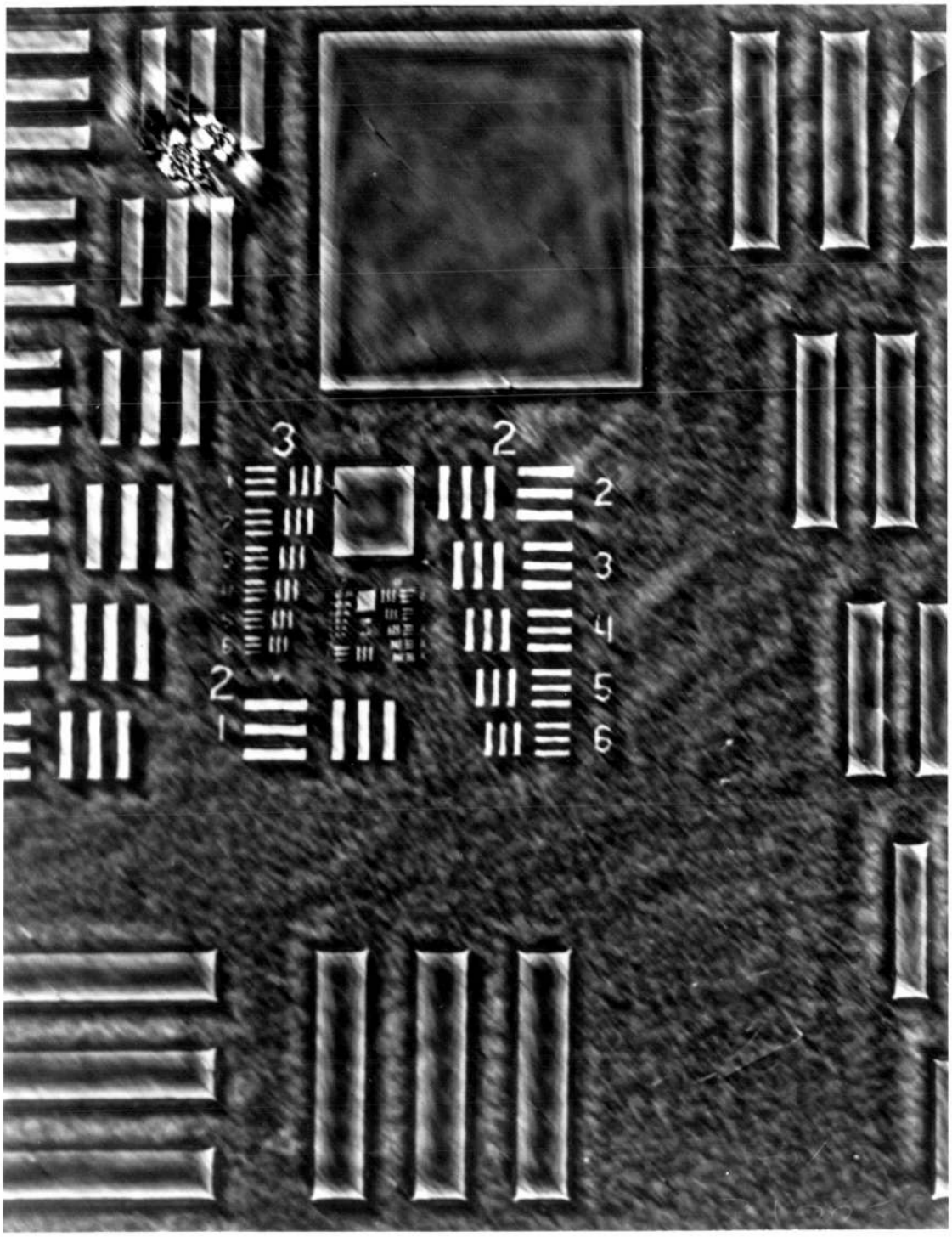

Figure 4.6

Integral of Phase Object Derivative

Phase Resolution Target #1

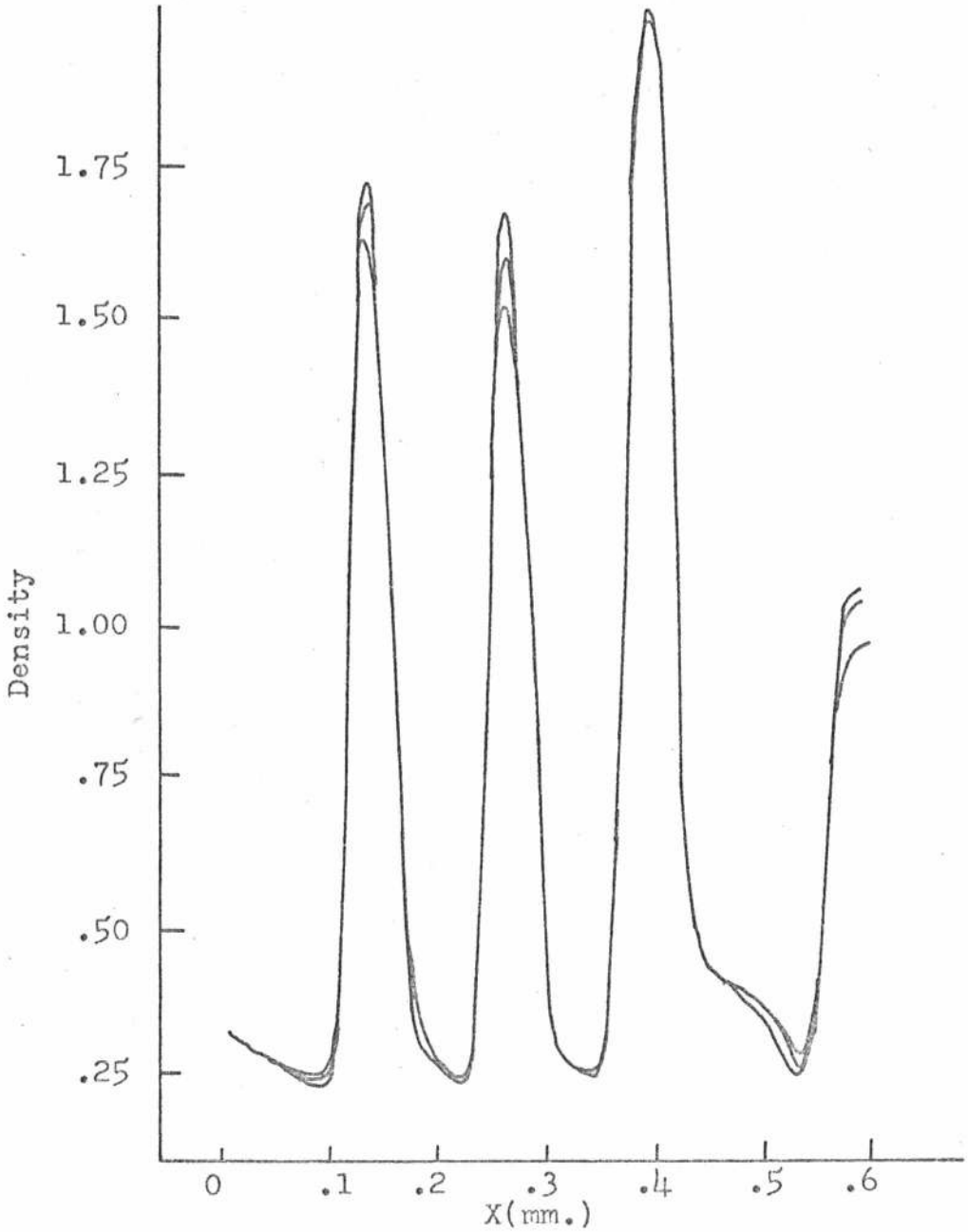

Figure 4.7

Densitometer Trace

Integral of Phase Object Derivative

Phase Resolution Target #1

Bar Group 3-1

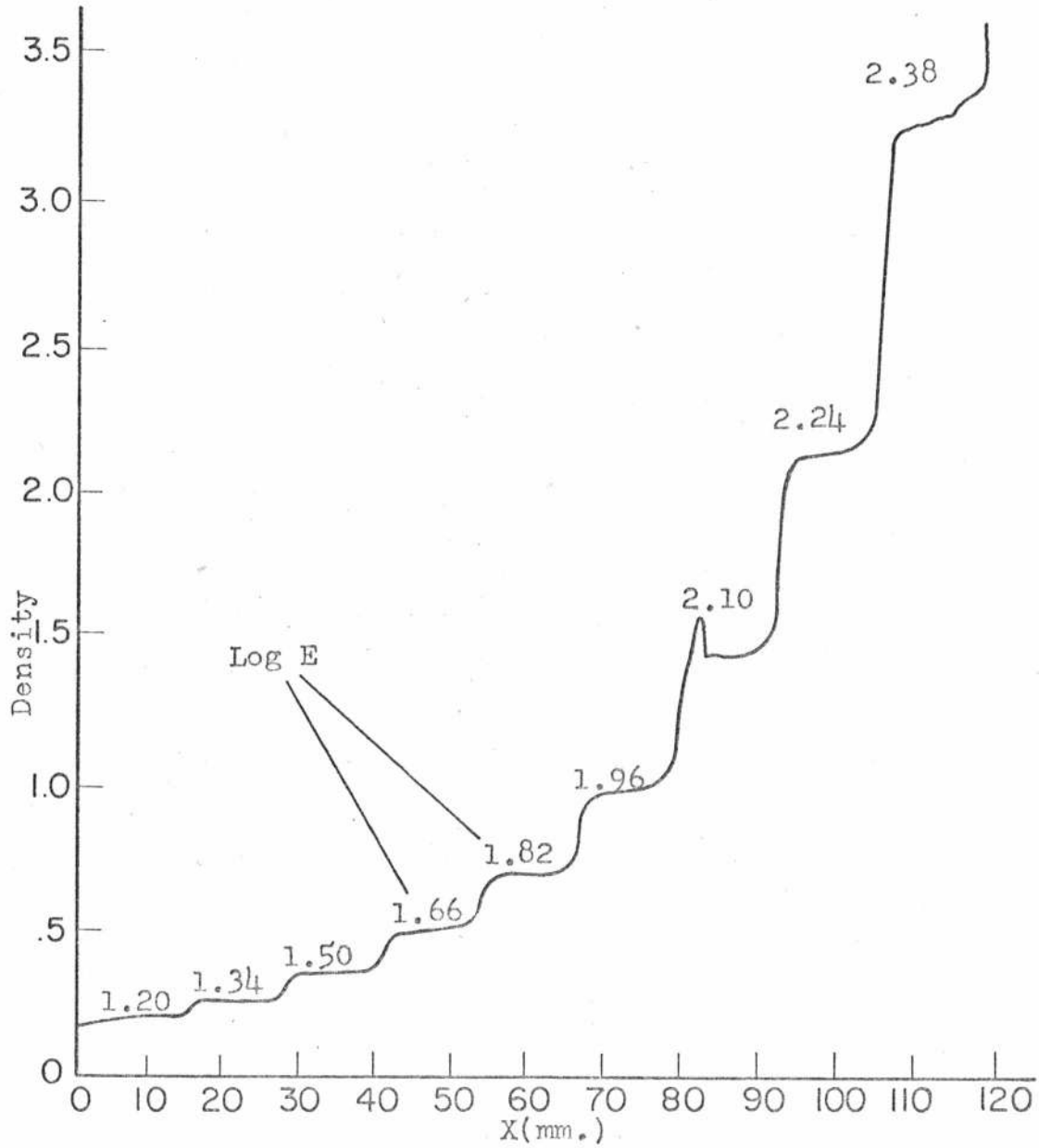

Figure 4.8

Densitometer Trace--Step Wedge Exposure

Integral of Phase Object Derivative

Phase Resolution Target #1

the resulting stepped density function. Since the density of the exposing step wedge is known, the exposing intensity function may be found and a graph of density vs. logE for Figure 4.6 and Figure 4.8 may be determined. (The log of the exposing intensity is listed above each density step in Figure 4.8.) This graph is exhibited in Figure 4.9. It provides a callibration so that the original exposing intensity which produced the density of Figure 4.6 can be calculated. The absolute exposure is arbitrary, but the relative exposure scale is determined from the step wedge. For this reason the scale has been arbitrarily set at logE = 0 for the first data point.

Density values may now be read off the trace of Figure 4.7 and the image intensity determined from Figure 4.9. The image amplitude is the square root of this intensity. The arbitrary normalization constant is chosen to make the amplitude bar height equal the phase height previously determined for one set of bars. Since this normalization constant represents the absolute light level in the image, once it is determined for one set of bars, the same constant must be used for all others in the same photograph. Since the low spatial frequency response of the integration system is expected to be poor, the normalization constant was chosen for the smallest set of bars.

The dashed line in Figure 4.10 is the final trace of the image amplitude. It is to be compared with the previously

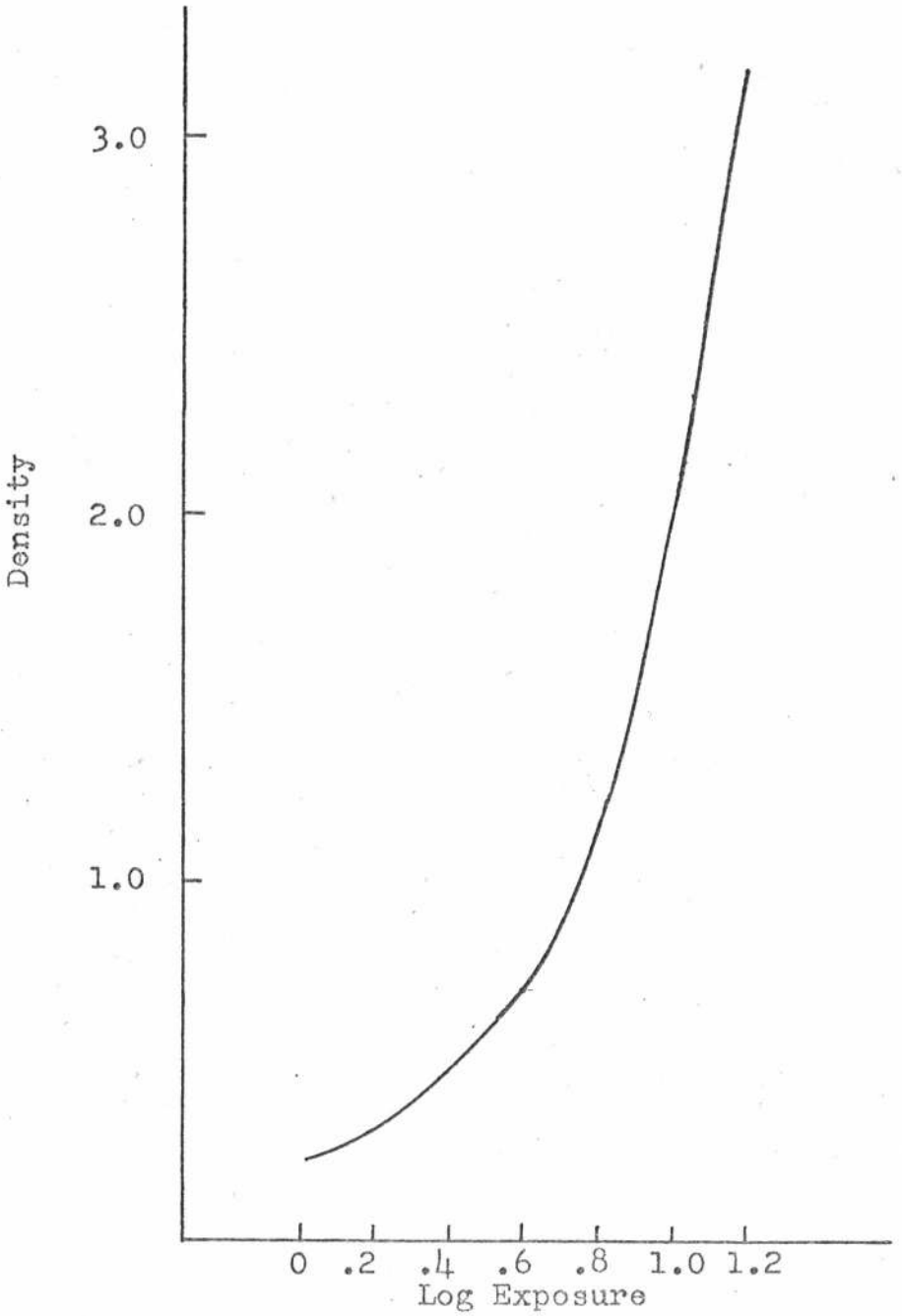

Figure 4.9

Callibration Curve

Integral of Phase Object Derivative

Phase Resolution Target #1

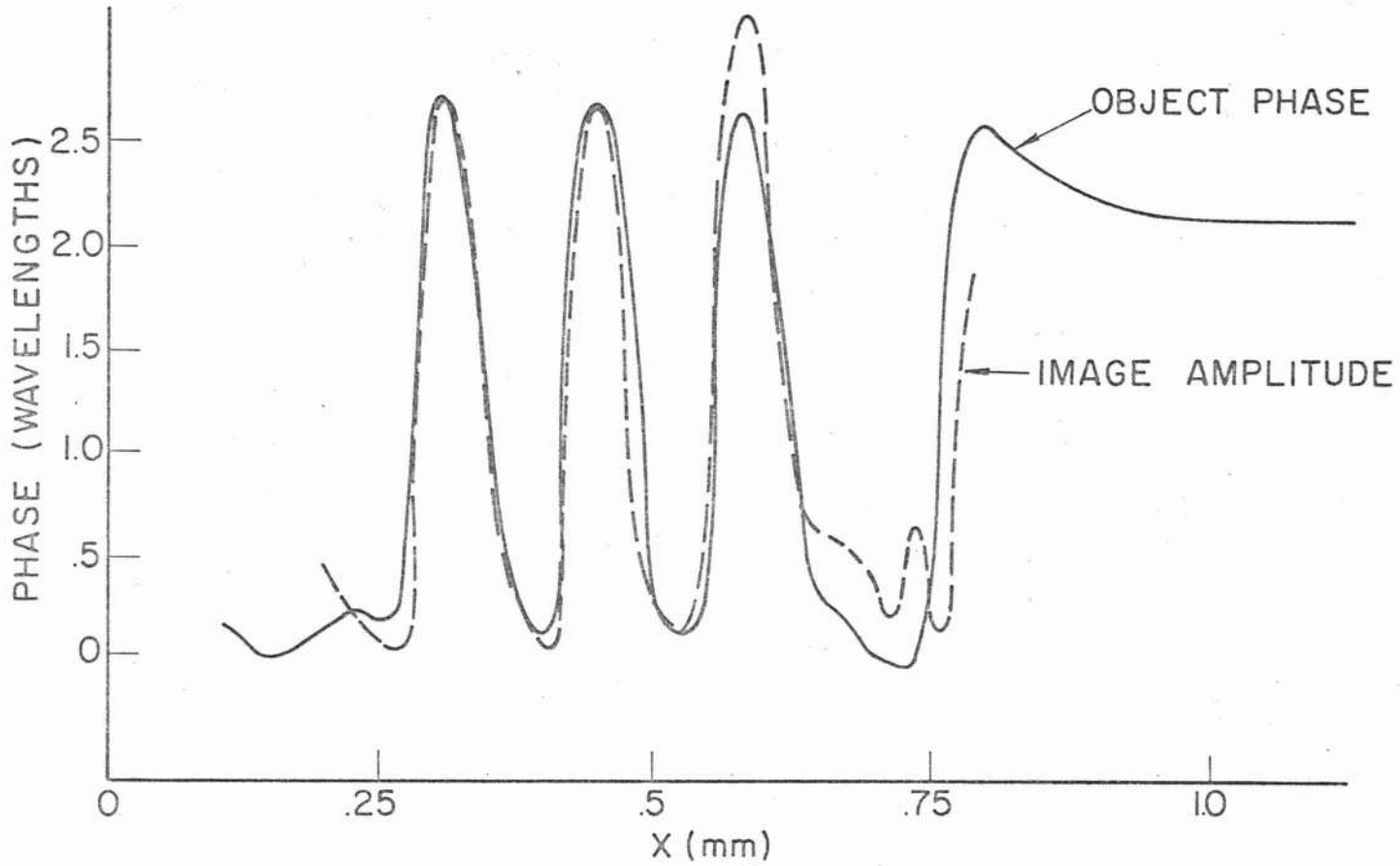

Figure 4.10

Comparison of Image Amplitude With Object Phase

Phase Resolution Target #1--Bar Group 3-1

determined phase contour of the surface. Since there is no such thing as absolute phase, the relative phase trace already determined has been translated along the vertical axis until the two curves match as closely as possible.

This same entire procedure is used to evaluate the rest of the bars on this target and all the bars on another target of smaller maximum step height. The results are presented in Figures 4.11 through 4.27. The results are similar for both bar targets and show the expected characteristics; for high spatial frequency phase bars, the comparison of the image amplitude and the object phase is quite good. For the wider bars, a distinct edge sharpening is apparent due to the truncation of the integration filter.

Circular Phase Depressions

The transmission phase of the circular phase depressions could not be measured in reflection because little is known about the internal index changes of the Duco Cement due to compression by the depression-forming sphere. Instead, a transmission interferometer was used to measure the phase. The idea for this technique is due to Sommargren.[38] It involves translating the phase object in front of the image of two coherently illuminated pinholes. The diffraction pattern formed by these two pinholes contains a cosine function whose lateral position is determined by the phase difference between the pinholes. If this position is measured as the phase object

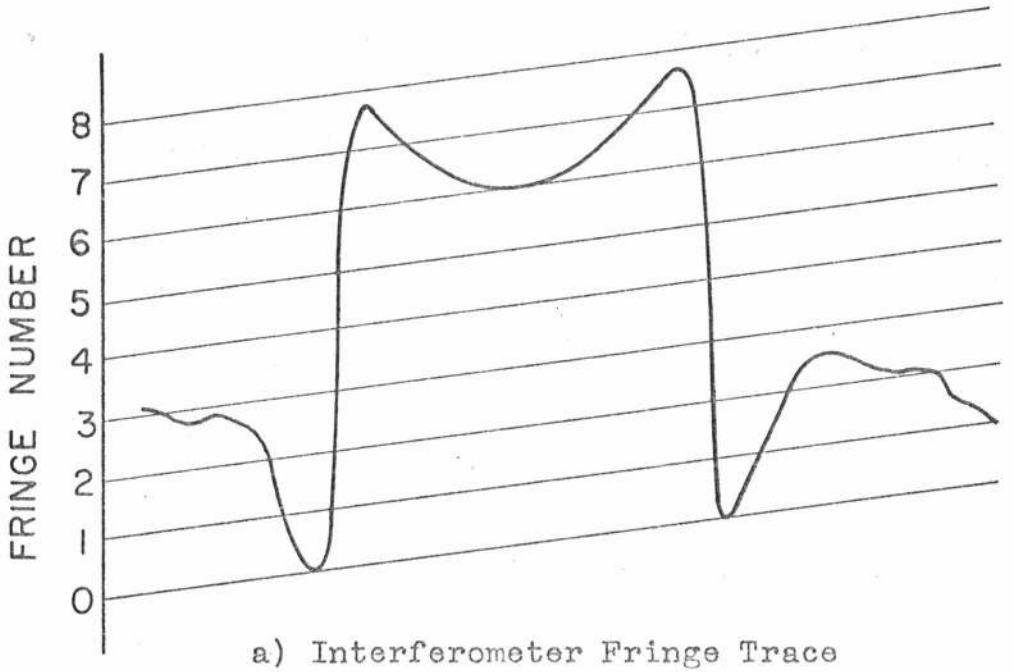

a) Interferometer Fringe Trace

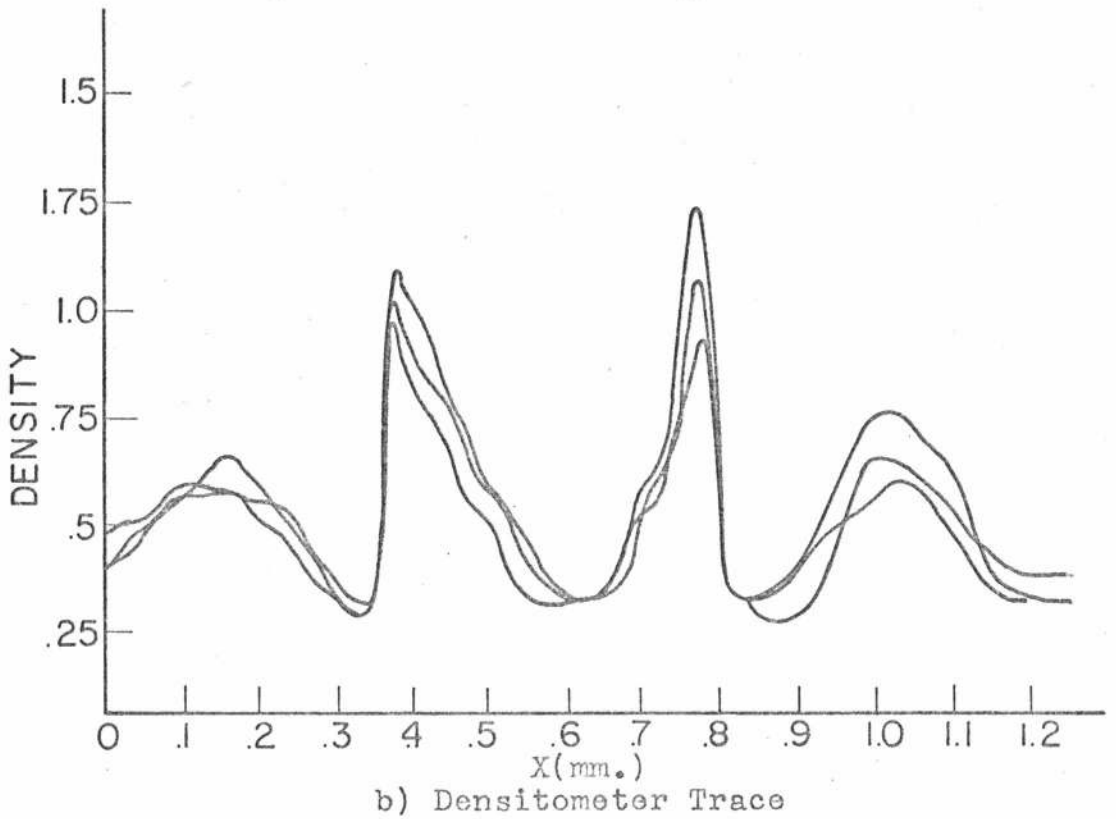

b) Densitometer Trace

Figure 4.11

Phase Resolution Target #1--Bar Group 0-2

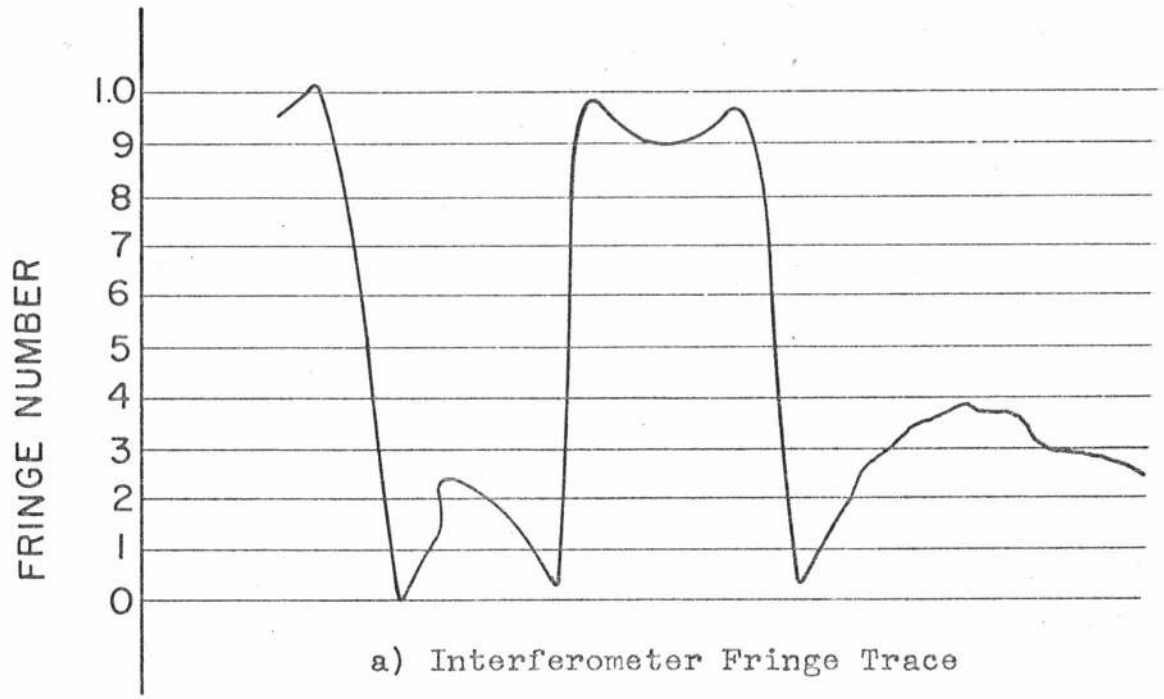

a) Interferometer Fringe Trace

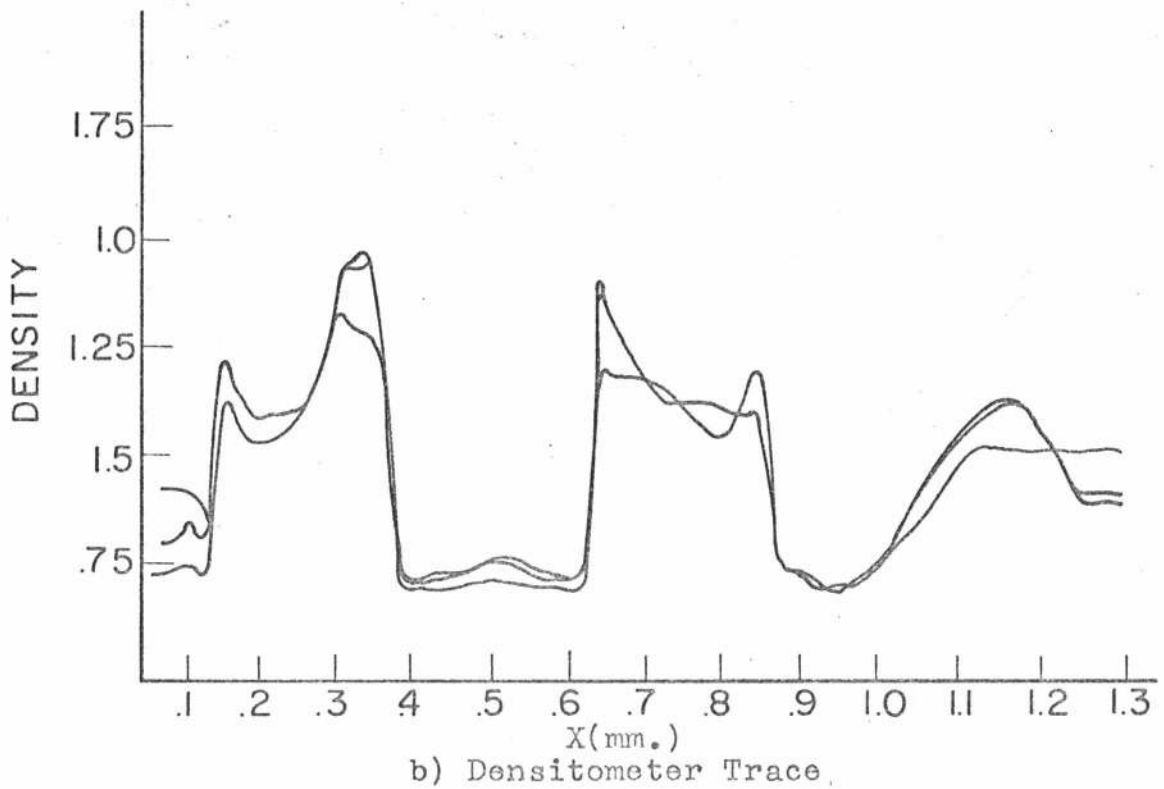

b) Densitometer Trace

Figure 4.12

Phase Resolution Target #1--Bar Group 1-1

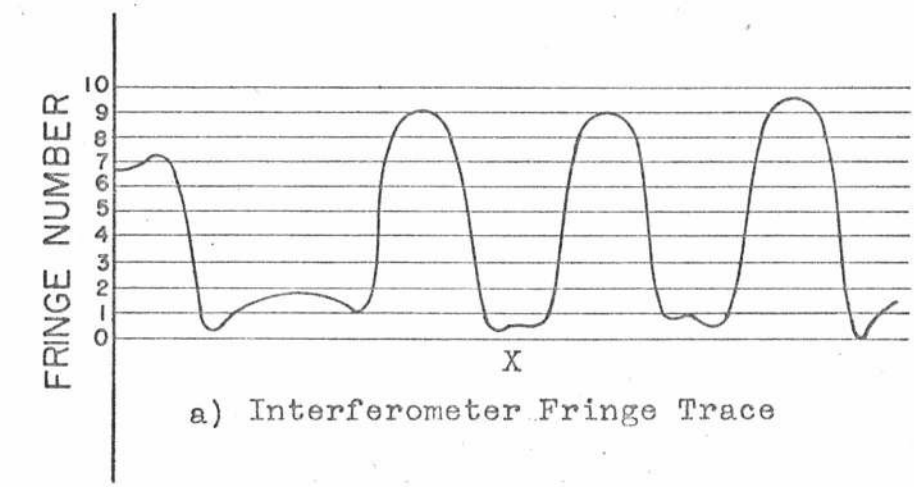

a) Interferometer Fringe Trace

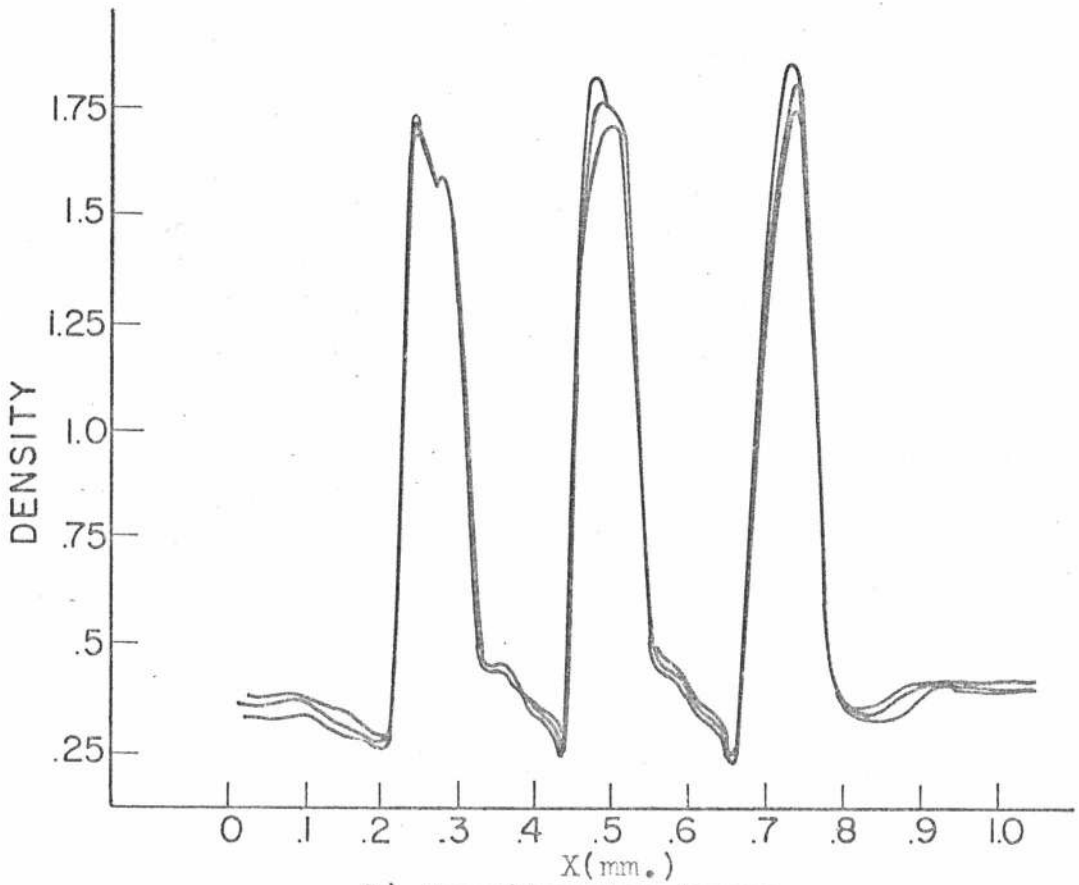

b) Densitometer Trace

Figure 4.13

Phase Resolution Target #1

Bar Group 2-2

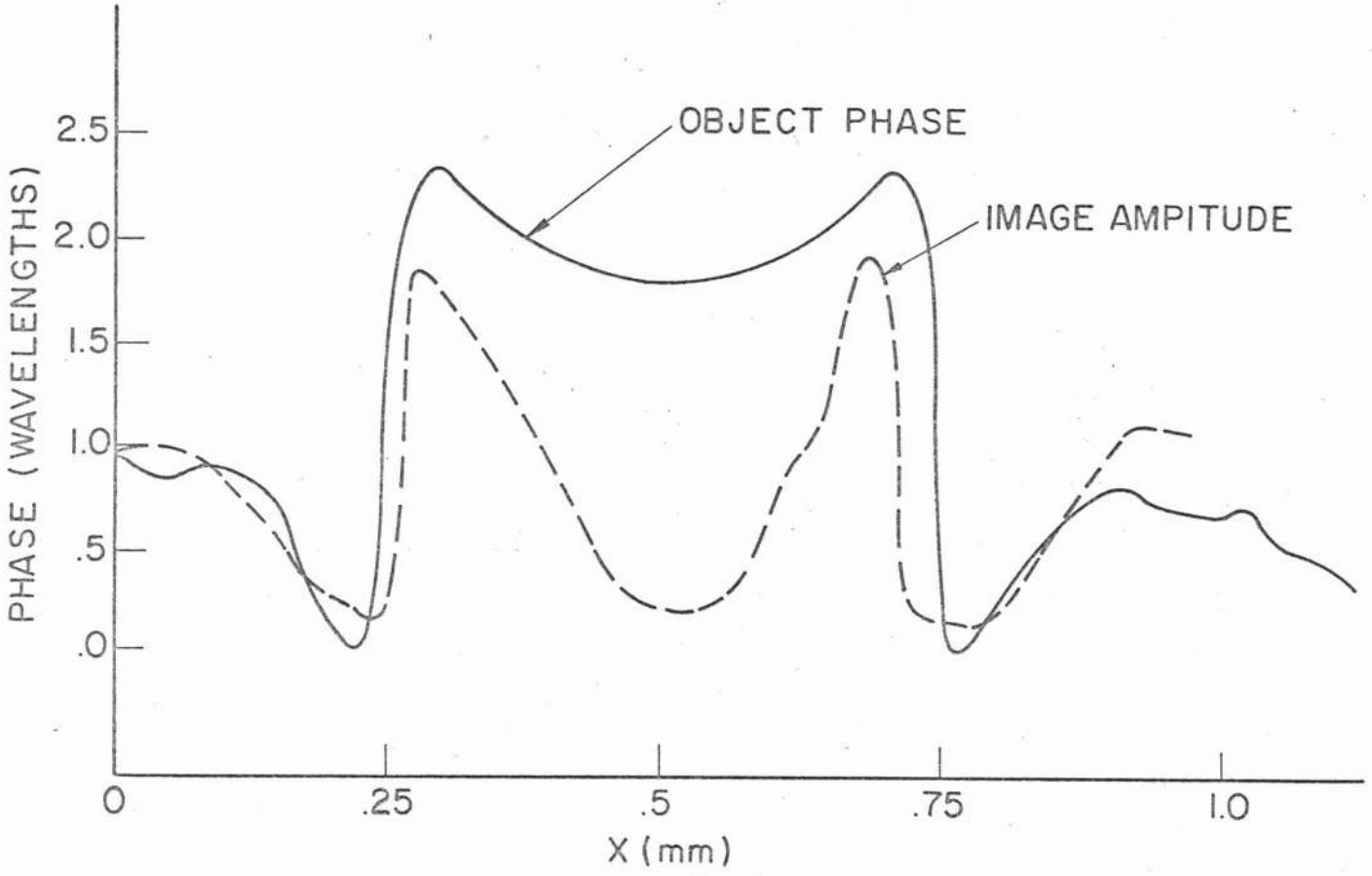

Figure 4.14

Comparison of Image Amplitude With Object Phase

Phase Resolution Target #1--Bar Group 0-2

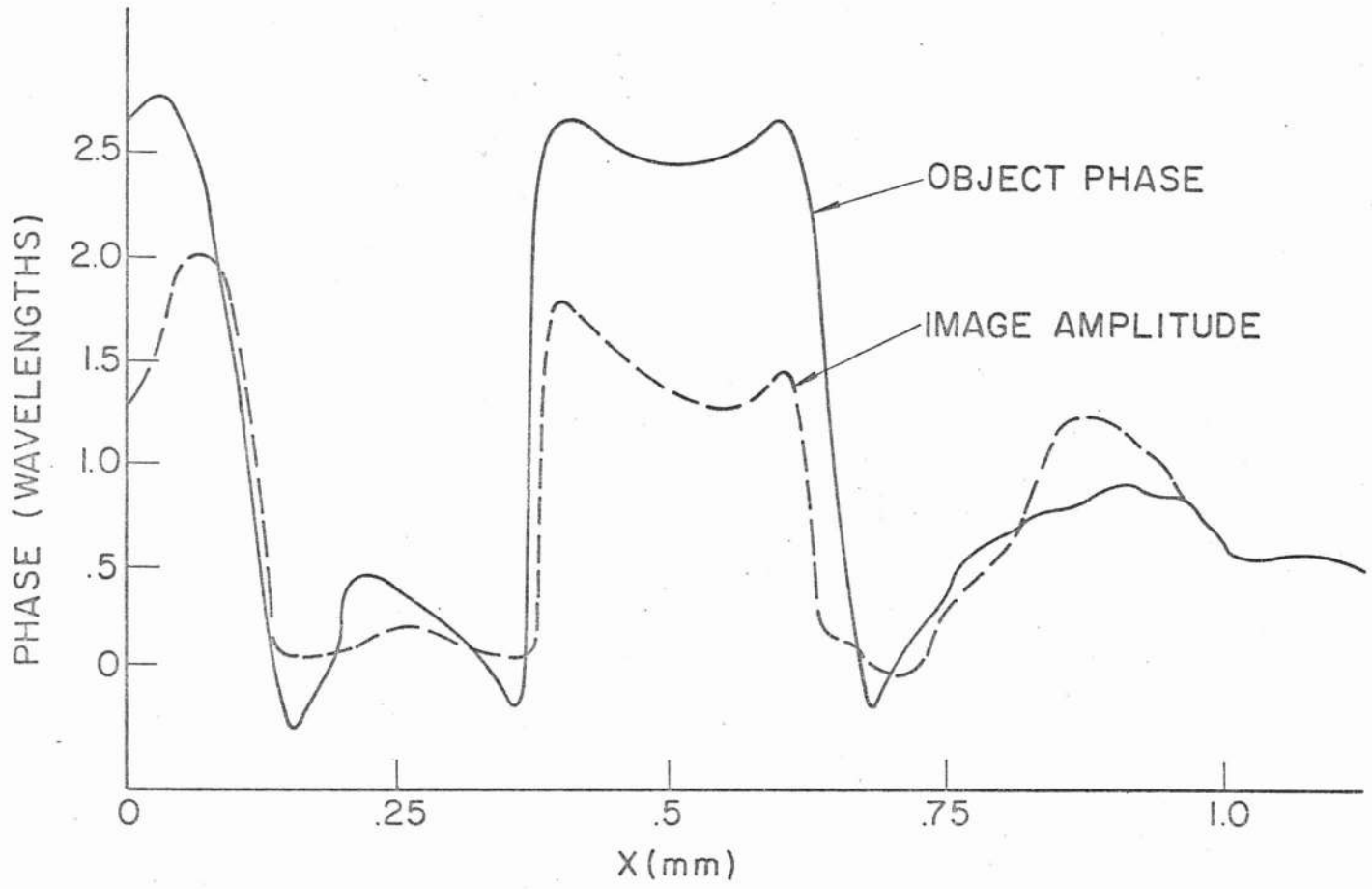

Figure 4.15

Comparison of Image Amplitude With Object Phase

Phase Resolution Target #1--Bar Group 1-1

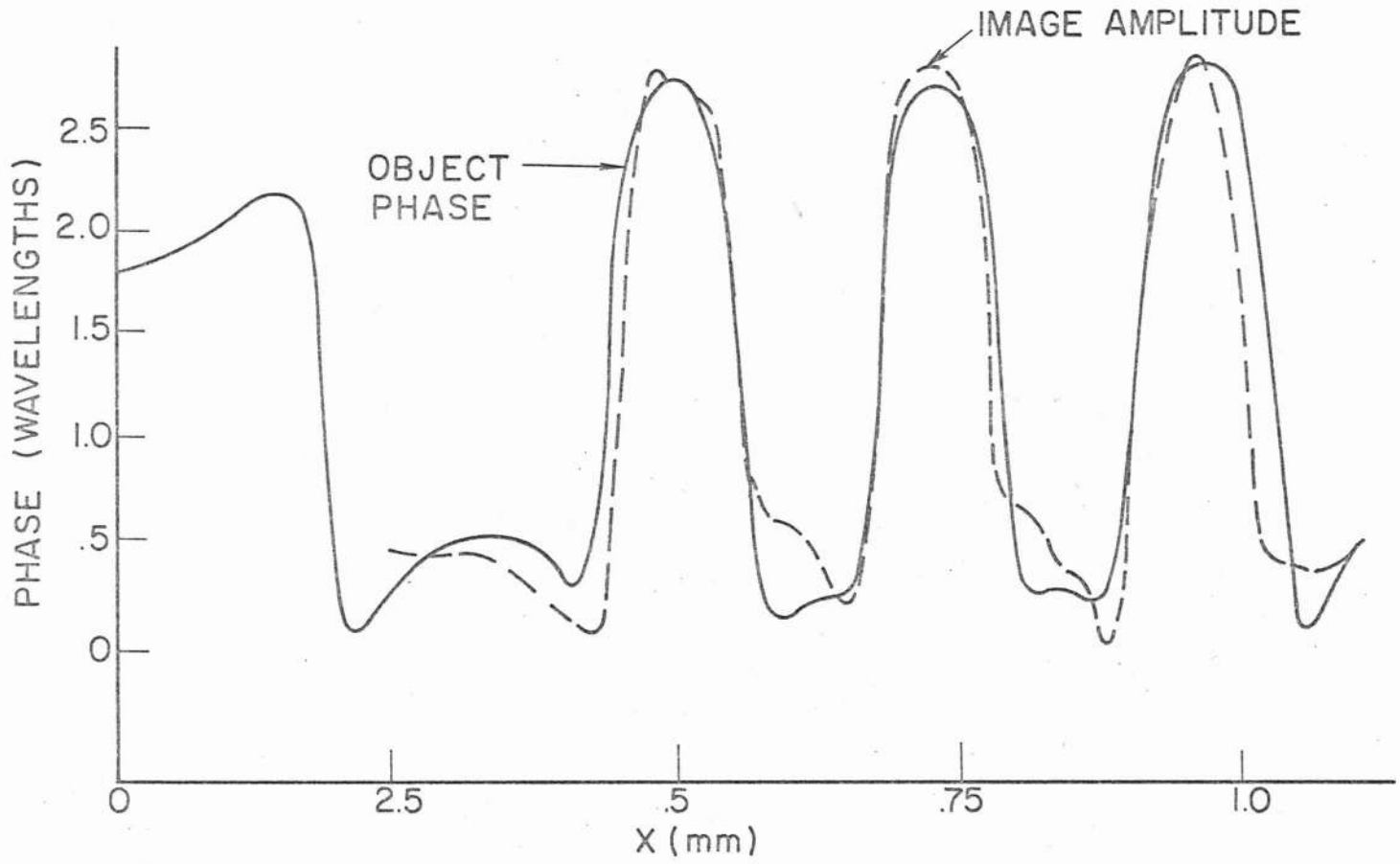

Figure 4.16

Comparison of Image Amplitude With Object Phase

Phase Resolution Target #1--Bar Group 2-2

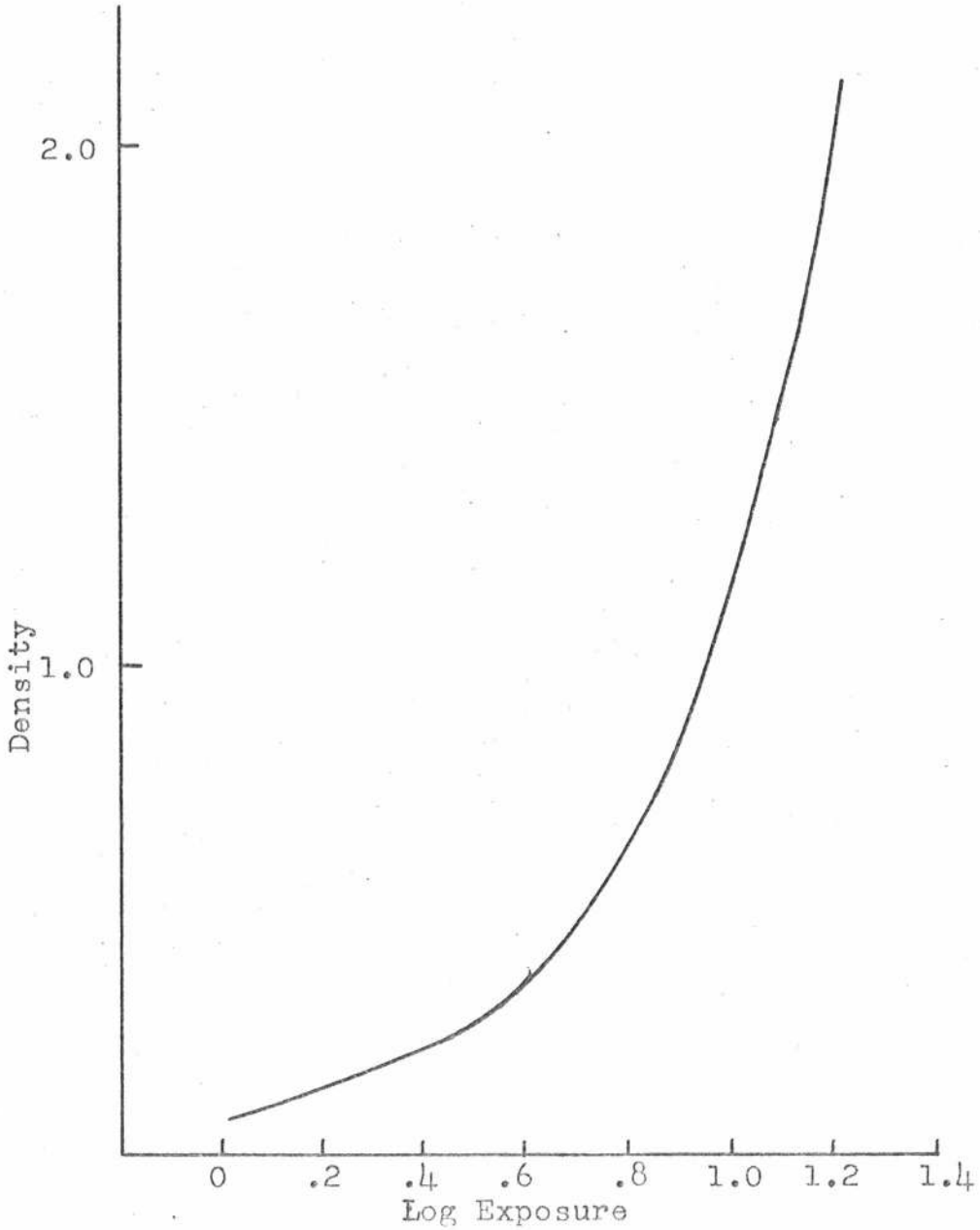

Callibration Curve

Integral of Phase Object Derivative

Phase Resolution Target #2

Figure 4.17

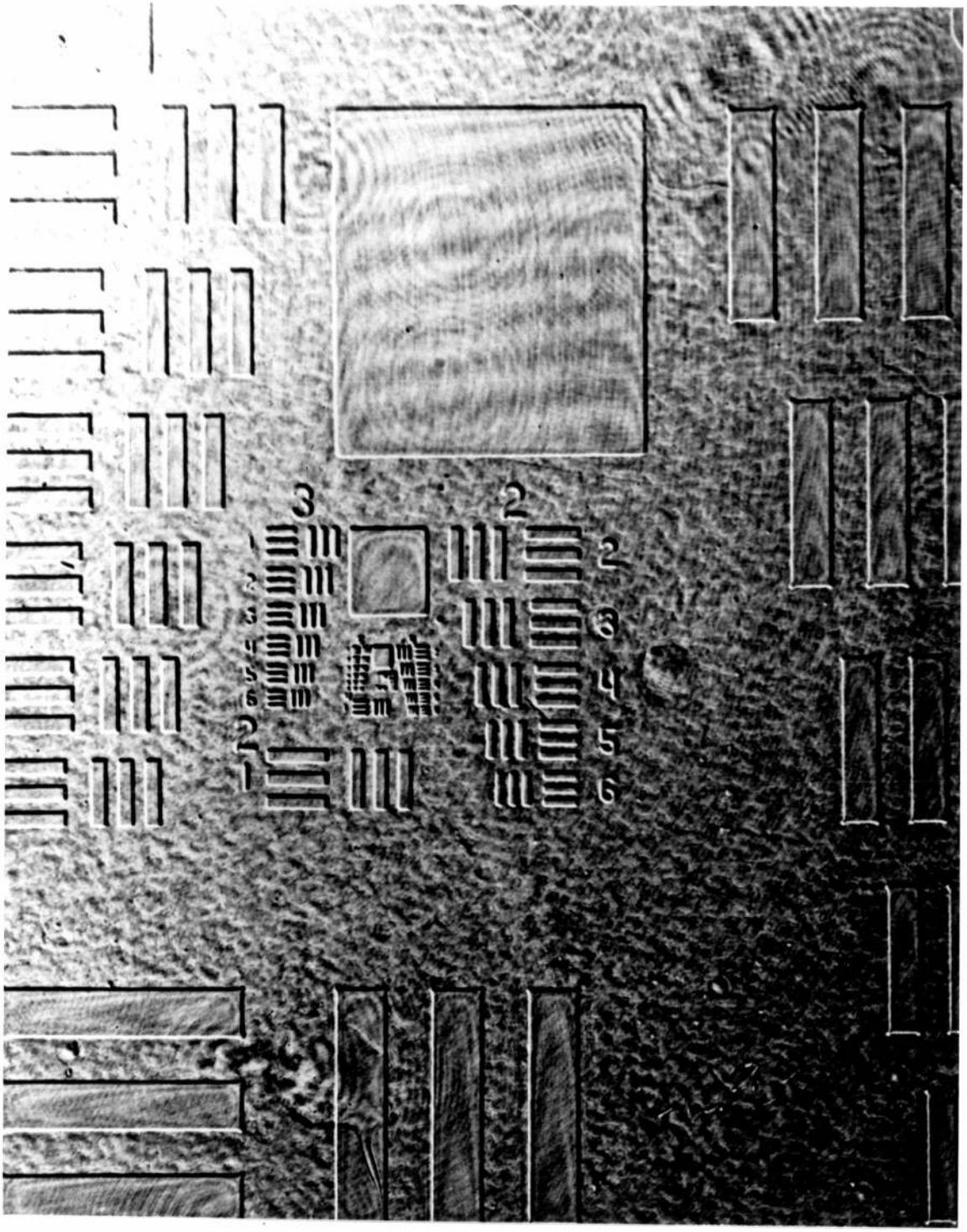

Figure 4.18

Phase Object Derivative

Phase Resolution Target #2

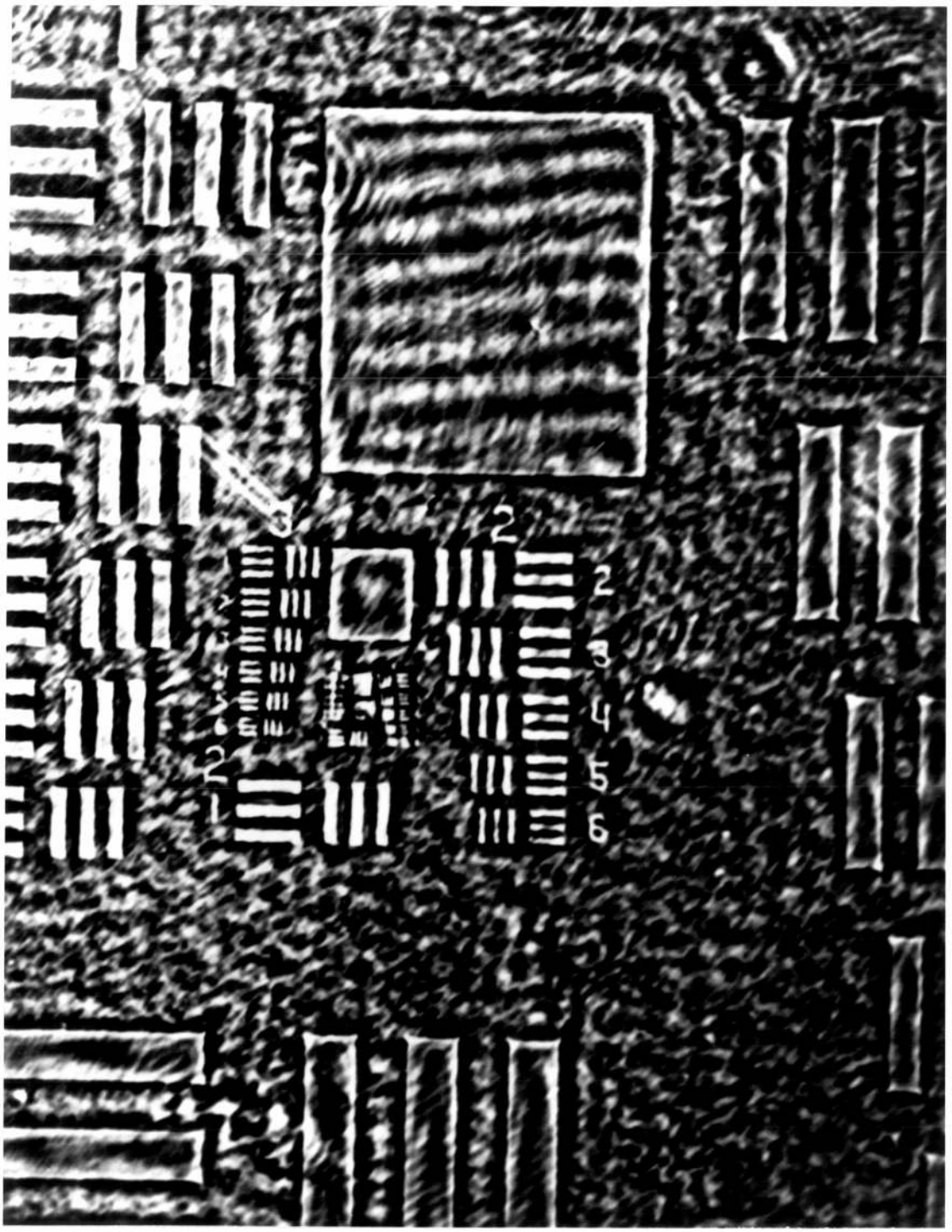

Figure 4.19

Integral of Phase Object Derivative

Phase Resolution Target #2

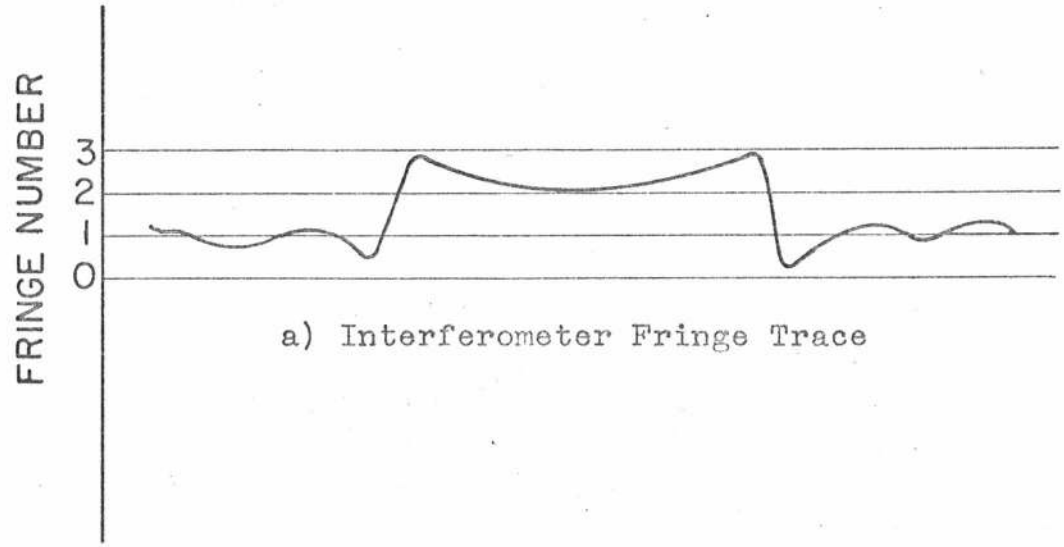

a) Interferometer Fringe Trace

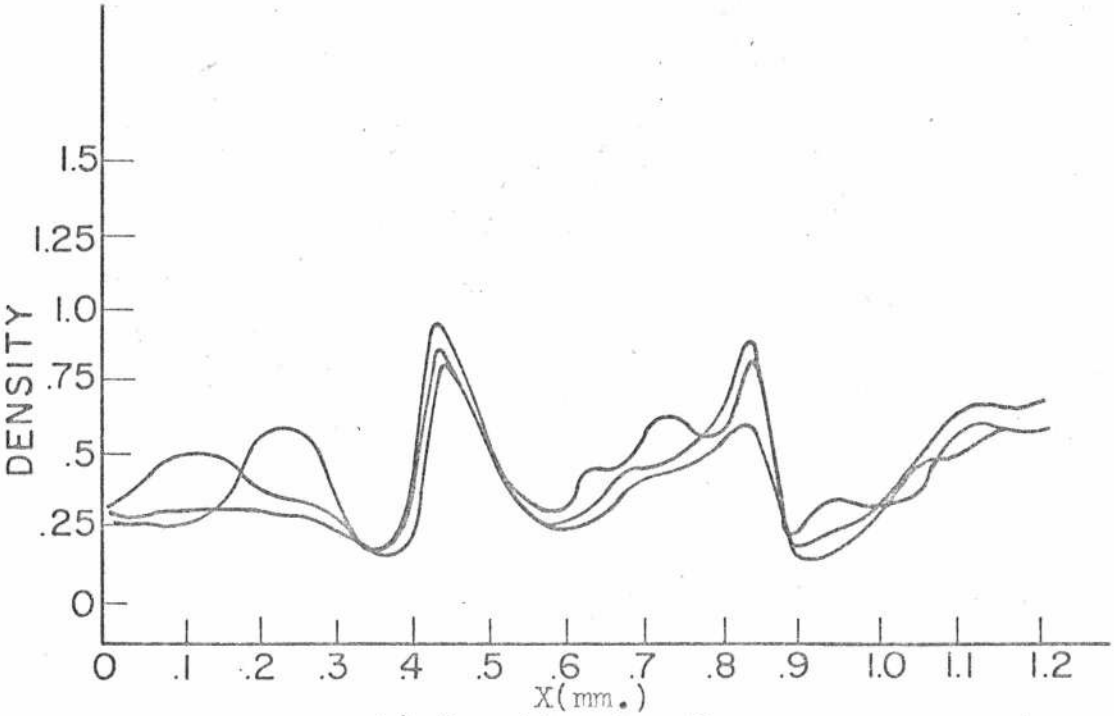

b) Densitometer Trace

Figure 4.20

Phase Resolution Target #2

Bar Group 0-2

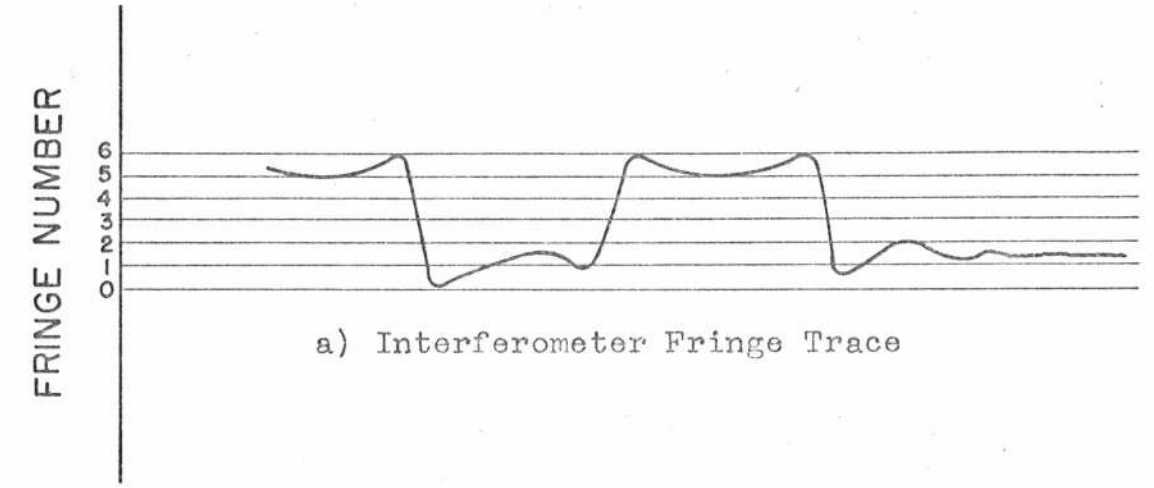

a) Interferometer Fringe Trace

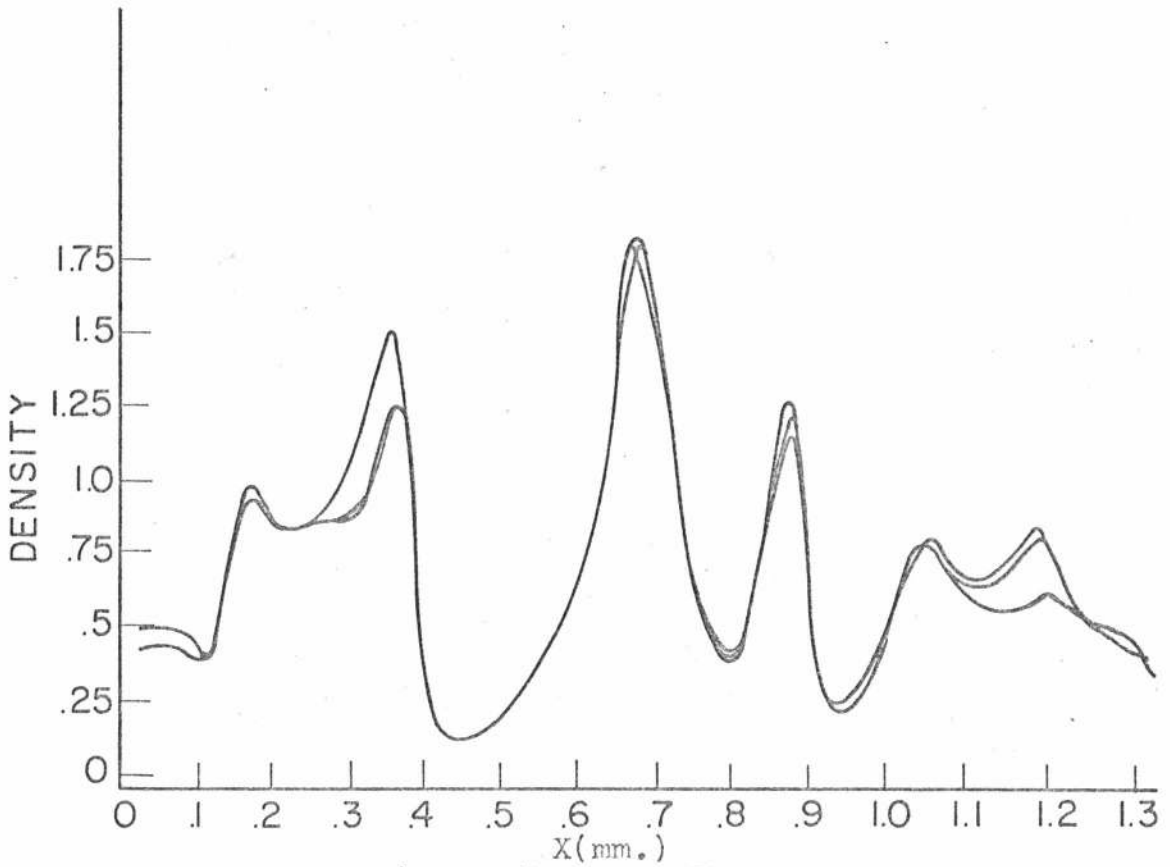

b) Densitometer Trace

Figure 4.21

Phase Resolution Target #2

Bar Group 1-1

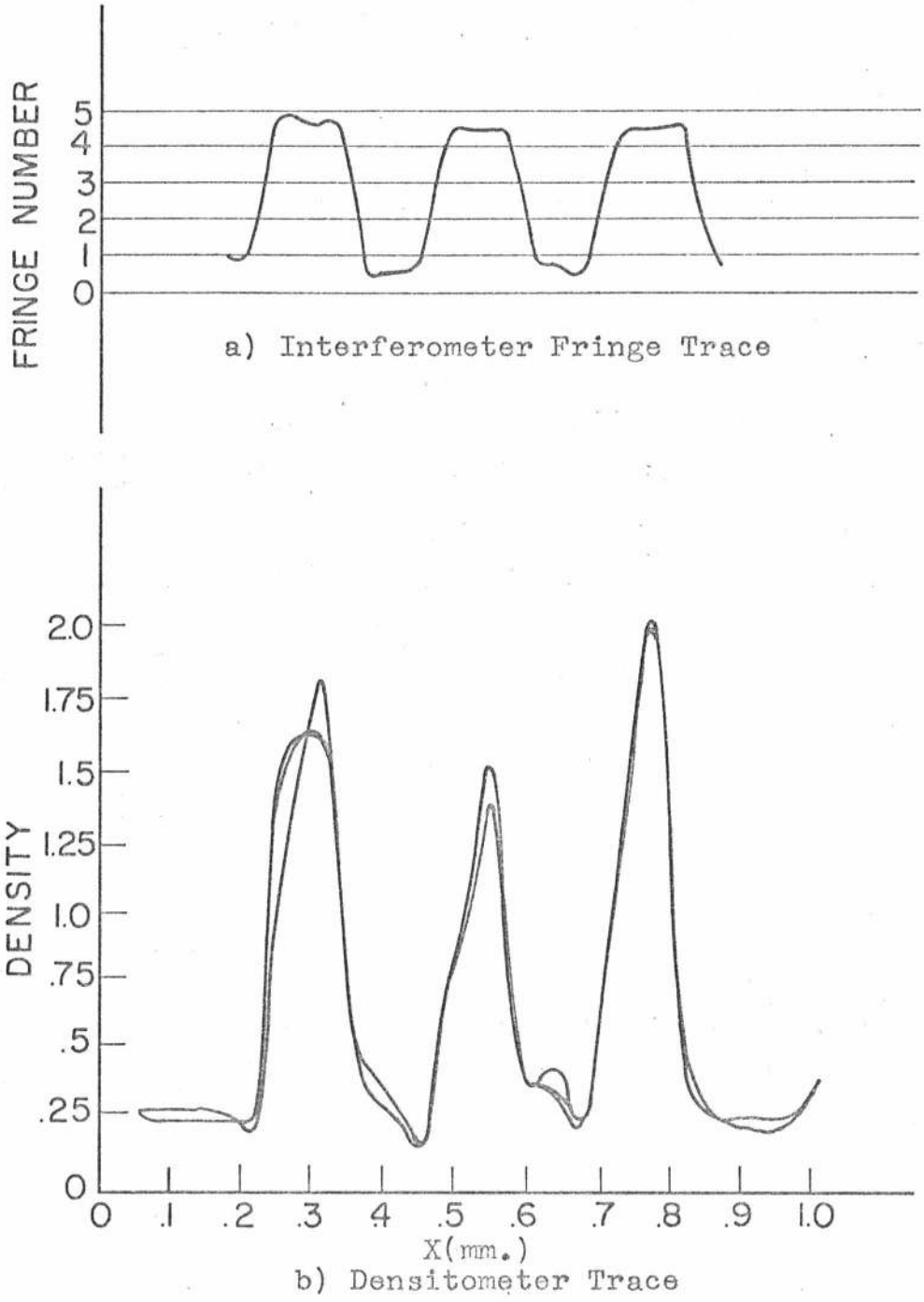

a) Interferometer Fringe Trace

b) Densitometer Trace

Figure 4.22

Phase Resolution Target #2

Bar Group 2-2

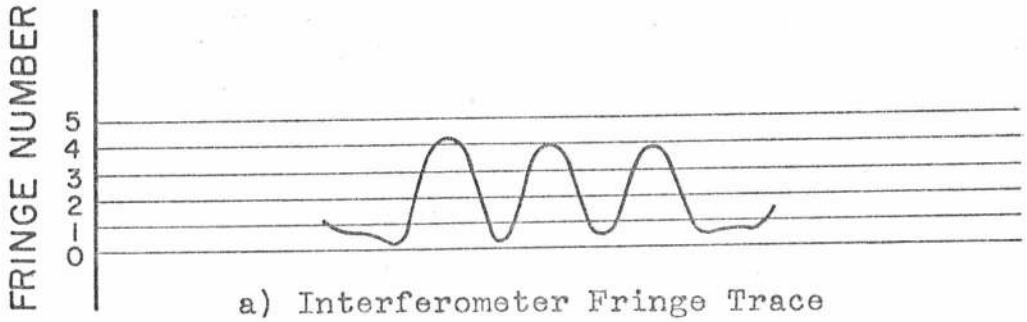

a) Interferometer Fringe Trace

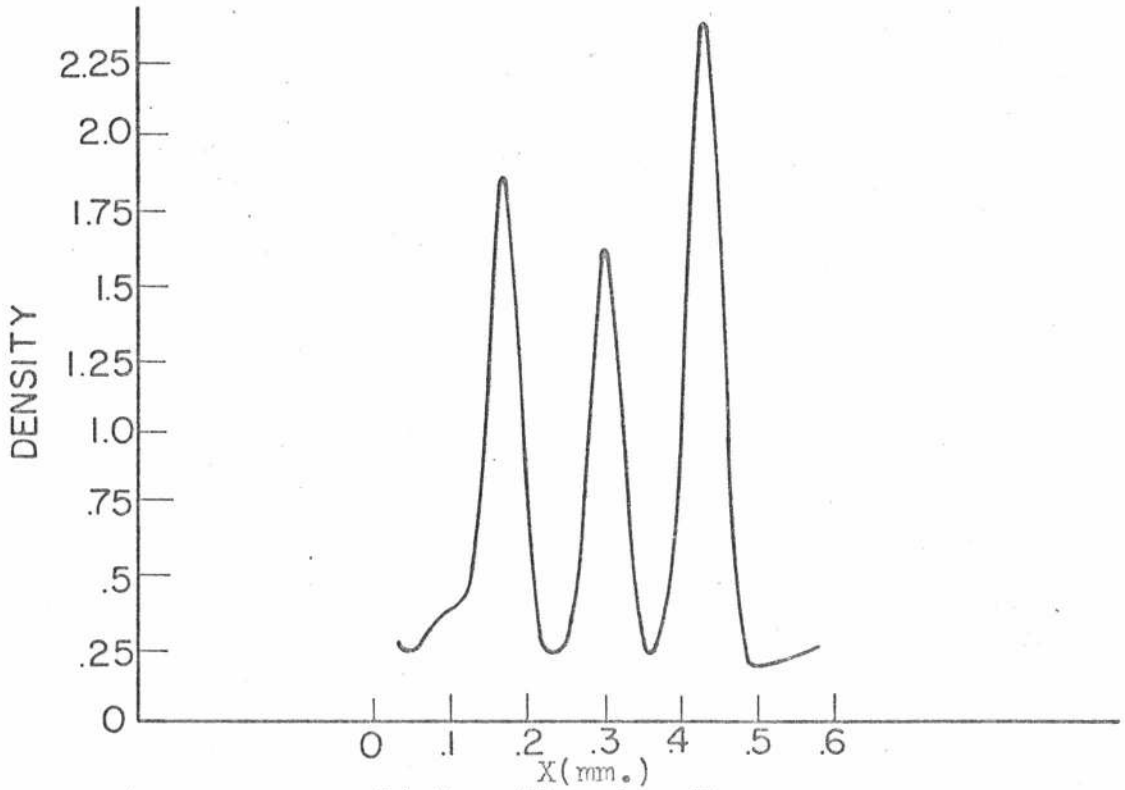

b) Densitometer Trace

Figure 4.23

Phase Resolution Target #2

Bar Group 3-1

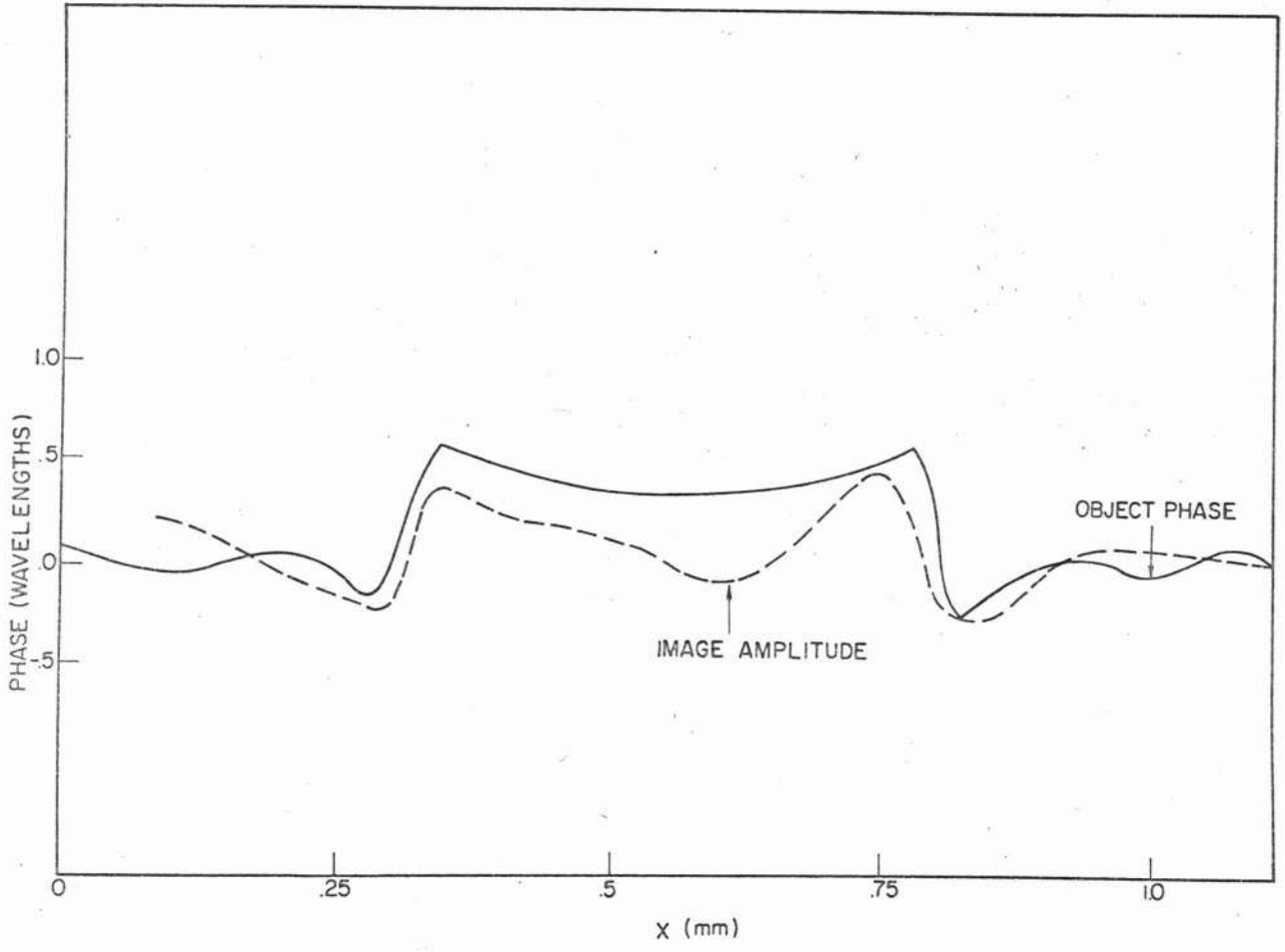

Figure 4.24

Comparison of Image Amplitude With Object Phase

Phase Resolution Target #2

Bar Group 0-2

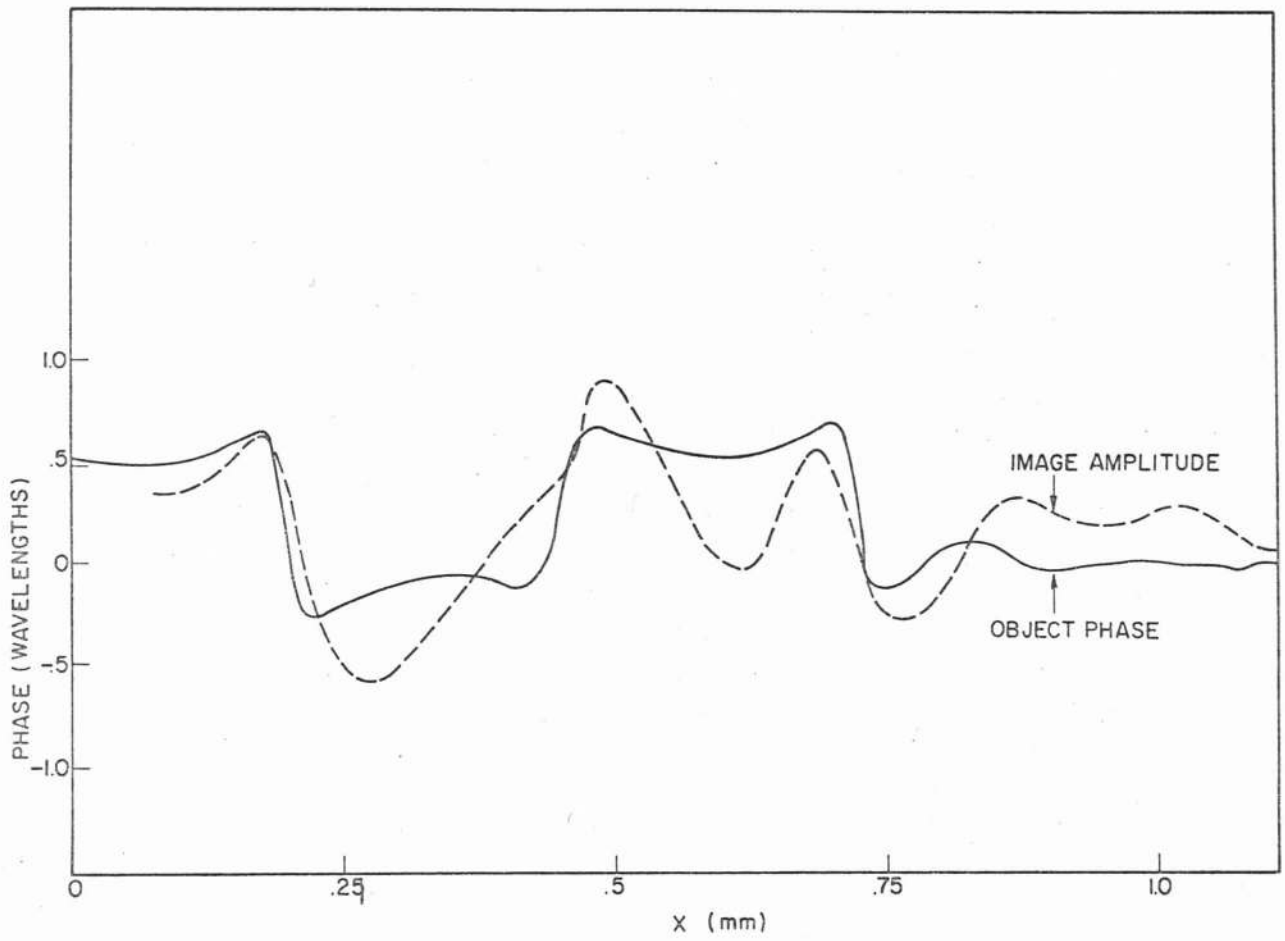

Figure 4.25

Comparison of Image Amplitude With Object Phase

Phase Resolution Target #2

Bar Group 1-1

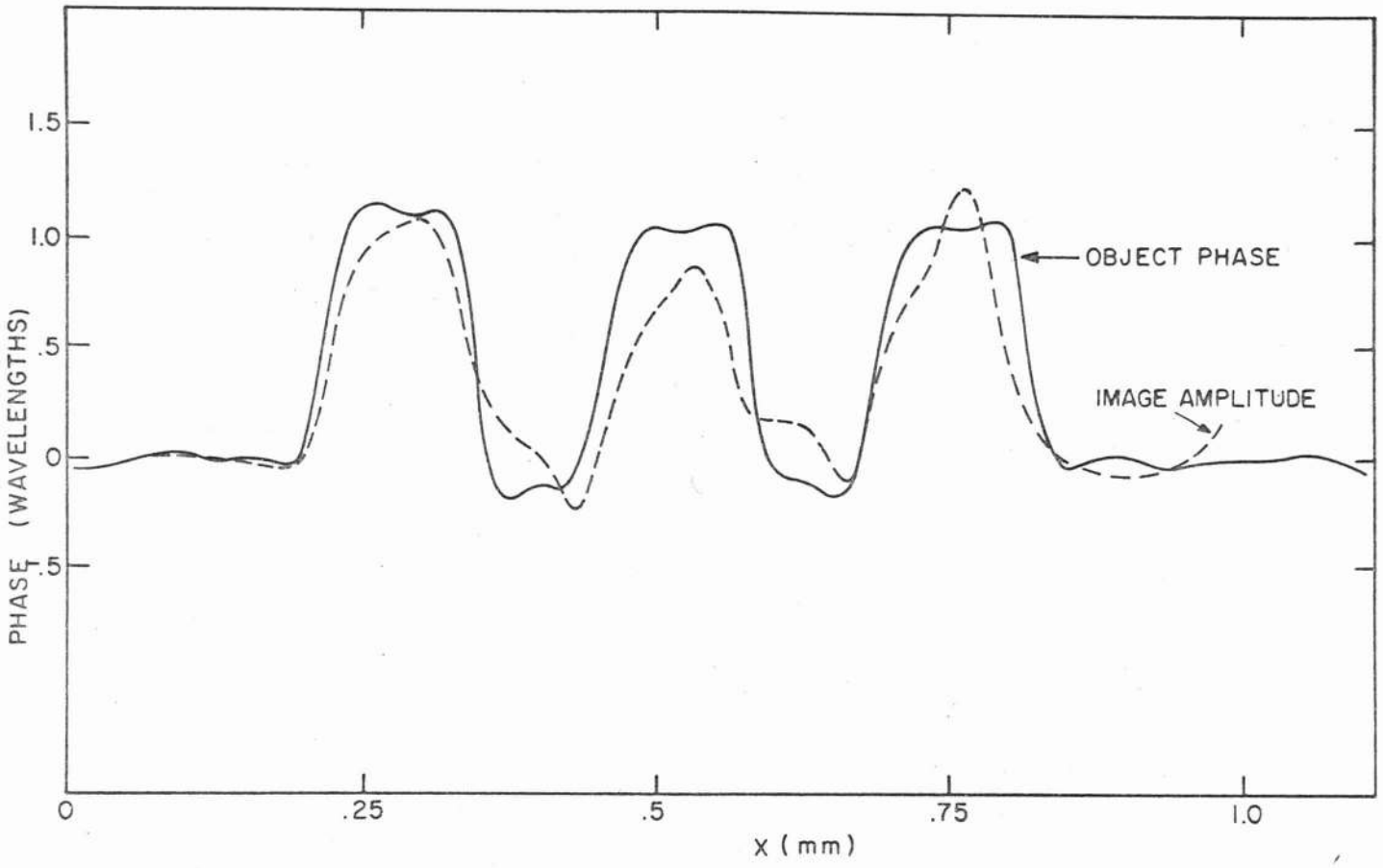

Figure 4.26

Comparison of Image Amplitude With Object Phase

Phase Resolution Target #2

Bar Group 2-2

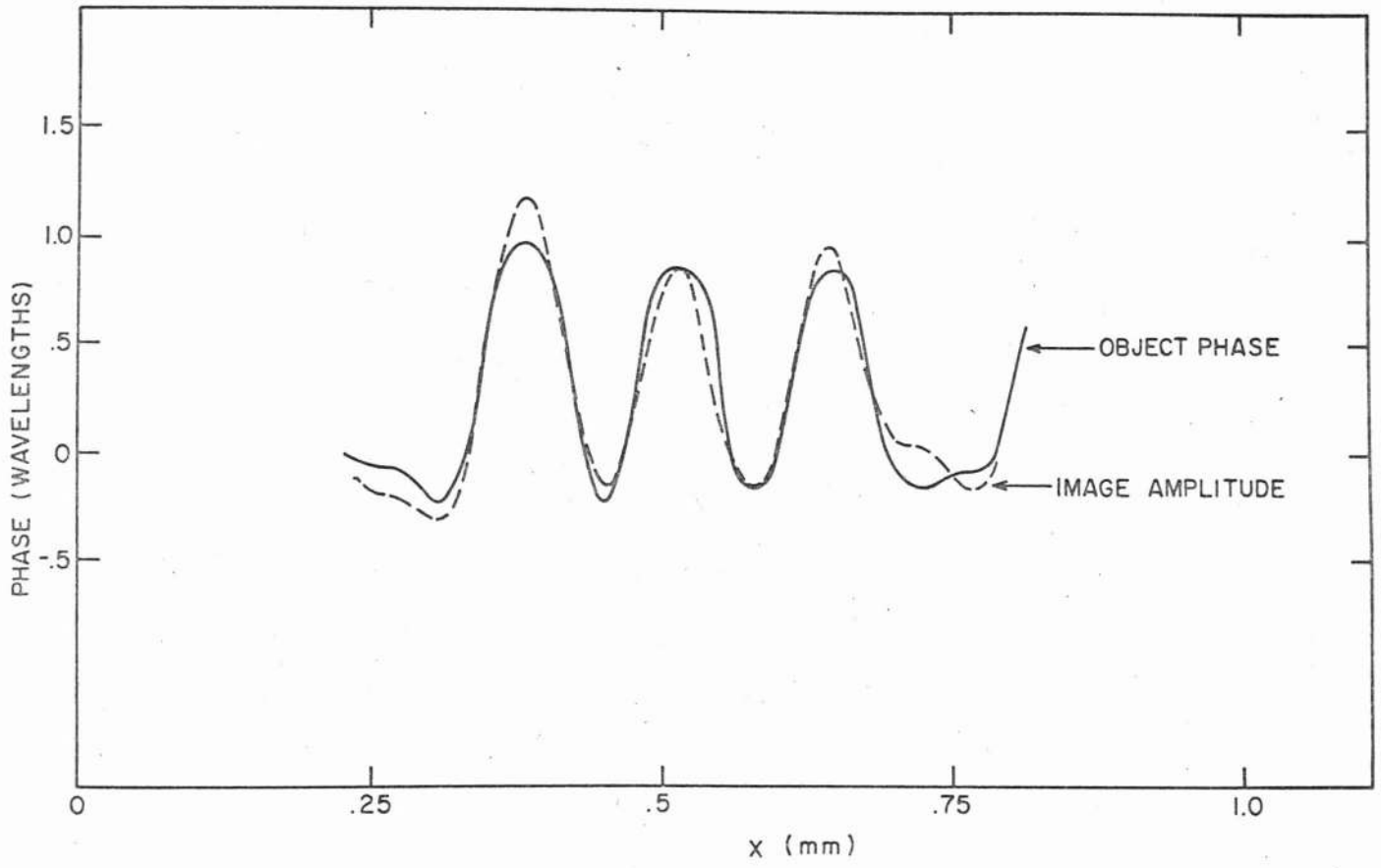

Figure 4.27

Comparison of Image Amplitude With Object Phase

Phase Resolution Target #2

Bar Group 3-1

detail is translated across one pinhole, it gives a direct measure of the object phase.

A diagram of the setup used is reproduced in Figure 4.28. The fringe position is monitored with a bench microscope equipped with a filar eyepiece. The pinholes are imaged onto the phase object, one in the region of phase detail and one in a nearby smooth area. Although it is preferable for the reference pinhole to not traverse the object at all, this was inconvenient with the available apparatus. The effect of imaging the reference through a smooth area of the target will be at worst the measurement of object phase detail superimposed on a slowly increasing or decreasing function. This function may be estimated and subtracted from the total phase function to give the correct result.

When using this technique to measure the circular phase depressions, centering was achieved by first moving the test pinhole to the apparent center of the spot and then adjusting its x and y positions to give a minumum phase reading for both. Traces were than taken in both directions across the depression.

The phase of the circular depressions as measured with the two point scanning interferometer is represented by the traces in Figures 4.29 through 4.31. The smooth curves drawn in Figures 4.29 through 4.31 were subtracted from the phase readings to give the actual phase in Figures 4.41 thorugh 4.46.

PHASE MEASUREMENT APPARATUS

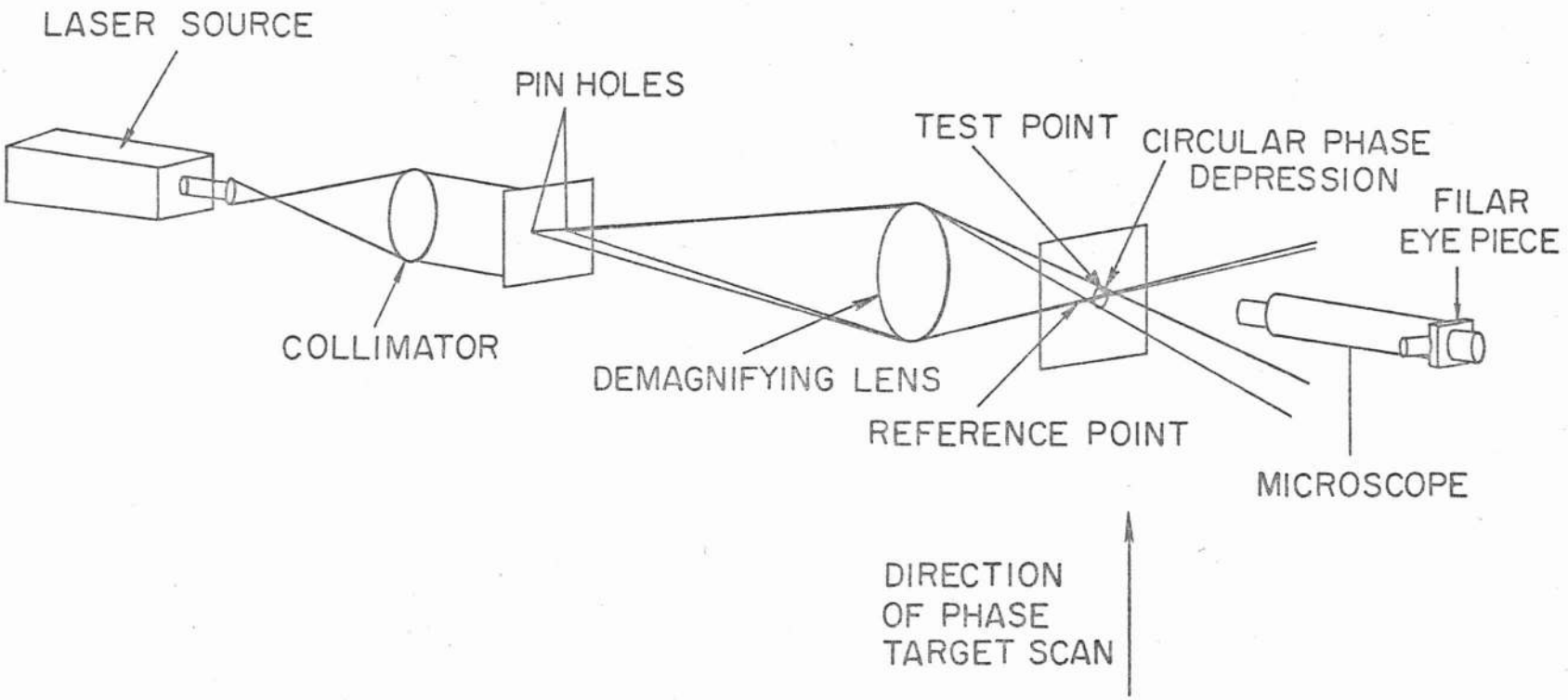

Figure 4.28

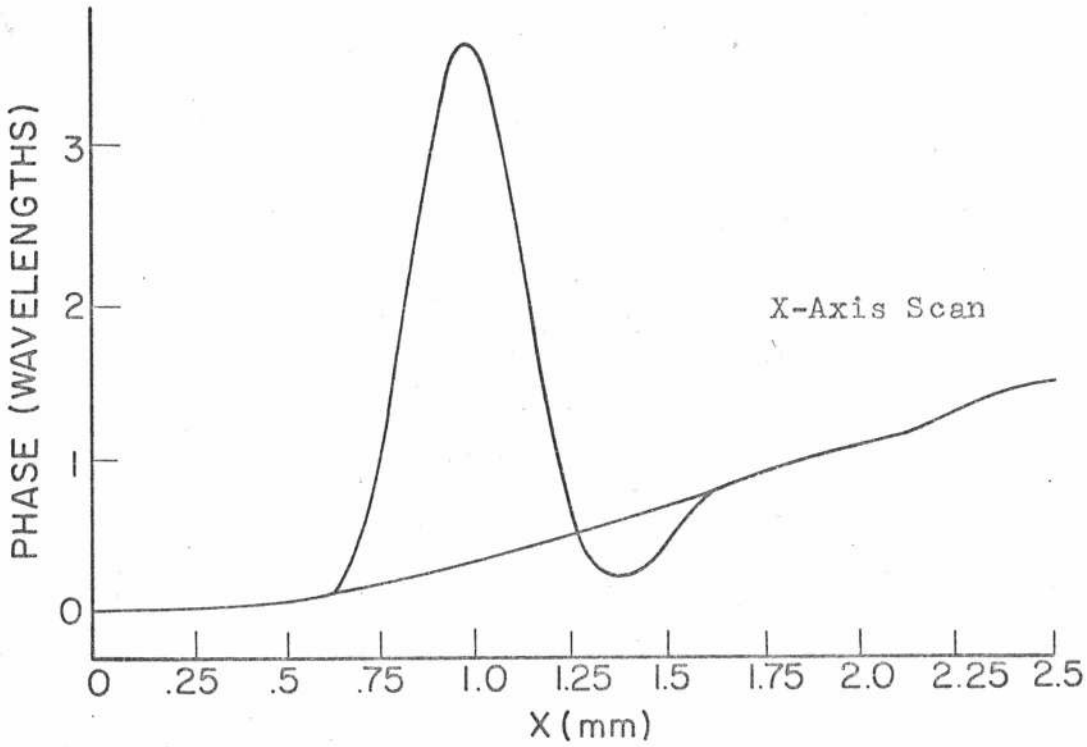

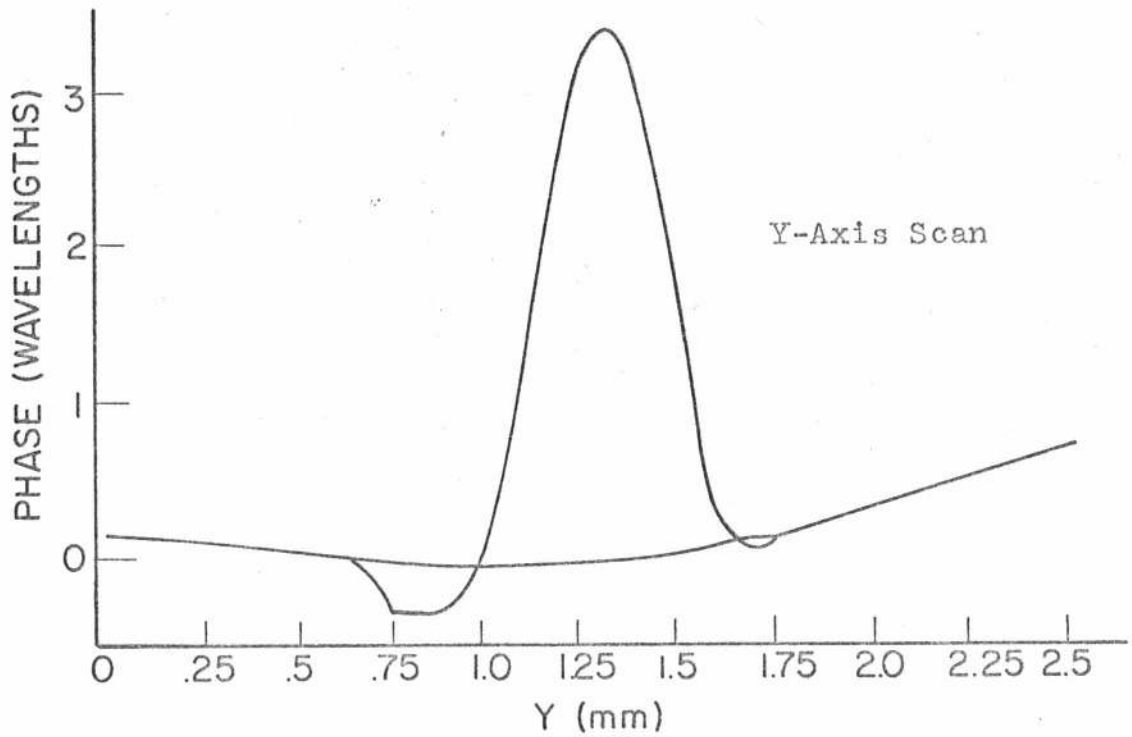

Figure 4.29

Transmission Phase Measurements

Circular Phase Depression #1

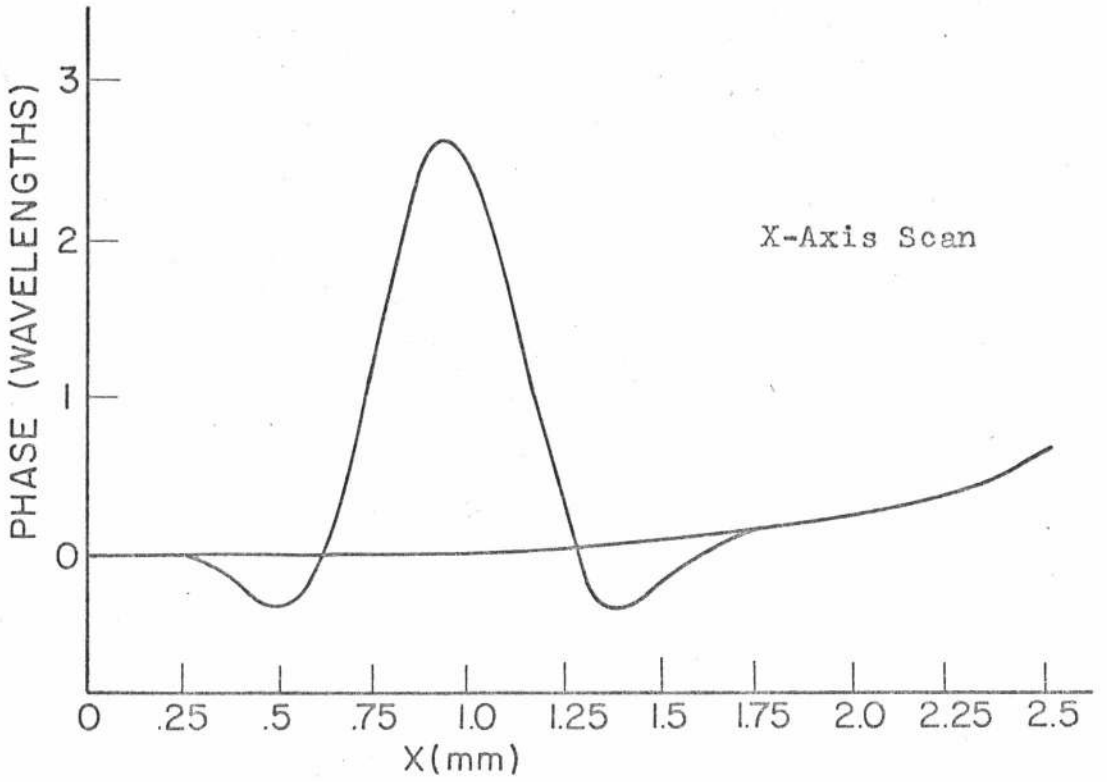

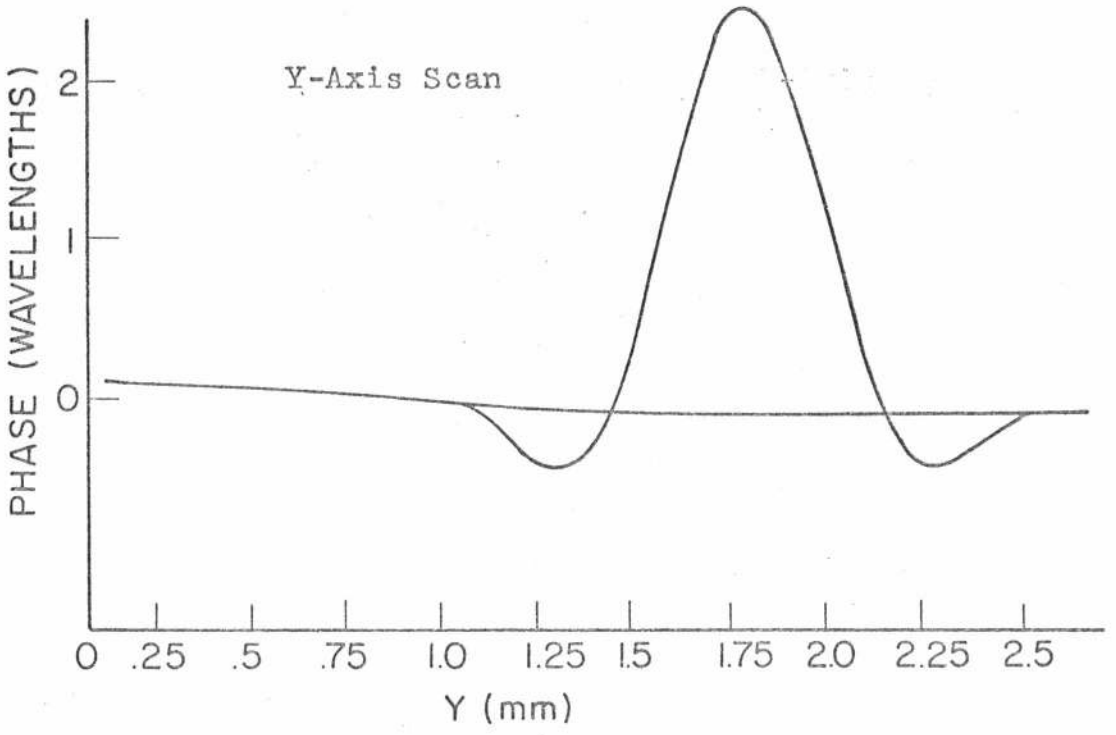

Figure 4.30

Phase Measurements--Circular Phase Depression #2

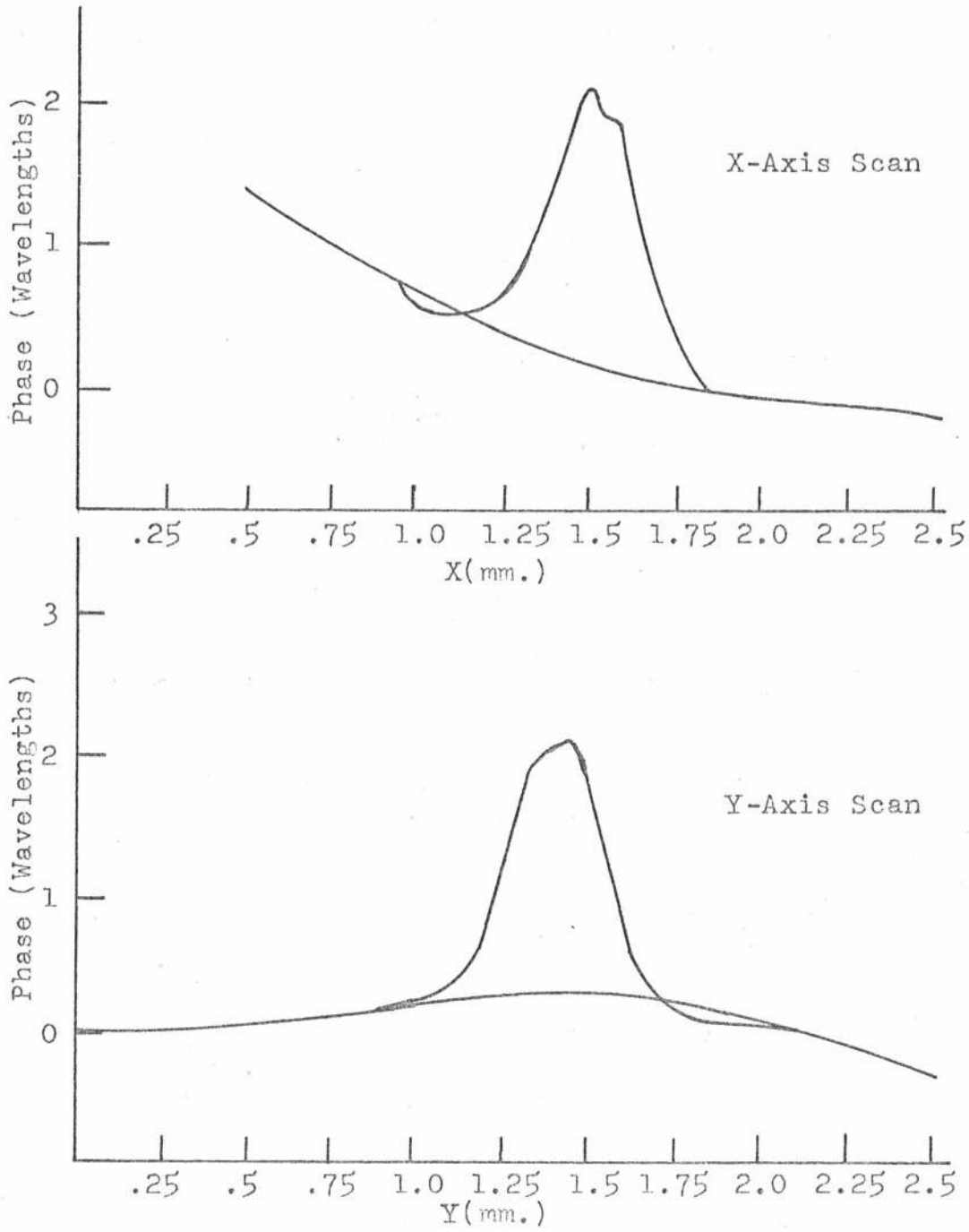

Figure 4.31

Transmission Phase Measurements

Circular Phase Depression #3

The coherent derivative of the circular phase depressions is reproduced in Figure 4.32 and the integral in Figure 4.33. The actual spatial width of the depressions is misleading, as this width is too broad for proper integration with the truncated filter. To circumvent this problem, a demagnification of 4.5x of the derivative was effected in making a contact print. This demagnified derivative was used as the input to the integration system to give the results shown.

It is unfortunate that the dark surrounding line on the derivative was drawn for orientation purposes, as this line also integrates to add extraneous terms to the image. These terms are slowly changing and must be subtracted out. Microdensitometer traces were taken in the x and y directions across three of these spots. The traces were made to traverse the maximum density region of each spot by centering the scanning spot in both directions before scanning. The recordings made are reproduced in Figures 4.34a through 4.39a. These density recordings were callibrated to give exposure readings in a manner exactly similar to that used with the bar targets. The callibration D vs. log E curve is presented in Figure 4.40. The amplitude traces determined using this callibration are presented in Figures 4.34b through 4.39b.

To subtract the slowly changing term from the image, a smooth line was drawn across the base of each amplitude trace.

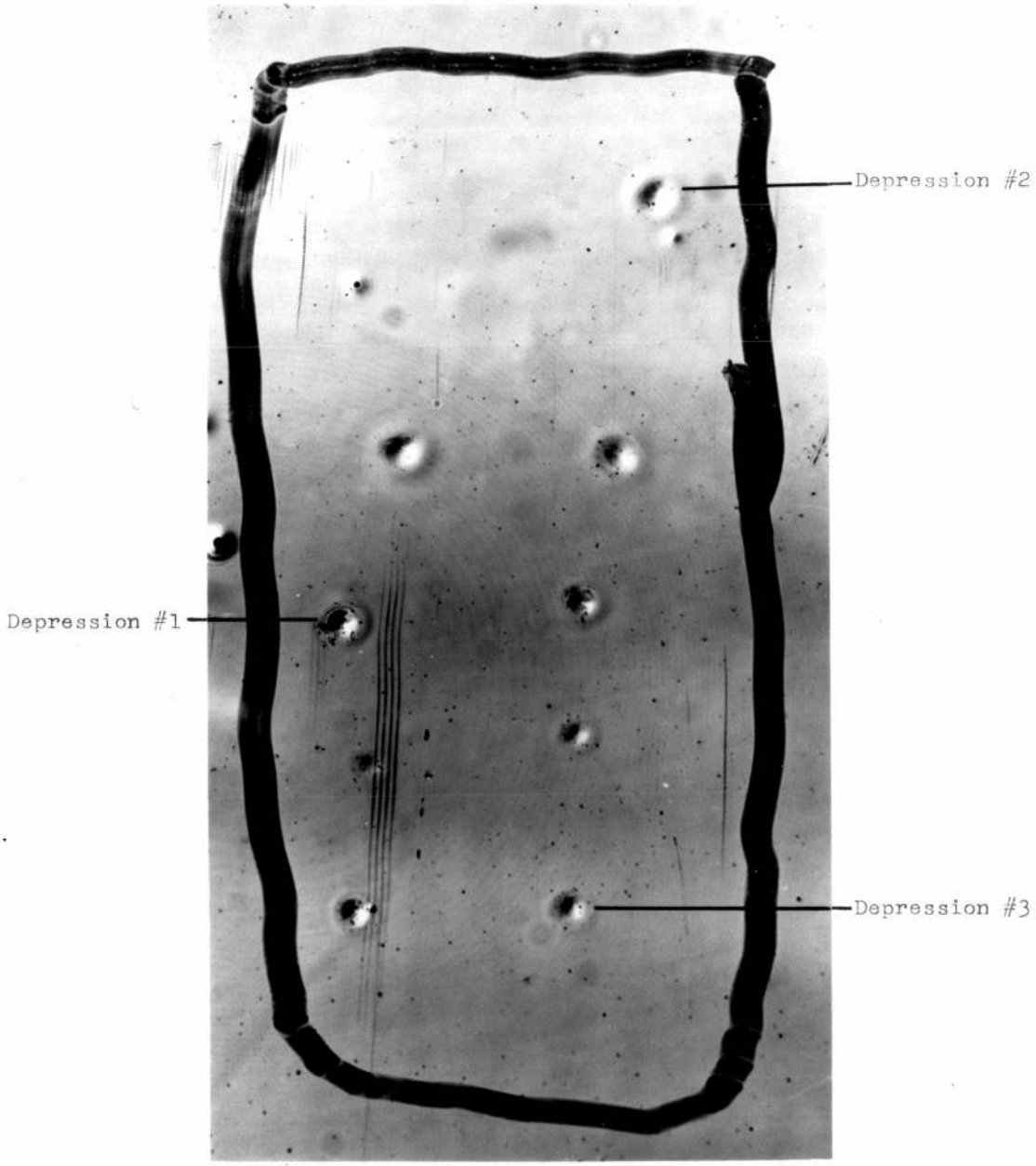

Figure 4.32

Phase Object Derivative

Circular Phase Depressions

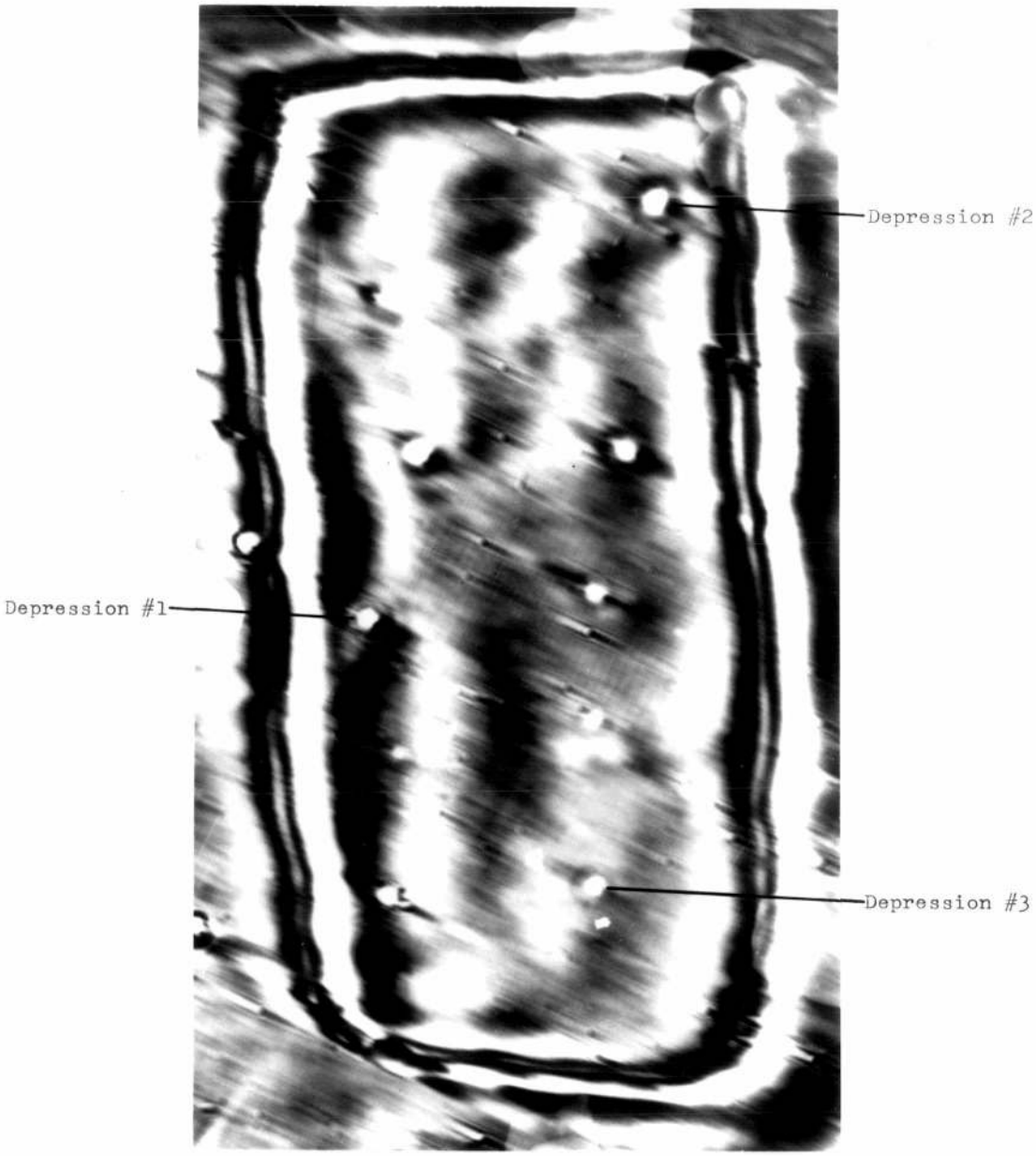

Figure 4.33

Integral of Phase Object Derivative

Circular Phase Depressions

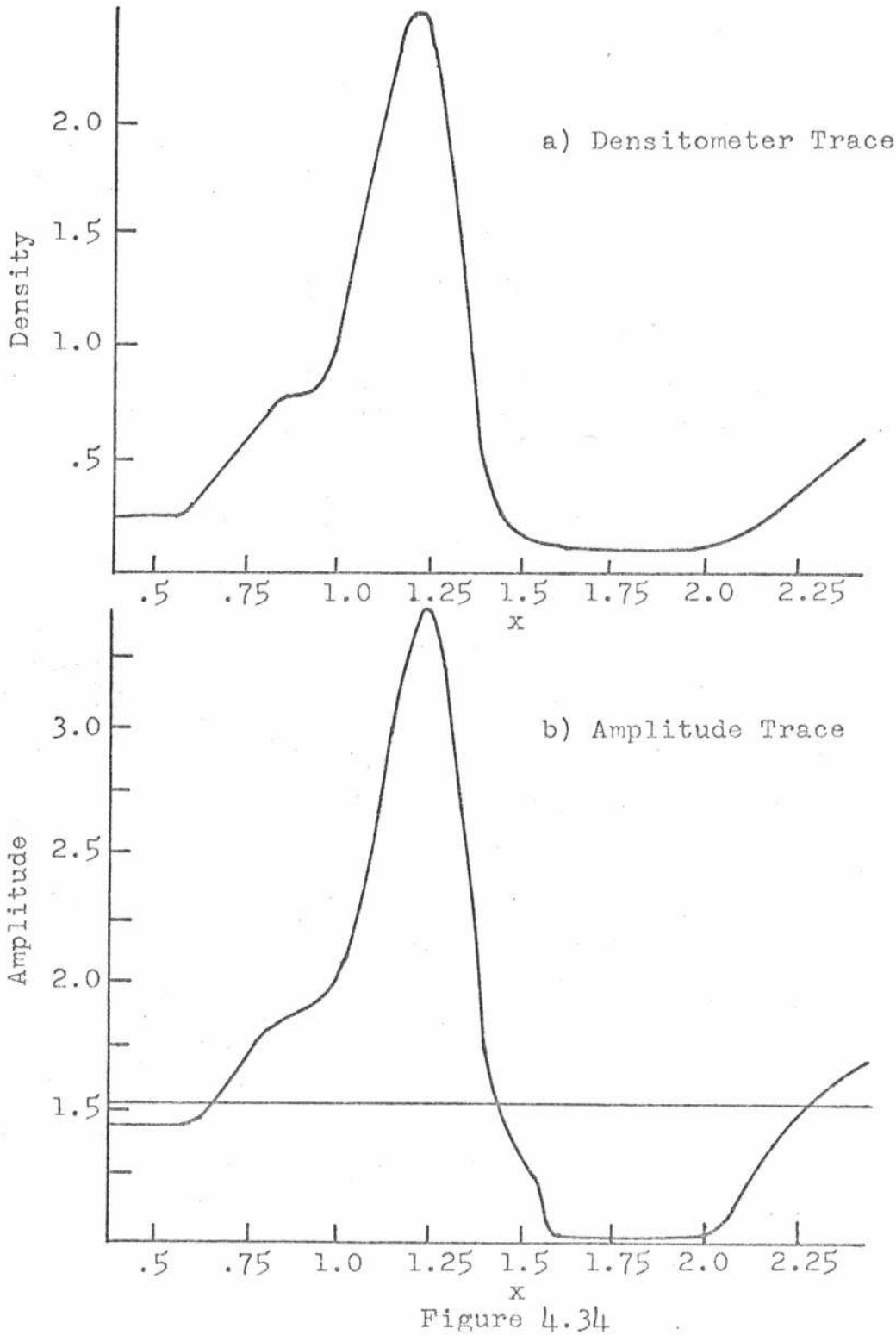

Figure 4.34

Circular Phase Depression #1--X-Axis Scan

Integral of Phase Object Derivative

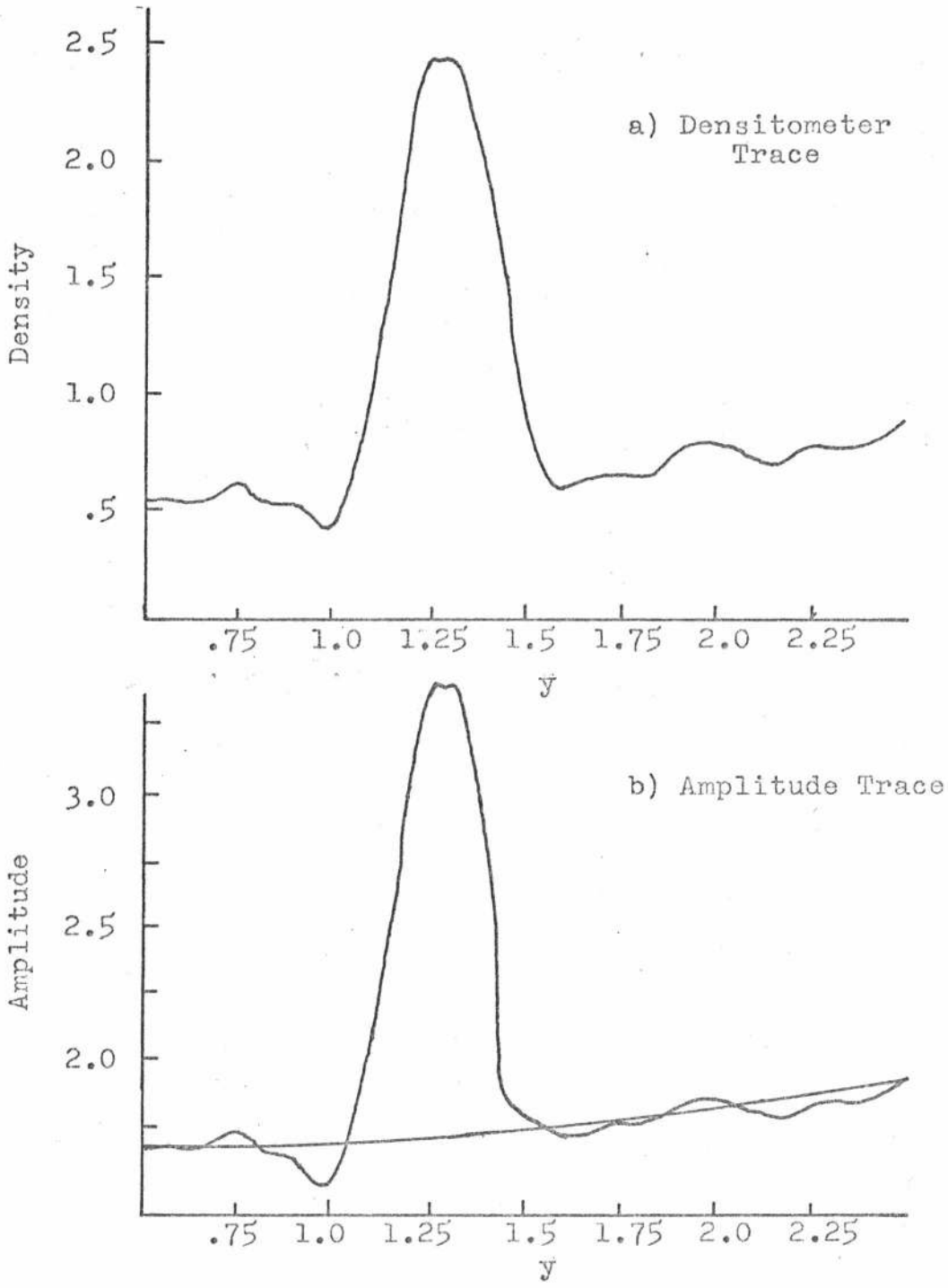

Figure 4.35

Circular Phase Depression #1--Y-Axis Scan

Integral of Phase Object Derivative

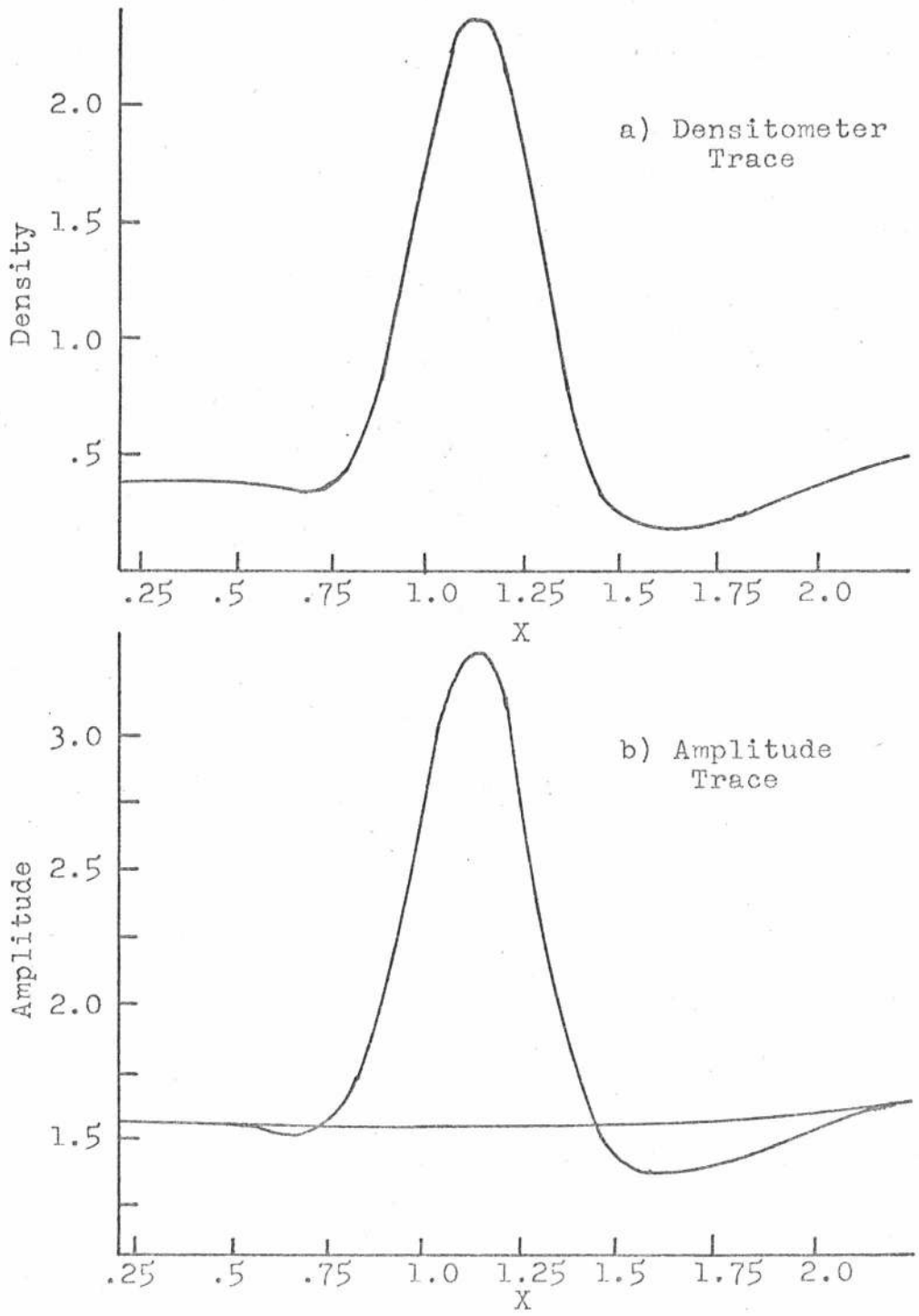

Figure 4.36

Circular Phase Depression #2--X-Axis Scan

Integral of Phase Object Derivative

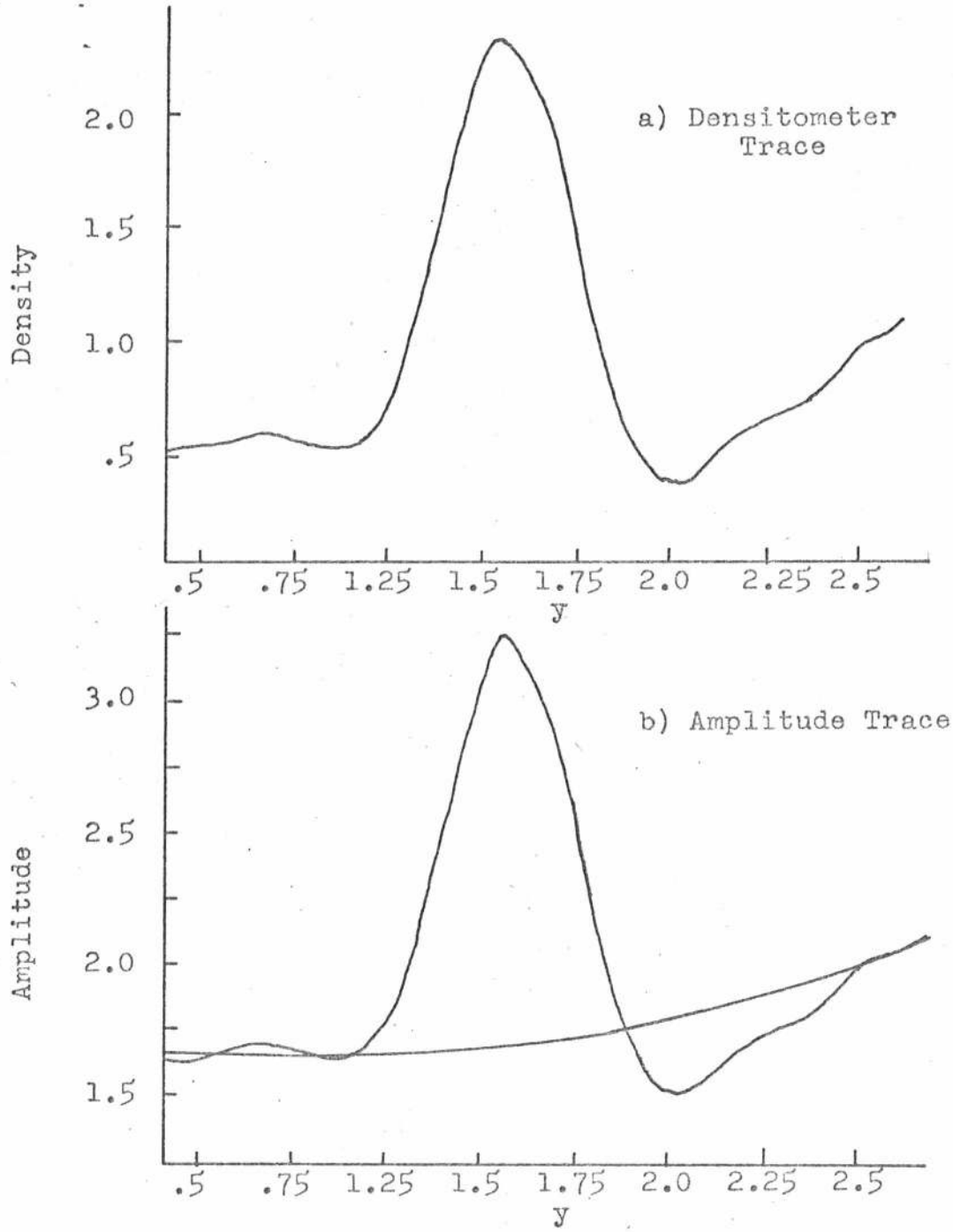

Figure 4.37

Circular Phase Depression #2--Y-Axis Scan

Integral of Phase Object Derivative

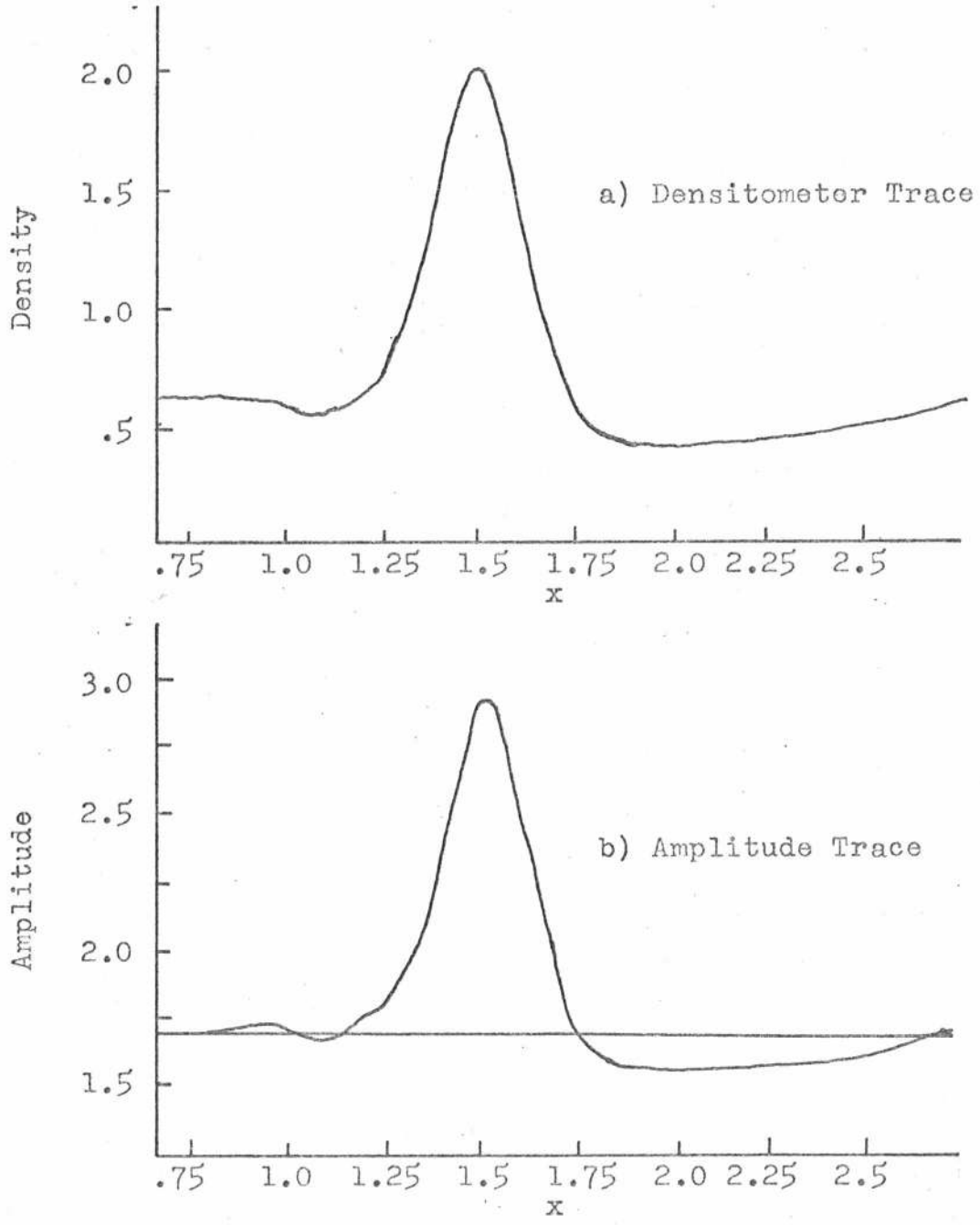

Figure 4.38

Circular Phase Depression #3--X-Axis Scan

Integral of Phase Object Derivative

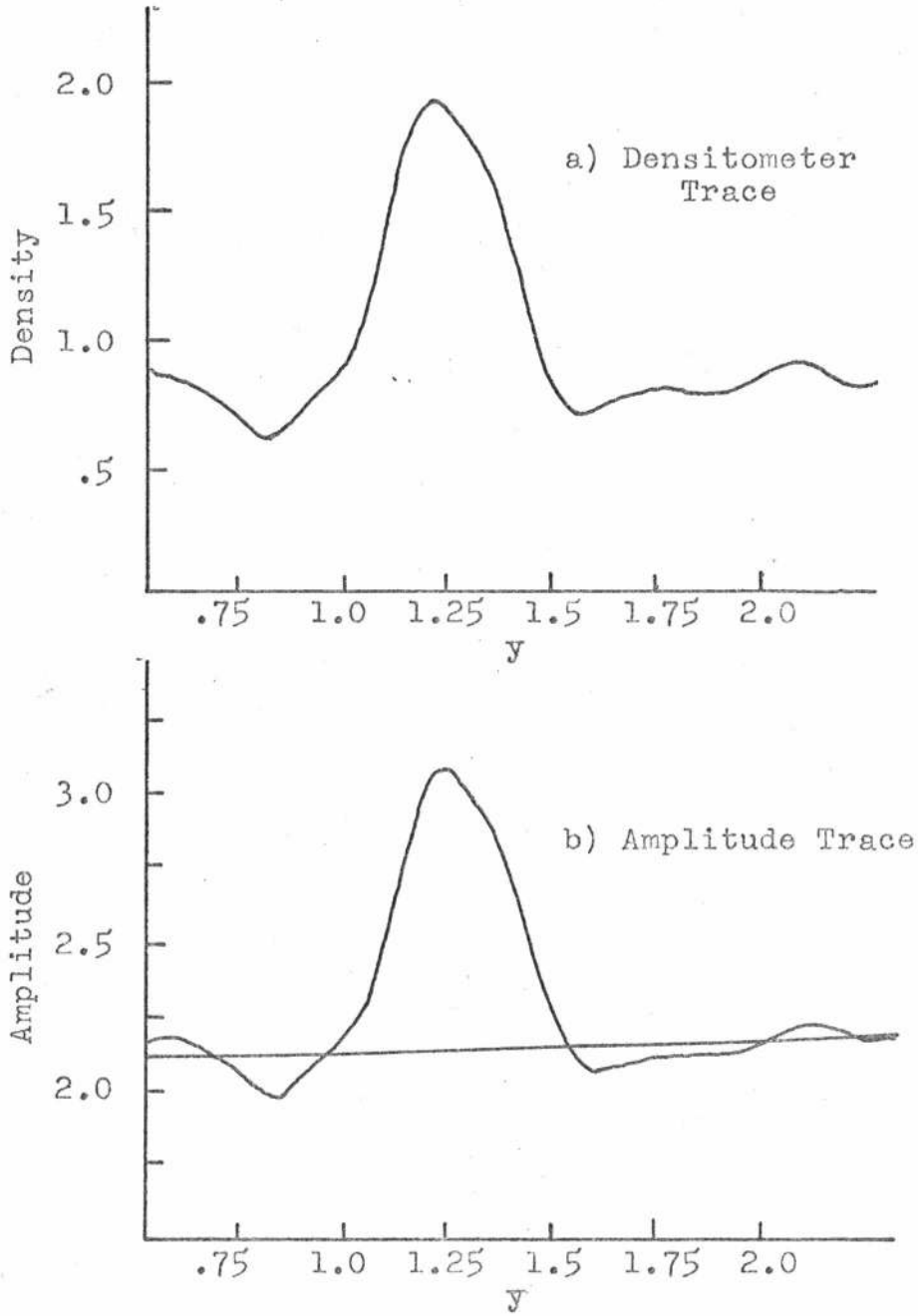

Figure 4.39

Circular Phase Depression #3--Y-Axis Scan

Integral of Phase Object Derivative

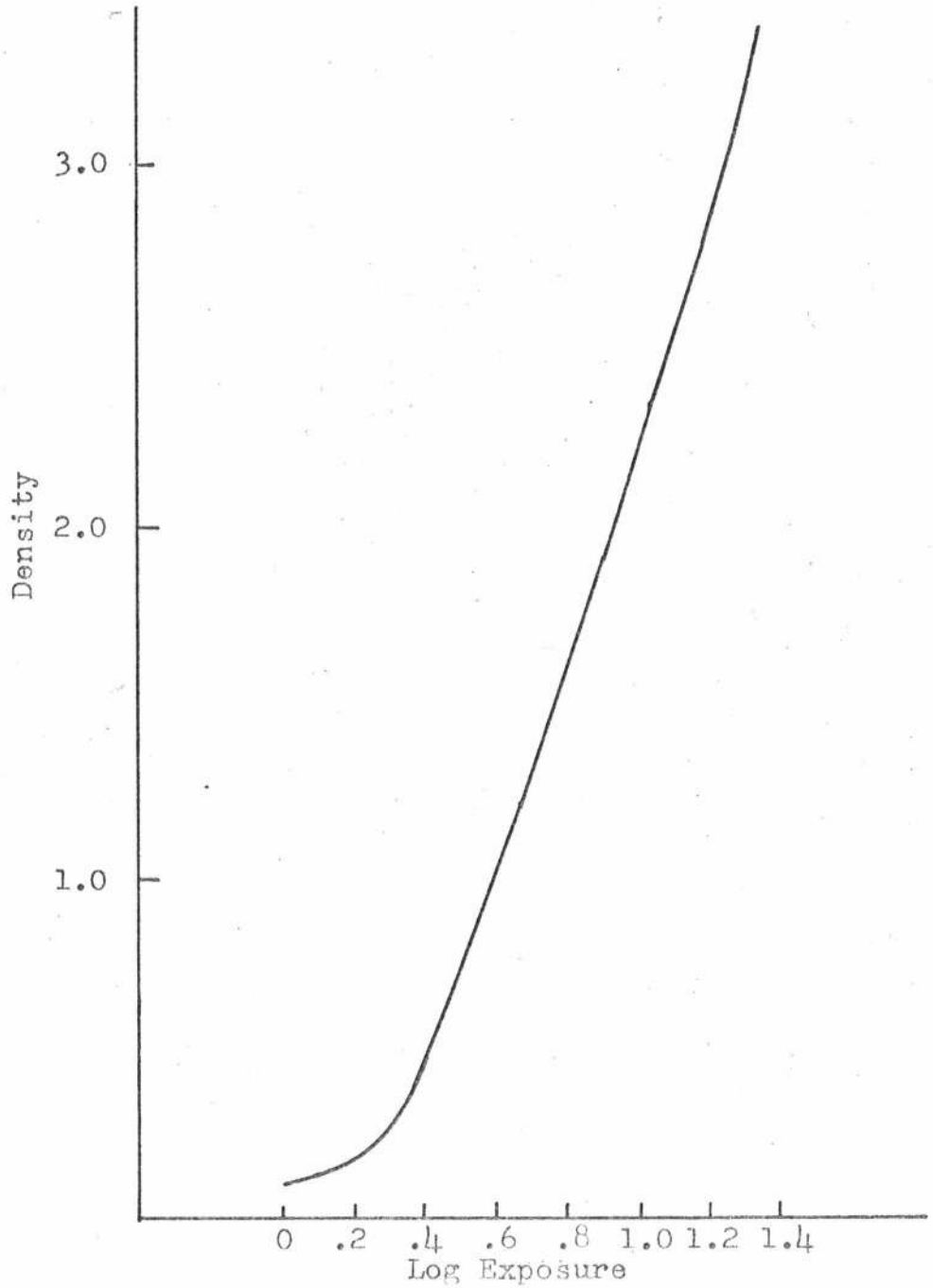

Callibration Curve

Integral of Phase Object Derivative

Circular Phase Depressions

Figure 4.40

The height difference between this line and the data values was then used to represent the actual exposure amplitude. The subtracted base lines are drawn with the amplitude traces in Figures 4.34 through 4.39. An identical normalization constant was chosen for all spot traces and the final results are drawn alongside the actual phase height measurements made with the interferometer in Figures 4.41 through 4.46. These traces show that the phase readout process is not at all binary but exhibits a continuous amplitude response from zero through a number of wavelengths.

Graded Phase Steps

The phase of the series of graded steps was measured with the interference microscope attachment. Several pictures were taken (Figure 4.47), each one overlapping the next so that a continuous phase trace could be made. One single trace was then recorded as the solid line in Figure 4.51.

The image exposure was also measured; the density trace is Figure 4.48, the callibration D vs. LogE curve is Figure 4.49 and the amplitude trace is Figure 4.50. This amplitude trace is seen to have a constant median bar height, the total bar height increasing from one step to the next. The base level of the bars decreases slowly as a broad randomly varying function superimposed on a linear taper. This randomly varying function could arise from image noise or thickness variations in the glass backing of the phase target. Since the

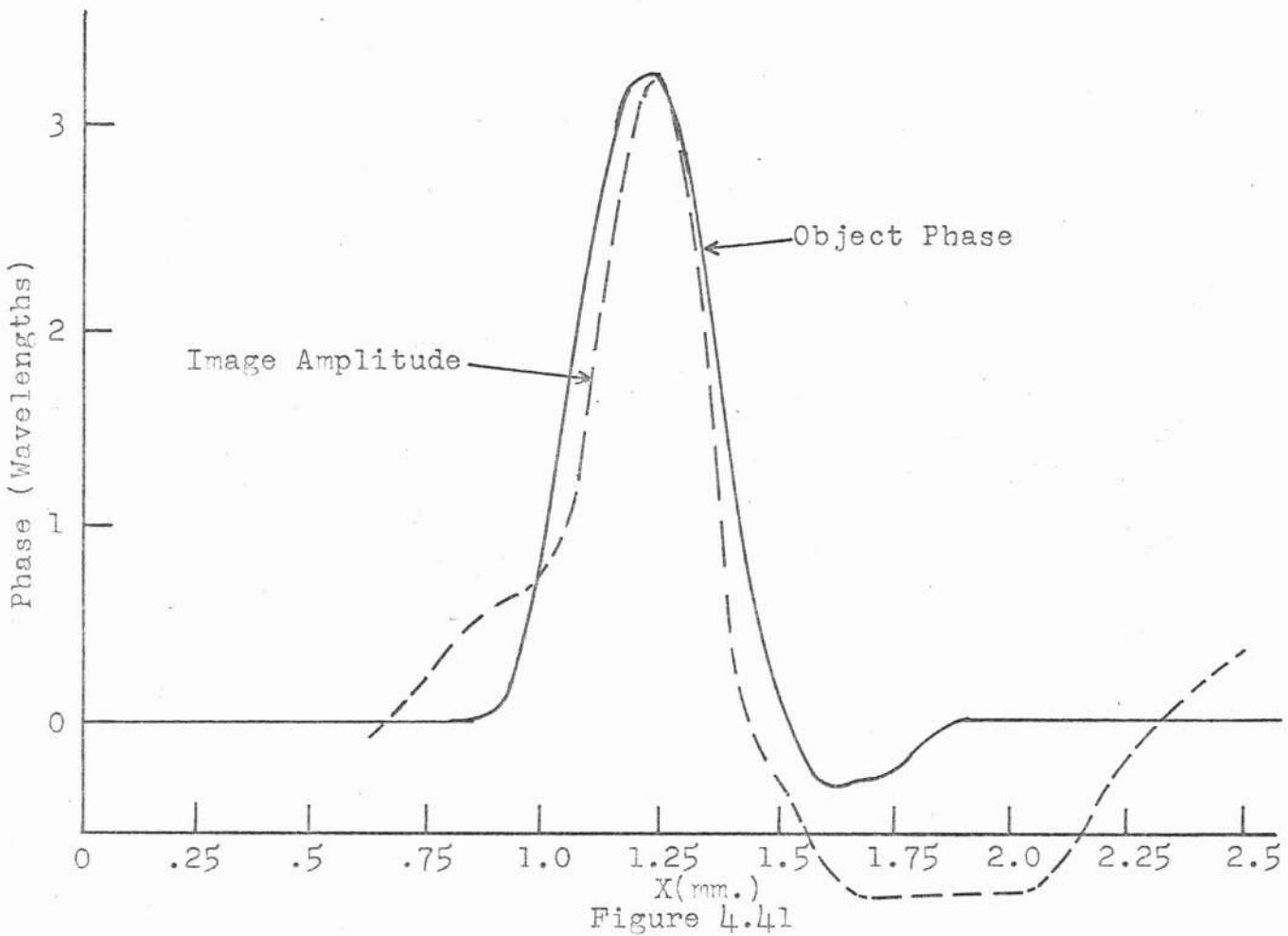

Figure 4.41

Comparison of Image Amplitude With Object Phase

Circular Phase Depression #1

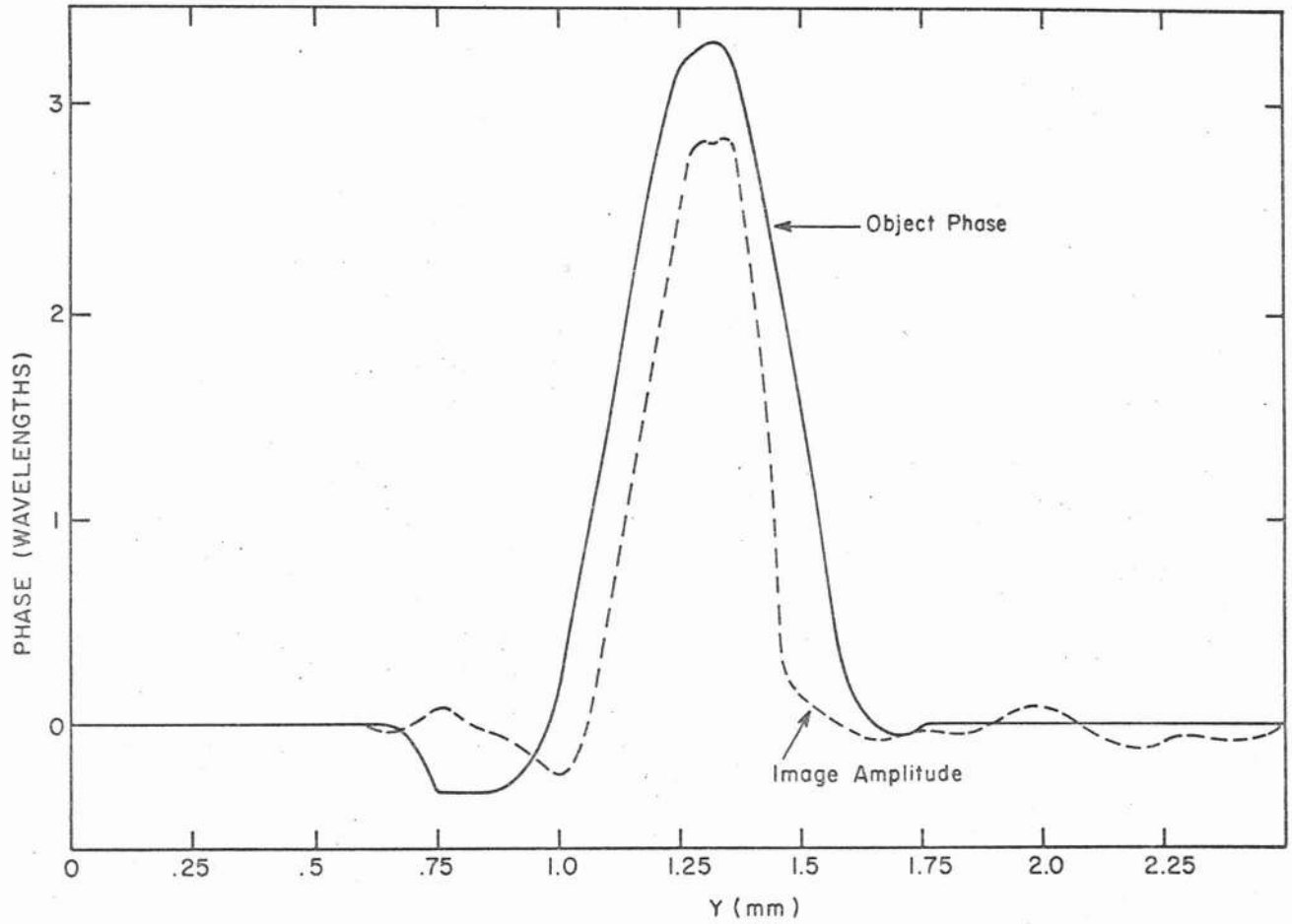

Figure 4.42

Comparison of Image Amplitude With Object Phase

Circular Phase Depression #1

Y-Axis Scan

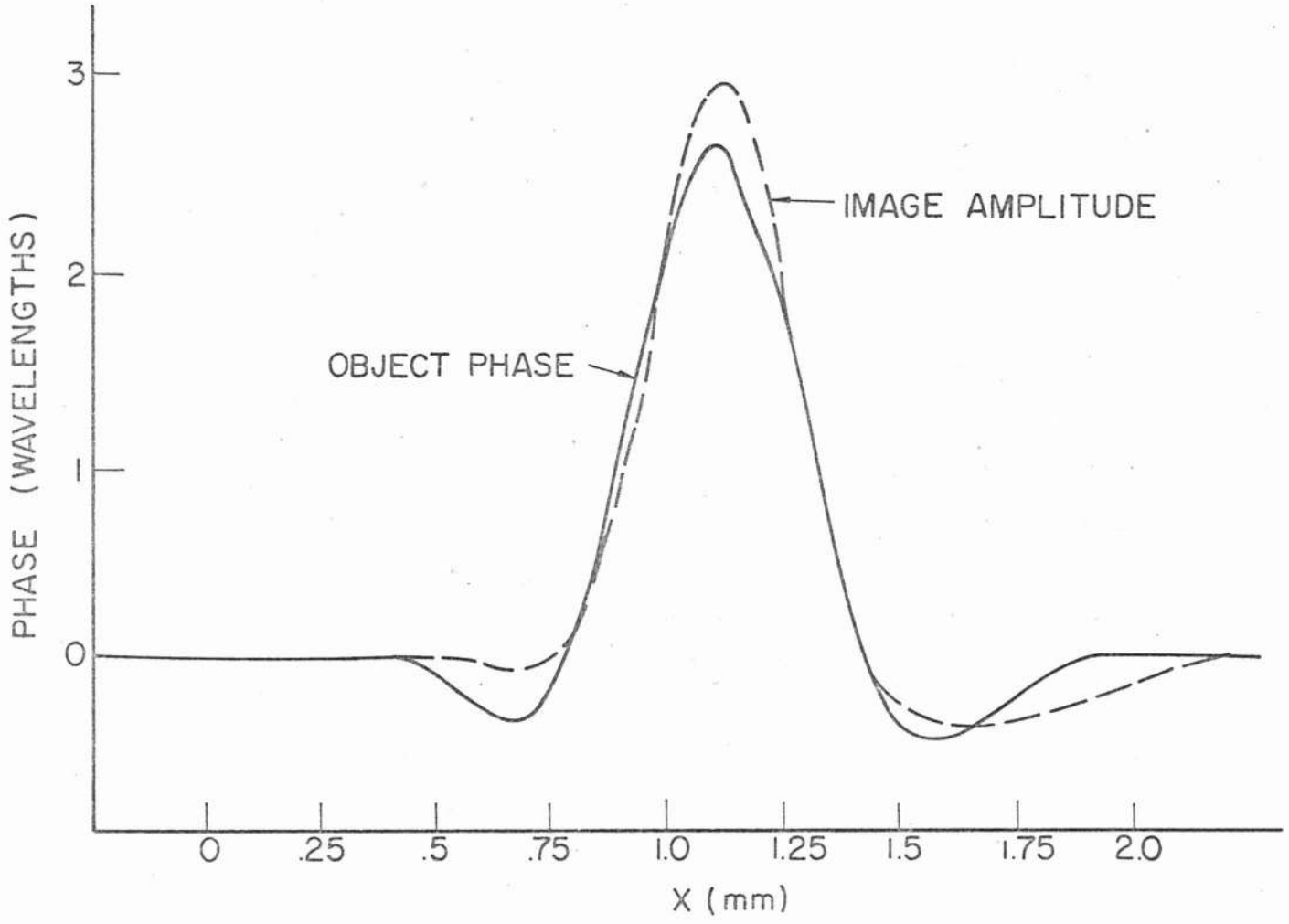

Figure 4.43

Comparison of Image Amplitude With Object Phase--Circular Phase Depression #2

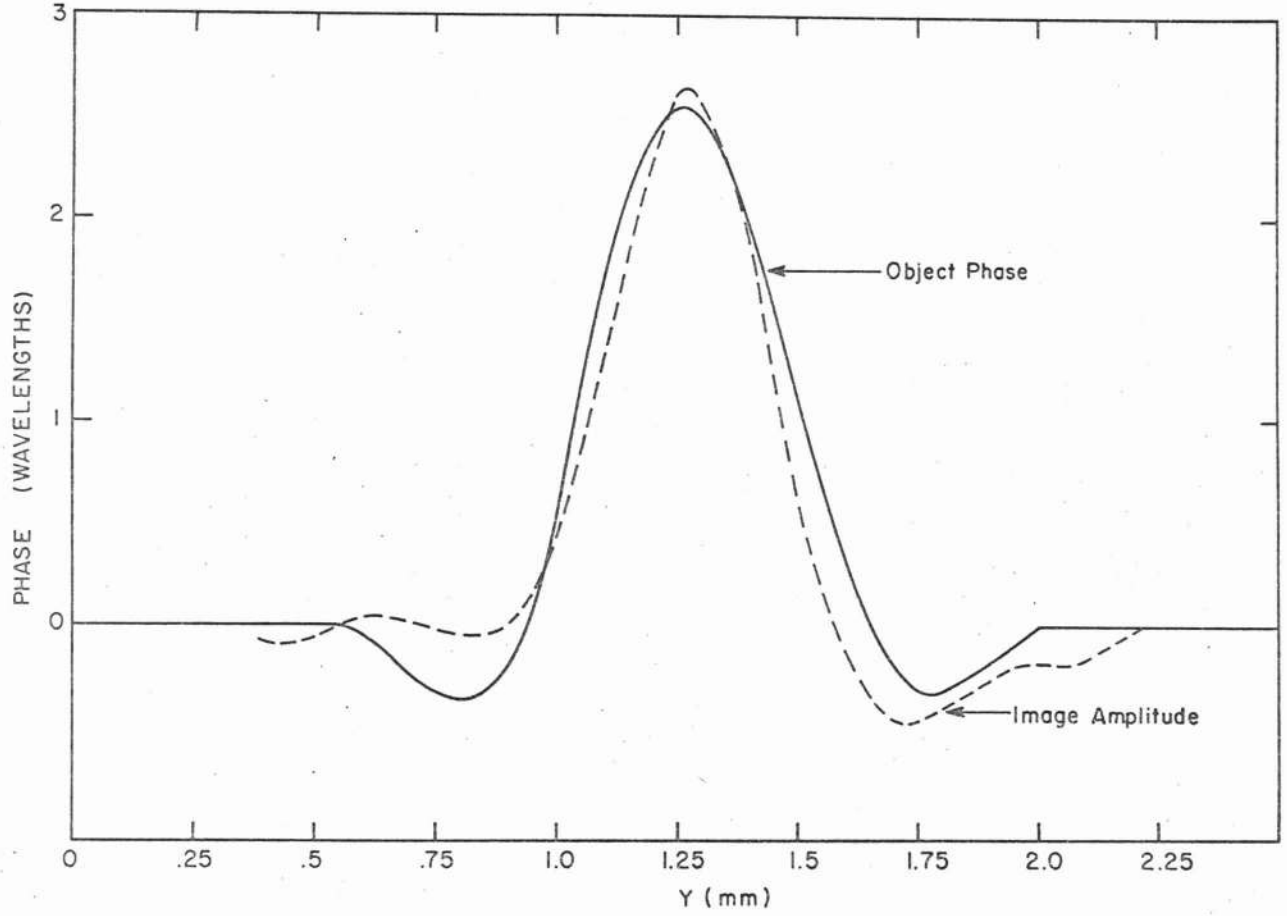

Figure 4.44

Comparison of Image Amplitude With Object Phase

Circular Phase Depression #2

Y-Axis Scan

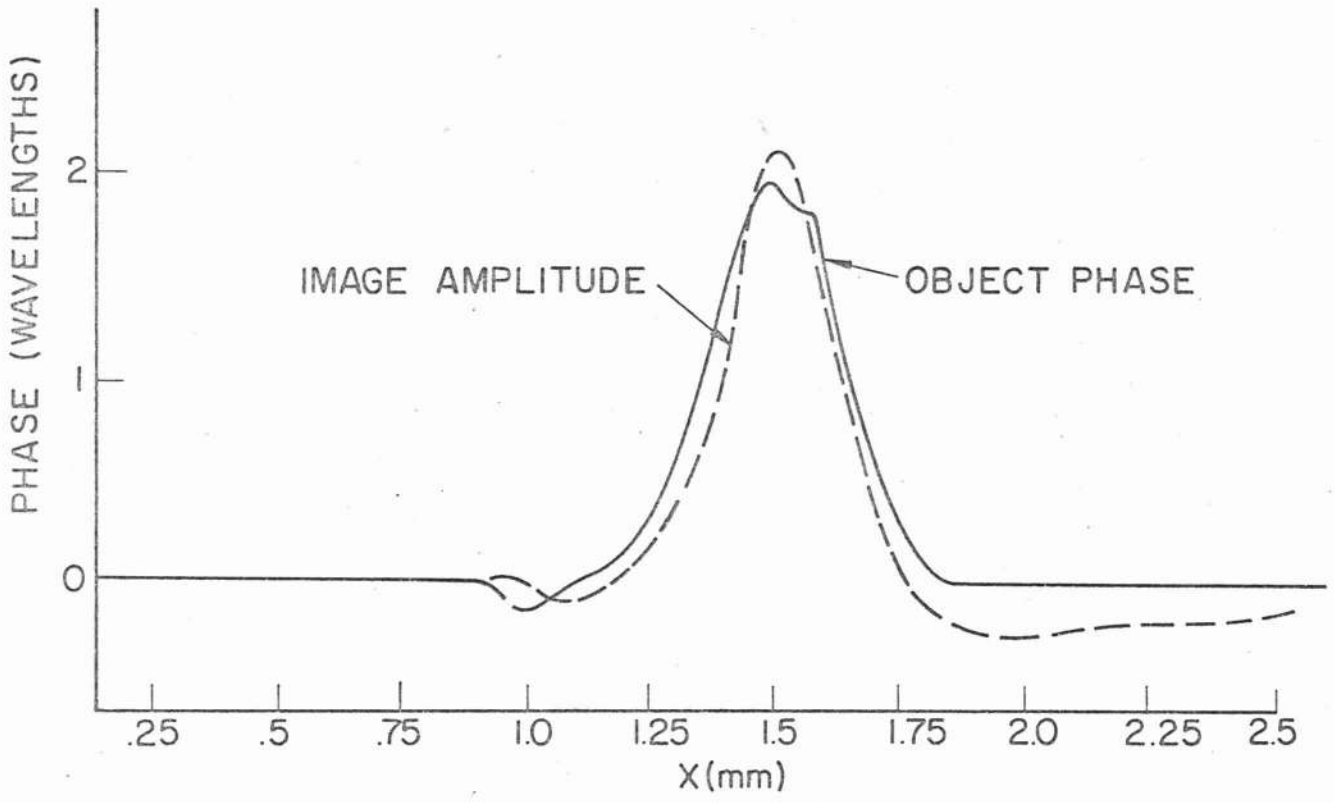

Figure 4.45

Comparison of Image Amplitude With Object Phase

Circular Phase Depression #3

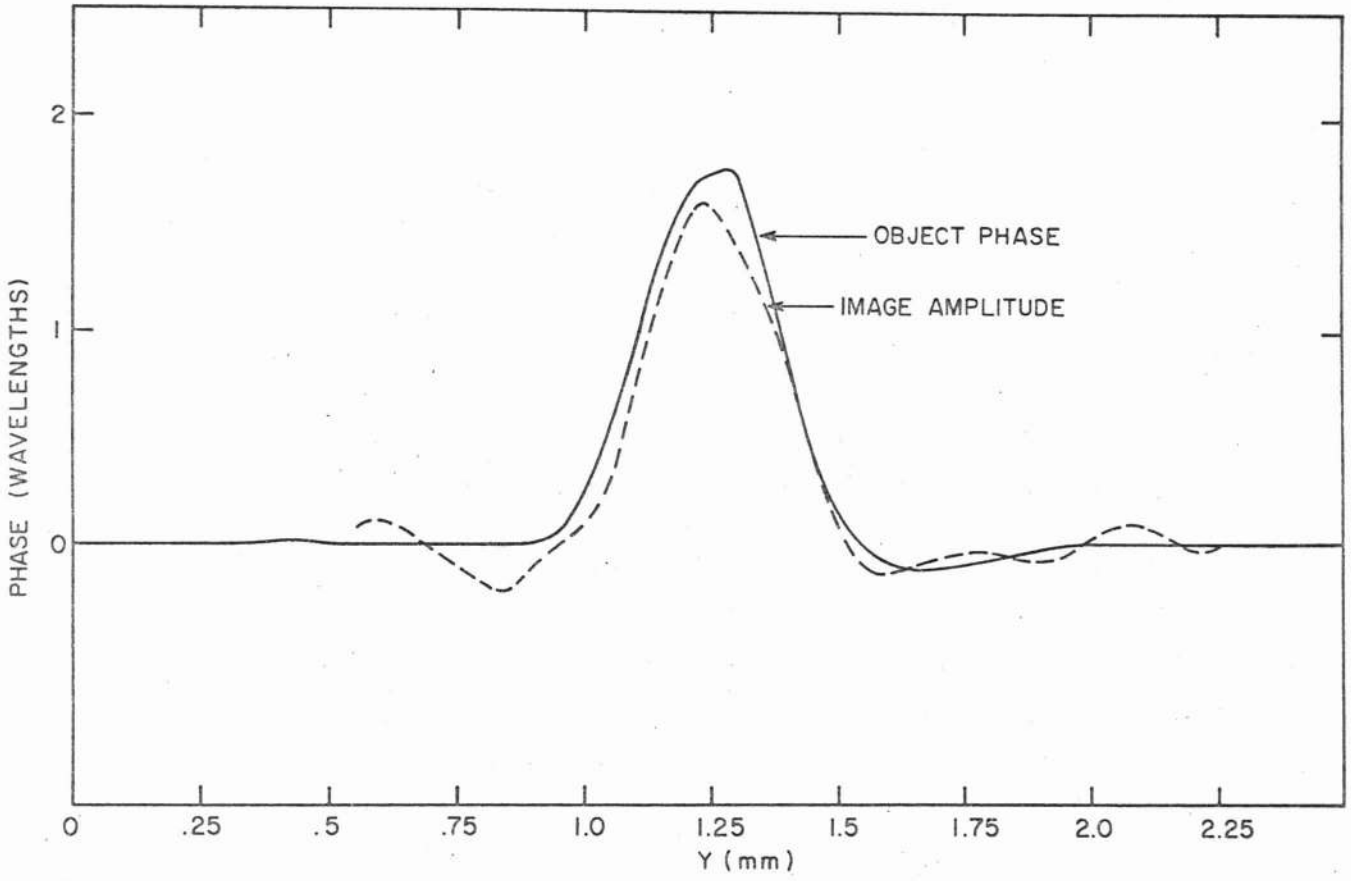

Figure 4.46

Comparison of Image Amplitude With Object Phase

Circular Phase Depression #3

Y-Axis Scan

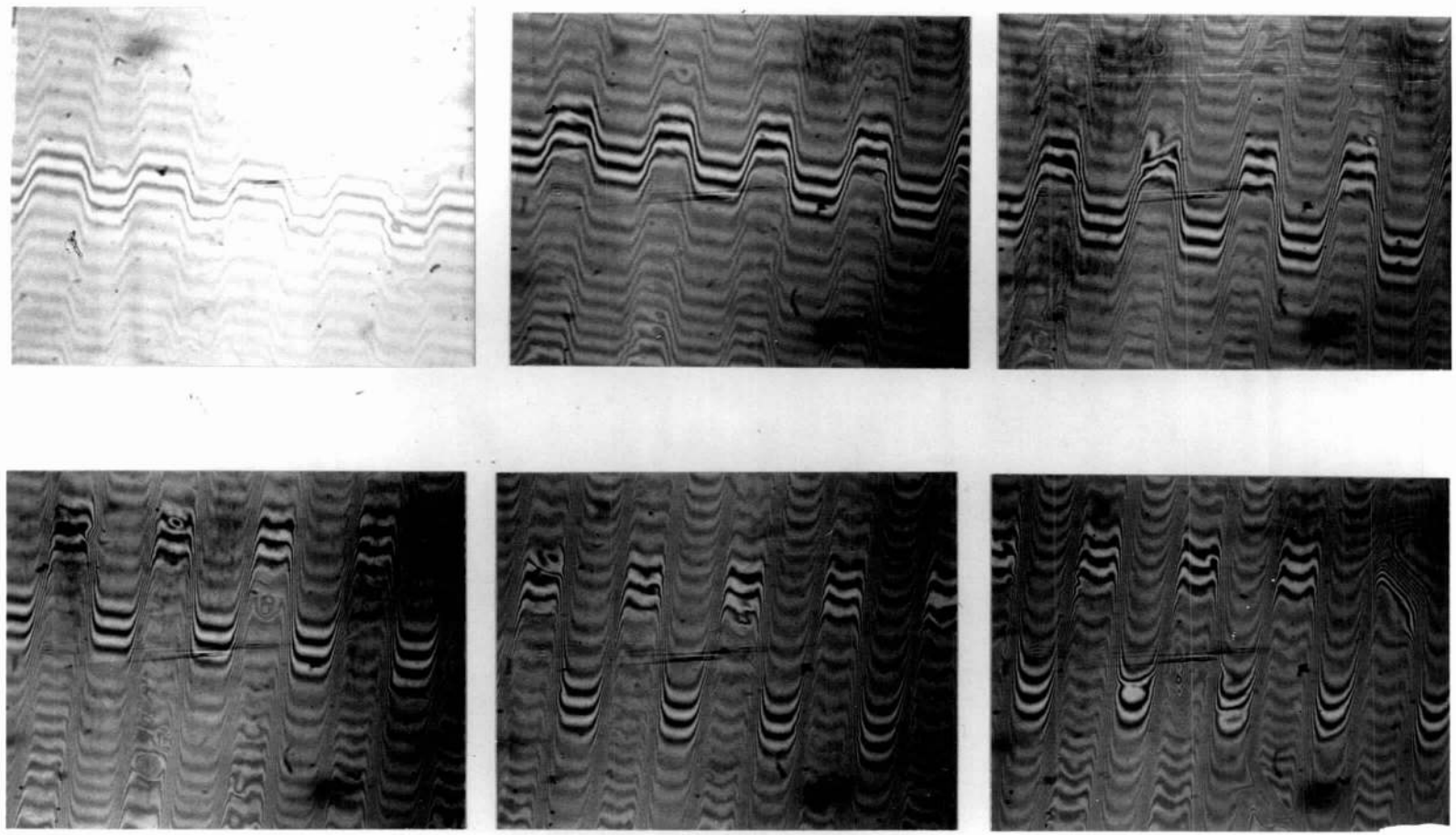

Figure 4.47

Interferometer Fringe Patterns

Graded Phase Steps

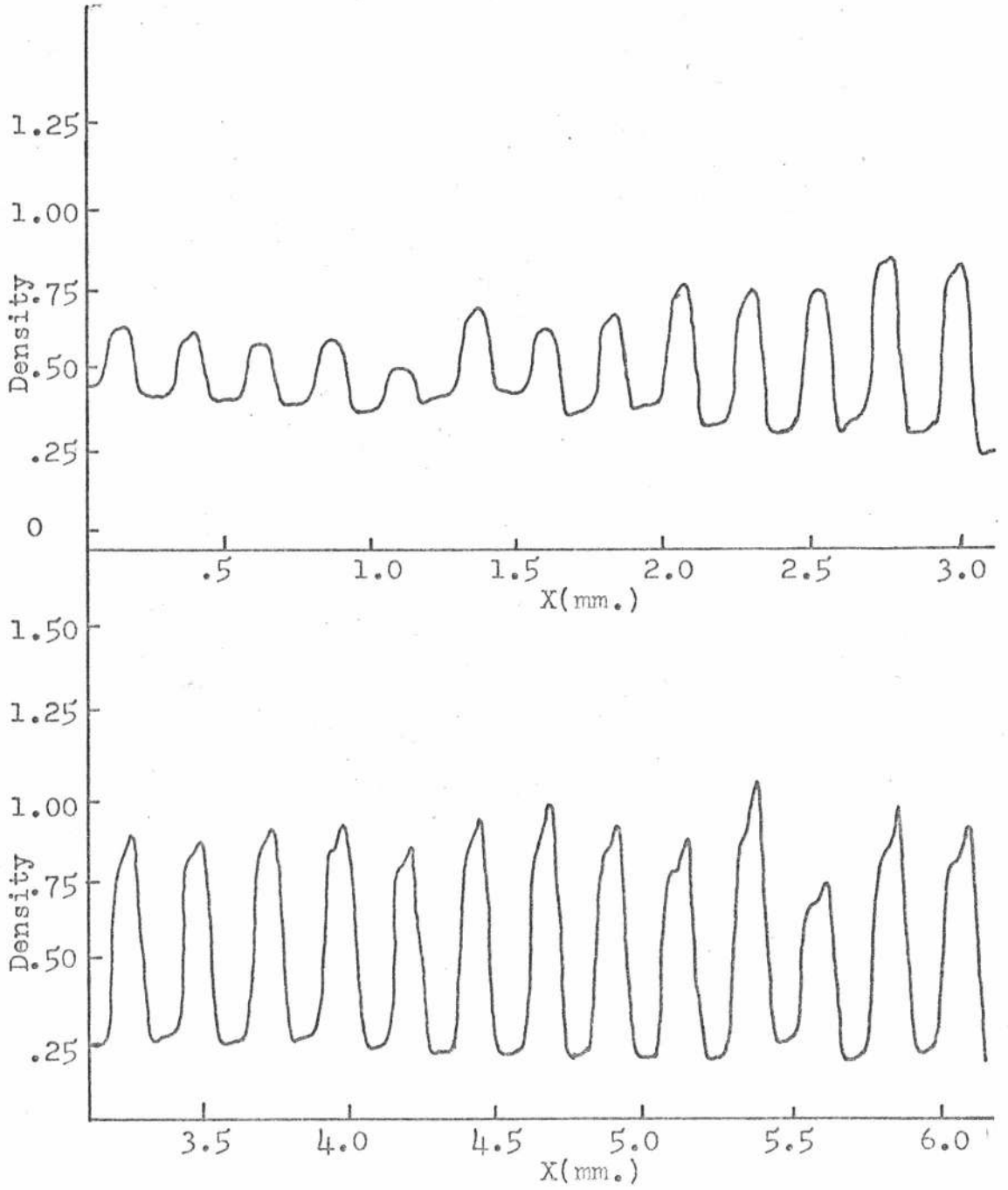

Densitometer Trace

Integral of Phase Object Derivative

Graded Phase Steps

Figure 4.48

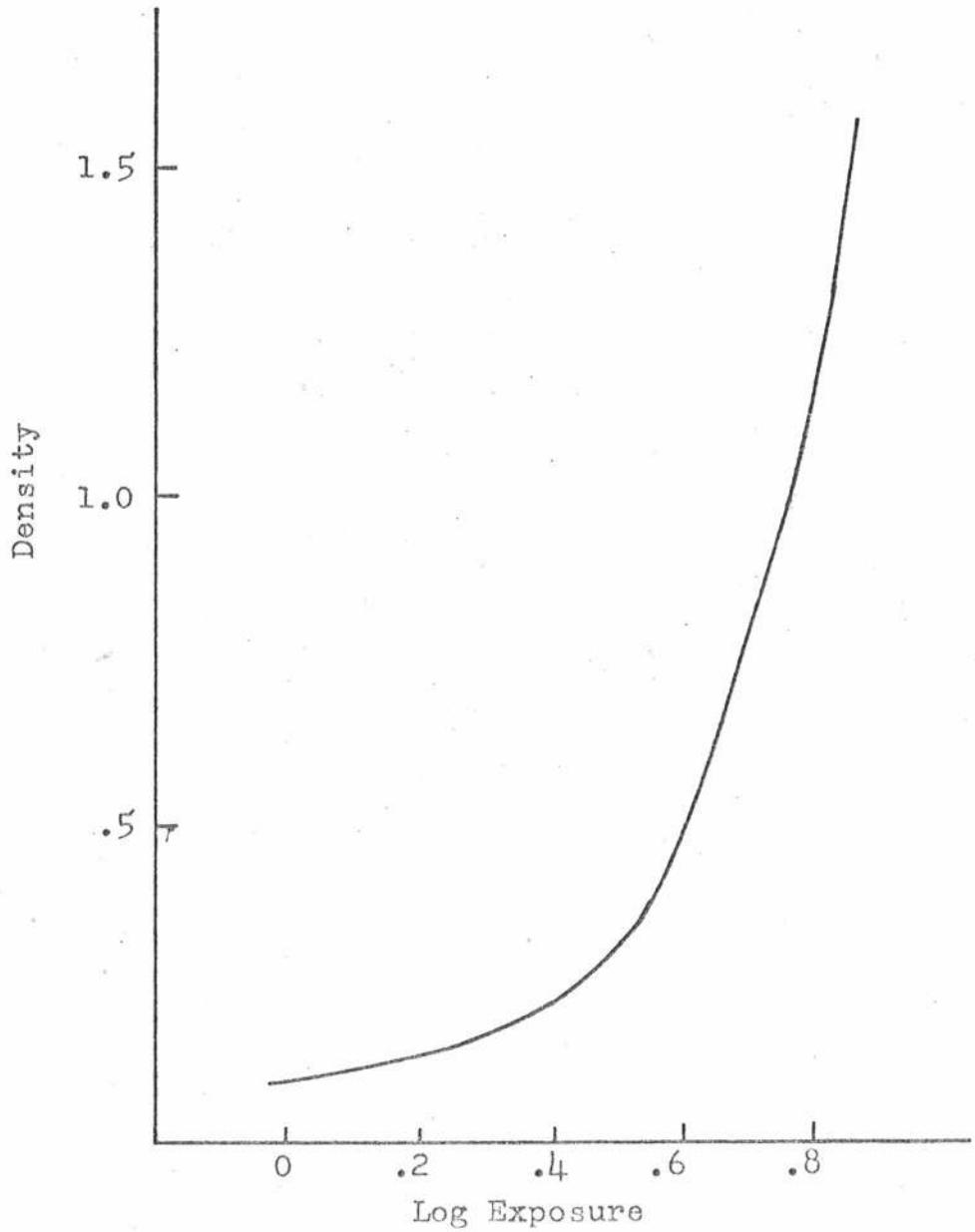

Callibration Curve

Integral of Phase Object Derivative

Graded Phase Steps

Figure 4.49

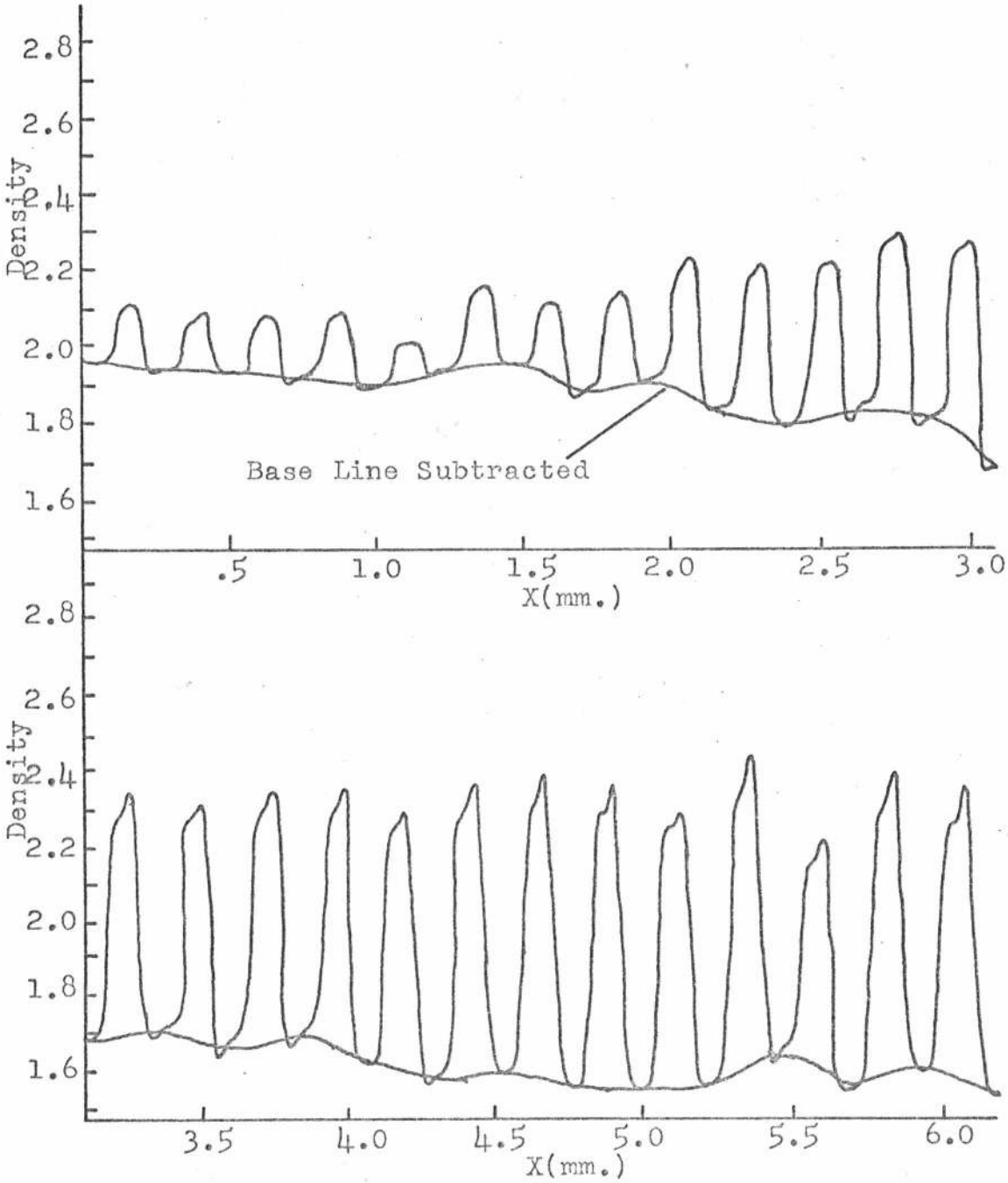

Image Amplitude

Integral of Phase Object Derivative

Graded Phase Steps

Figure 4.50

interferometer would measure neither of these effects, this random function has been subtracted out and the base of each bar set at zero for comparison with the phase trace. With the normalization constant determined, this amplitude trace is compared with the phase trace in Figure 4.51. The traces agree quite well with the exception of slight differences in bar height due to noise or failure to locate the density trace and the phase trace on the same position of each bar. This result especially shows that the photographic recording of the derivative was performed with the proper gamma.

Limitations of Coherent Differentiation

The phase object derivative of Figure 4.52 is an experimental verification of the limitations of coherent differentiation applied to phase objects as discussed in the analysis section. This derivative was formed from Phase Resolution Target #1 with a differentiation filter which extended over a range of ±30 lines/mm. (See Figure 3.4). The phase edges were too steeply sloped to be differentiated properly with the broad point spread function characteristic of this narrow filter. The same filter worked properly however, to give the results of Figure 4.18 for Phase Resolution Target #2, which had less steeply sloped edges. Although actual traces have not been made across the derivative of Figure 4.52, its appearance is quite similar to that represented in Figure 2.3c, which was calculated for approximately the same edge slope and point spread function. When a broader differentiation filter extending over ±60 lines/mm. was placed in the system, the correct derivative of Figure 4.5 was obtained.

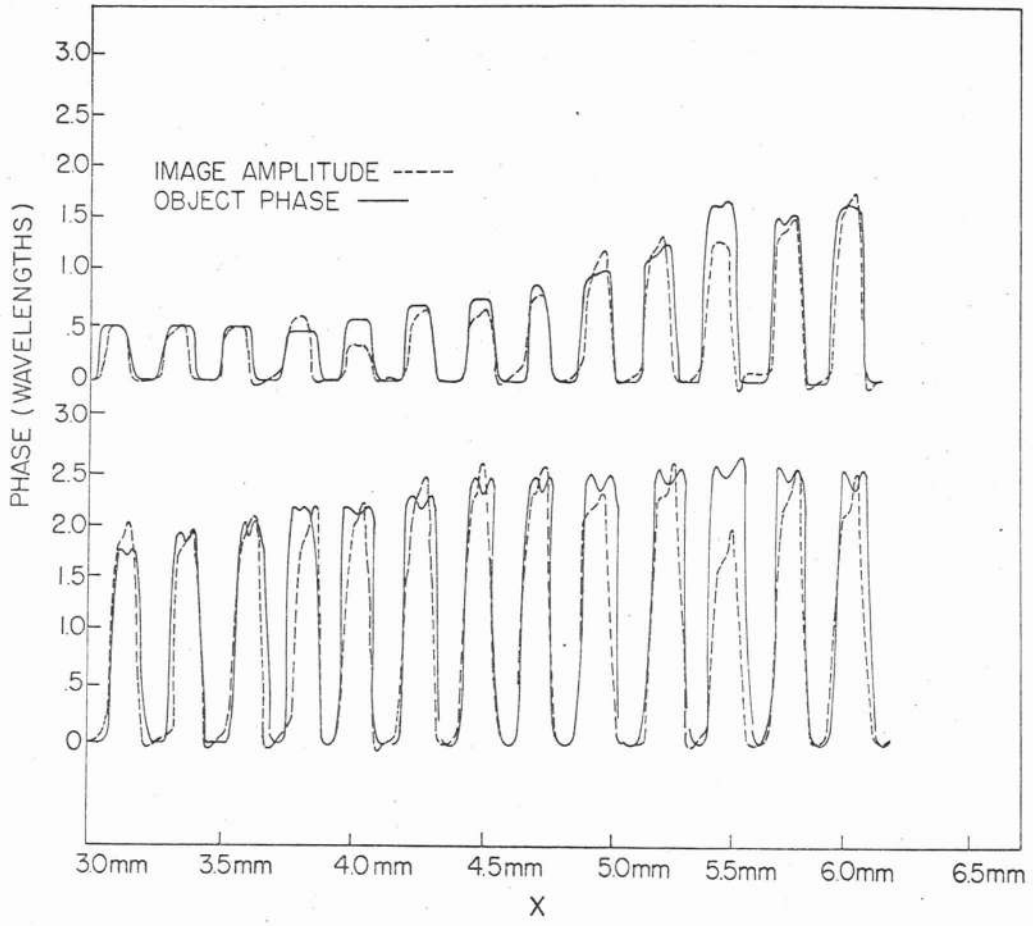

Figure 4.51

Comparison of Image Amplitude With Object Phase

Graded Phase Steps

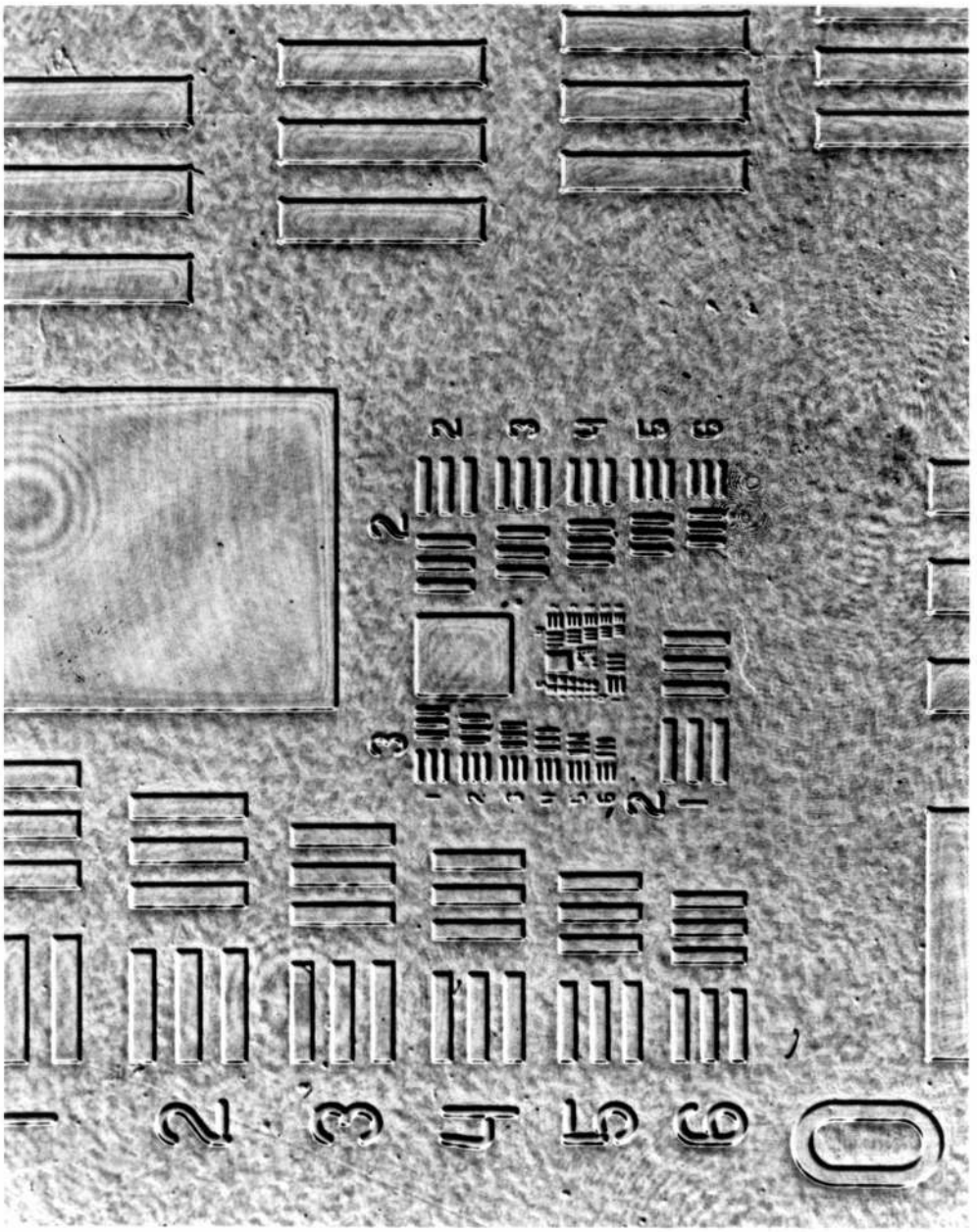

Figure 4.52

Phase Object Derivative Formed in Low Resolution System

Phase Resolution Target #1

Chapter V

Application To Microscopic Phase Object

Although the apparatus previously described was designed for a resolution range of 1 to 45 lines/mm., an attempt was made to observe a pure phase biological specimen. The specimen was a slide containing dragon fly liver cells immersed in water, an object which exhibited large phase variations. Differentiation was achieved by using the setup of Figure 5.1, in which a 96X microscope objective is used to form an enlarged image of the object. This image is used as the input to the differentiation system. The only additional alteration of the original system involves a displacement of the spatial filter to the new Fourier Transform plane, which is located where an image of the source is formed.

Diffraction-limited performance was difficult to achieve with this crude setup, so that substantial image amplitude variations were present even with no differentiation filter in the system. An attempt was made to remove these amplitude variations through photographic division as described on pages 30-31.

The experimental results are displayed in Figure 5.2 and Figure 5.3. Figure 5.2a is the original derivative $f_3(x_3)$ Figure 5.2b is $1/(a^2(x))^{\frac{1}{2}}$, and Figure 5.3a is the final phase object derivative. This last derivative (Figure 5.3a) was integrated to produce the result of Figure 5.3b. Although the

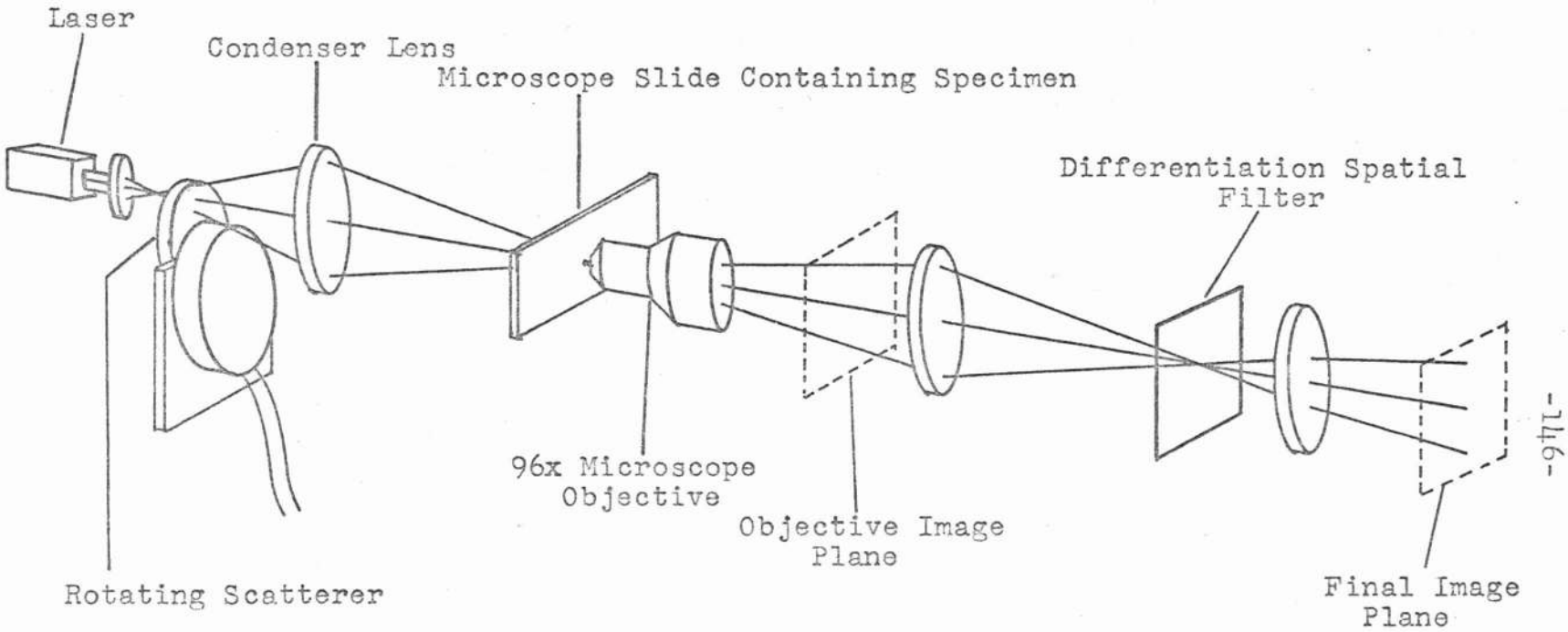

Figure 5.1

Microscope Setup For Differentiation

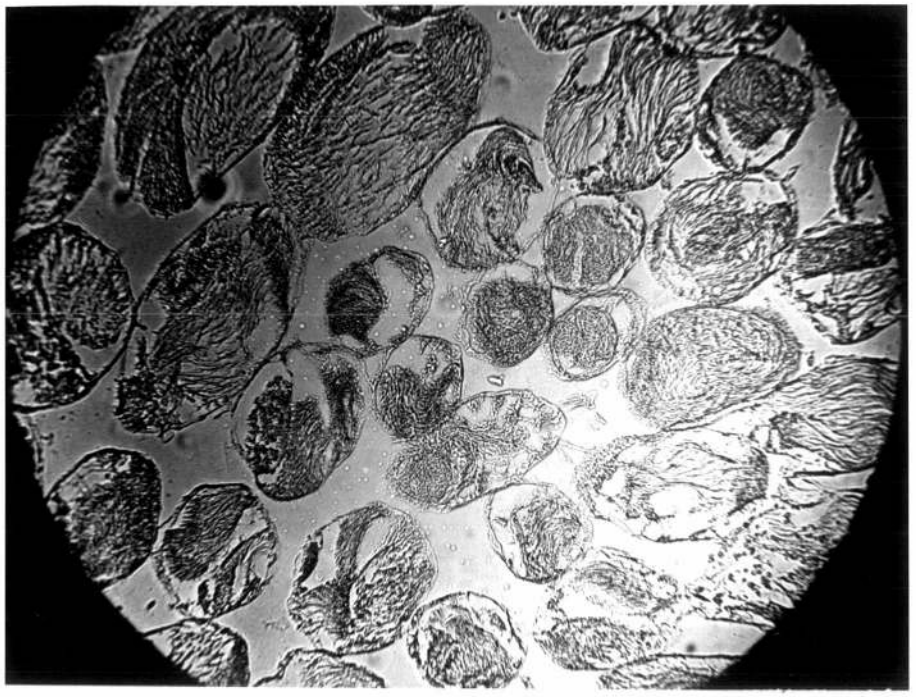

Figure 5.2a
Image With Differentiation Filter

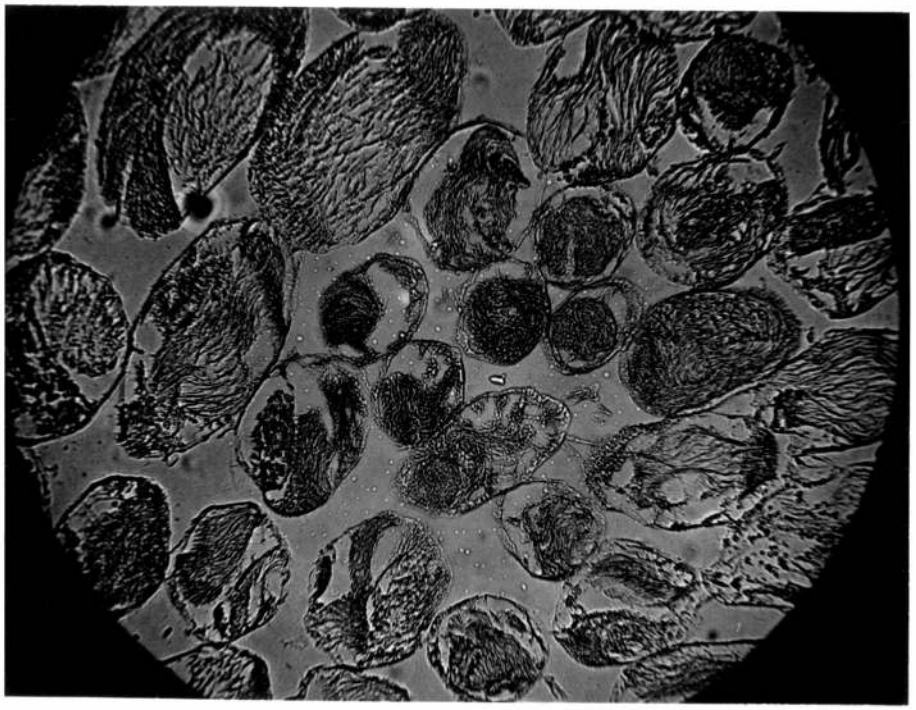

Figure 5.2b
Image Without Differentiation Filter

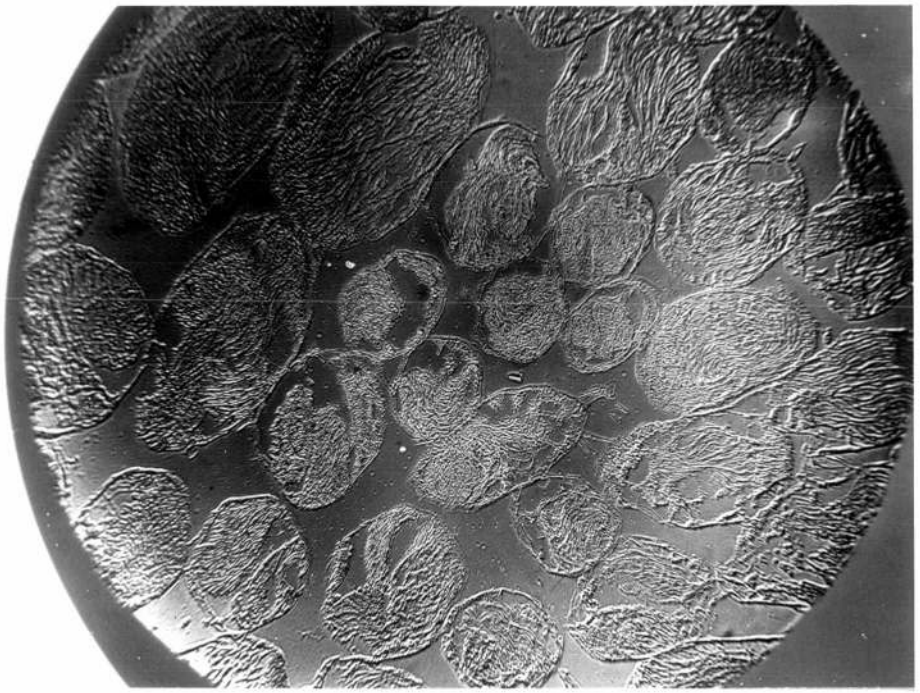

Figure 5.3a
Phase Object Derivative

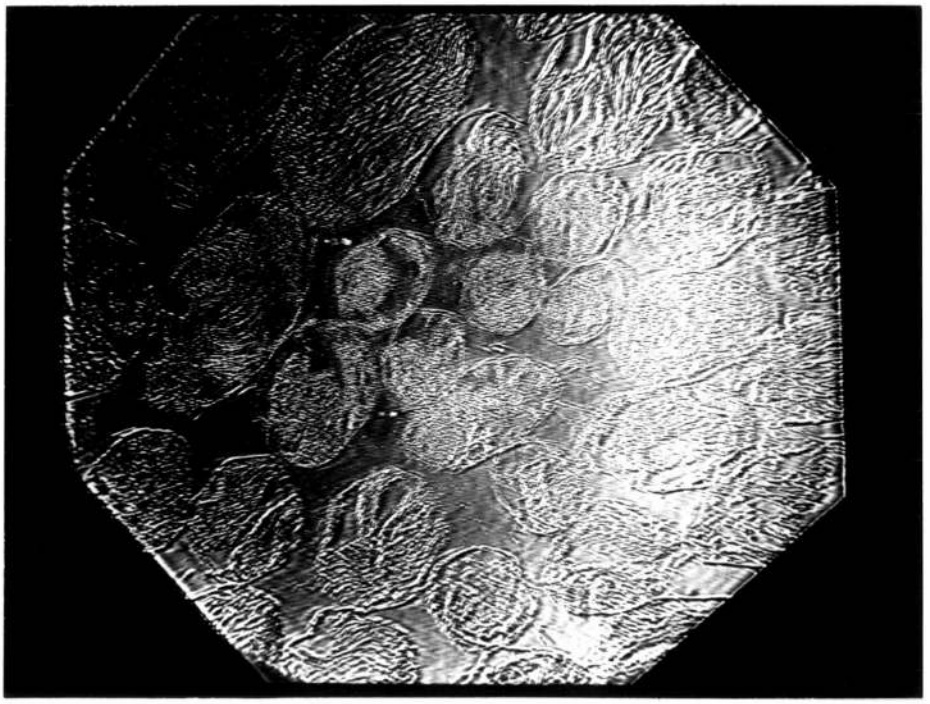

Figure 5.3b
Integral of Phase Object Derivative

shapes of the cells show up in this result, the picture is considerably blurred. This blurring arises from extraneous amplitude terms in the derivative. When these terms are imaged with the broad point spread function of the integration system, they appear very blurred in the final image. This problem could be considerably lessened in a number of ways which are described in Chapter VI, but this work was felt to be beyond the scope of this thesis.

Chapter VI

Future Work

Improvement of Present System

The experience gained in doing this experiment has generated a number of ideas of ways in which it could be improved. One simple improvement would be the use of multilayer antireflection coatings on the elements of the first lens of the integration apparatus. This would eliminate the necessity to tilt the optical flat to prevent light reflected off the aluminum strip from back-scattering into the system. Although tilting this flat introduces no third order aberrations if the tilt is small (as it was for this system), residual fifth order aberrations are still present.

The spatial filters could be made through thin film coating rather than photographic recording. These thin film filters would be less grainy than the photographic film, introducing less noise into the system. A greater dynamic range in transmission could also be achieved allowing for a greater spatial frequency range. Production of the thin film filters could be accomplished by evaporating aluminum onto a glass substrate. Thickness variations in the aluminum coating could be produced by using the evaporation analogue of the knife edge shadowing technique used to produce the photographic integration filter.

In the enlarging setup used for the microscopic work,

the object Fourier Transform lies not in a plane but on a curved surface. Because of this, it may be advantageous to form the spatial filter on a curved glass which contours this surface. It is intuitively felt that since the differentiation filter has a slowly varying transmittance function, its failure to lie on the curved transform surface will not significantly alter the filtering operation. However, further theoretical analysis of this situation would be useful.

One very significant problem with the apparatus used was curvature of field in the image plane caused by the high magnification. Since a flat photographic plate was used to record the derivative, a significant portion of the image may have been out of focus. Although this field curvature was perhaps not large enough to cause focus problems for incoherent light, when coherent illumination is used the focus criterion becomes very severe. To circumvent this problem it will be necessary to either record the derivative on film contoured to fit the curved field or to restrict viewing to a narrow region of the field. Another alternative is to design the optical system to give a very flat field.

A wide source could be substituted for the point source. This will not only increase the system resolution but will also help to remove noise. In addition, use of a wide source would significantly alleviate the problem of out-of-focus phase variations in the object. These out-of-focus

variations introduce image amplitude variations which somewhat obscure the phase function derivative. These extraneous amplitude variations would be considerably smoothed with a broader source. Since the broadening of this source limits the coherence of the system, the requirement on its maximum size must be that the coherence function in the object plane be broader than the extent of the image area over which interference is desired. Remembering from the shearing interferometer analogy that this region has a width equal to that of the unfiltered system point spread function, the requirement on the source size is that its image not overfill the objective aperture. This is hardly surprising, as overfilling the aperture is a rule of thumb for incoherent imaging. To form a good contrast image, the source should be considerably smaller than this limit.

The monochromatic laser source may be replaced with a broad-band white light lamp. This will alleviate the problem with out-of-focus portions of the phase object, reduce optical noise, and also render the image considerably easier to view and interpret. Since each spectral element of the source forms its own coherent image, the action of the differentiation filter will not be affected. Achromatic optics will of course be necessary.

Optical differentiation is limited in application to phase variations of less than a wavelength across the width of the point spread function. For this reason, it is very important that imaging be achieved in a near-diffraction-limited

situation with as high a numberical aperture as possible. A high resolution objective should be used, with low magnification achieved through use of a low power eyepiece. Because of the critical focus position characteristic of coherent systems, a very fine focus should also be available.

One final improvement which may be made involves the sample preparation. Since out-of-focus portions of the phase object is one of the major limitations of the system, great care should be taken that the samples are as thin as possible. The samples will still be very large phase of course, but should be physically quite thin. The same techniques used in sample preparation for phase contrast work are applicable.

Additional Techniques

This thesis has attempted to analyze in detail one technique for quantitative visualization of large-variation phase objects. Since the conception of this idea, several other possible techniques for achieving the same result have become evident.

Video Integration

One of the drawbacks of the present system is the necessity to expose a photographic plate, develop it, make a contact print, and reimage this in the final system. It is desirable to achieve the same end result in real time without the necessity to wait for photographic development. Unfortunately, this can not be done entirely optically because an

intermediate nonlinear process is required between the differentiation and integration steps. This nonlinear process could be effected by introducing a moving scatterer in the image plane of the differentiation system. The resulting intensity distribution transmitted by the scatterer could then be integrated incoherently by convolving it with a knife edge. However, incoherent convolution of this sort has poor resolution.

Another more promising possibility is the use of a video system to obtain the nonlinear process. If the derivative image is allowed to fall on the surface of a vidicon, the output signal will be proportional to the derivative intensity. This signal may be fed into an electronic integrating circuit and the output used to modulate a scanning electron beam. This beam can then be used to scan an emulsion or a phosphor surface (TV) to provide the desired output. If the TV is used, this output may be seen in real time. Electronic integration circuits are commercially available, as they are widely used in analogue computers. The only drawback of this system is the use of electronic video apparatus with its characteristic limitations in grey scale and resolution. However, the real time aspect of such a system is very attractive.

Differentiation With A Shearing Microscope

It was noted in the introduction that the shearing interference microscope exhibits an image amplitude proportional to the derivative of the object phase. This image could be recorded on film and used as the input to a coherent optical

integration system or integrated using a video system. Although the apparatus involved is much more complicated and difficult to adjust than a simple differentiation filter, it has several advantages over it. First, because interference microscopes are production items, no detailed development work is required for the first stage process. Second, since the amount of shear can be varied at will, the fundamental limitation of the spatial filter technique to not-too-rapidly varying phase objects could perhaps be overcome. Whether the additional variability obtained surmounts the difficulty of adjustment in the use of this technique will depend upon the actual class of objects to be studied and upon the sensitivity of the instrument.

Holographic Integration

The integration process may also be performed in a different manner with the aid of an extra photographic step. The ideal spatial filter to perform integration has the transmittance $t(x_4) = D/x_4$. An amplitude distribution proportional to this function may be created simply by forming the Fourier Transform of a half wave phase step. Because of this, the integration procedure may be performed in the following way. The derivative is recorded on photographic film to produce a transparency whose amplitude transmittance is

$$t(x_3, y_3) = \phi_x'(x_3, y_3) + \frac{x_0}{f}. \qquad (6.1)$$

When this transparency is placed in the front focal plane of a

lens, a half wave phase step is placed next to it, and both are illuminated with a plane wave, the amplitude distribution in the Fourier Transform plane will be

$$f_4(x_4, y_4) = C\left[\tilde{\Phi}_x'(x_4, y_4) + \frac{x_0}{f}\delta(x_4)\delta(y_4)\right] + \frac{i}{2\pi x_4}\, e^{i\frac{k x_4 B}{f}} \quad . \tag{6.2}$$

$B = x_3$ coordinate location of the phase edge

The intensity distribution is the square modulus of this.

$$\begin{aligned} I_4(x_4, y_4) = C^2 \left| \tilde{\Phi}_x'(x_4, y_4) + \frac{x_0}{f}\delta(x_4)\delta(y_4)\right|^2 + \frac{1}{4\pi^2 x_4^2} \\ + \frac{iC}{2\pi x_4}\left[\tilde{\Phi}_x'(x_4, y_4) + \frac{x_0}{f}\delta(x_4)\delta(y_4)\right] e^{i\frac{k x_4 B}{f}} \\ - \frac{iC}{2\pi x_4}\left[\tilde{\Phi}_x'(x_4, y_4) + \frac{x_0}{f}\delta(x_4)\delta(y_4)\right] e^{-i\frac{k x_4 B}{f}} \end{aligned} \tag{6.3}$$

The fourth term of this intensity is

$$I_4(x_4, y_4) = -\frac{iC}{2\pi x_4}\left[\tilde{\Phi}_x'(x_4, y_4) + \frac{x_0}{f}\delta(x_4)\delta(y_4)\right] e^{-i\frac{k x_4 B}{f}} \quad . \tag{6.4}$$

When this intensity is recorded on film with $\gamma = 2$, the amplitude transmittance is proportional to the intensity except that the delta functions are density saturated. When the transparency is placed back in the focal plane and illuminated with a plane wave, the Fourier Transform of the fourth term is

$$f_5(x_5, y_5) = \frac{iC}{2\pi}\left[\Phi(x_5 - B, y_5) + F\right]. \quad F = \text{constant} \tag{6.5}$$

This is the desired phase function image centered about the

point (B, 0,). If the spatial extent of ϕ is less than $\pm B/2$, this term will be spatially separated from the other image terms. This is a pseudo-holographic technique because the phase step Fourier Transorm is added to the phase function derivative Fourier Transform, and the cross product formed by photographic recording.

This technique has the disadvantage that it requires another photographic step. It also has the problem that the Fourier Transforms $\tilde{\phi}'_x(x_4, y_4)$ and $i/2\pi x_4$ vary over a wide range of values, so that it will be difficult to expose entirely in the linear region of the film D vs. logE curve. (This problem might be circumvented by also adding a large plane reference wave.) This technique has the advantage that the function $i/2\pi x_4$ is formed automatically to within the limitations set by the point spread function of the lens, without any truncation except that due to film saturation.

Phase Compensation

The differentiation system produces an image amplitude distribution of the form

$$f_3(x_3, y_3) = \left(\phi'_x(-x_3, -y_3) + \frac{x_0}{f}\right) e^{ik\phi(-x_3, -y_3)} . \qquad (6.6)$$

In the present system, the phase portion of this term is removed by photographic recording. The phase portion may also be removed by holographic compensation. If the differentiation filter is removed from the system and a direct image of the

phase object is formed, the image amplitude is

$$f_3(x_3, y_3)_{\text{no filter}} = e^{ik\phi(-x_3,-y_3)}. \tag{6.7}$$

Holographic recording of this phase function will produce a transparency having the transmittance

$$t(x_3,y_3) = R^*R + 1 + R^* e^{ik\phi(-x_3,-y_3)} + Re^{-ik\phi(-x_3,-y_3)}. \tag{6.8}$$

R = reference wave

If the differentiation filter is now replaced in the system, the derivative of the phase object is formed in the image plane, and this hologram is placed in the image plane, the amplitude transmitted by the hologram will be

$$f_3(x_3,y_3)_t = \left(\phi_x'(-x_3,-y_3) + \frac{x_0}{f}\right) e^{ik\phi(-x_3,-y_3)}\, t(x_3,y_3). \tag{6.9}$$

Since the fourth term of the hologram transmittance is the complex conjugate of the phase function, it cancels the phase variation to give

$$f_3(x_3,y_3)_{t\,(4^{\text{th}}\text{ term})} = \left(\phi_x'(-x_3,-y_3) + \frac{x_0}{f}\right) R. \tag{6.10}$$

If the reference is an off axis plane wave, this term will be spatially separated from the others in the Fourier Transform plane. It can thus be separated out and used as the direct input to the integration system.

This technique of phase compensation has two desirable features: Firstly, the only photographic recording is holographic, so that the processing control required is considerably relaxed compared to that necessary to give $\gamma = 1$. Since a large reference is added to make a hologram, the limited dynamic range of the film is no problem. Secondly, no certain value of the bias level X_o is required to make the derivative positive definite as it was in the original system, because no photographic recording of the derivative is required. The major limitation of this technique lies in the alignment of the hologram recording to exactly cancel the phase function. This could be a significant problem if any emulsion shrinkage is involved.

Holographic Subtraction

The same linear relationship between image amplitude and object phase may be produced through two-wavelength holographic subtraction. If an image plane hologram of the phase object is recorded with illumination having a wave number $k+\Delta k$ and an off-axis reference, the resulting hologram transmittance will be

$$t(x,y) = \left| a e^{i(k+\Delta k)\phi(x,y)} + b e^{i(k+\Delta k)x\sin\theta} \right|^2$$

$$= a^2 + b^2 + ab e^{i(k+\Delta k)(\phi(x,y) - x\sin\theta)} + ab e^{-i(k+\Delta k)(\phi(x,y) - x\sin\theta)} . \qquad (6.11)$$

a, b = relative amplitudes of object and reference beams

When this hologram is illuminated with a plane wave reconstruction beam of wave number k at an angle θ' and the image produced is superimposed on that of the phase object itself, the resulting amplitude distribution is

$$a(x,y) = Ce^{i\delta} e^{ik\phi(x,y)} - \left[a^2+b^2+abe^{i(k+\Delta k)(\phi(x,y)-x\sin\theta)} + ab\, e^{-i(k+\Delta k)(\phi(x,y)-x\sin\theta)}\right] e^{+ikx\sin\theta'}. \tag{6.12}$$

C = relative amplitude of direct image

δ = relative phase shift of direct image

The reconstruction beam angle θ' may be chosen to satisfy

$$k\sin\theta' = (k+\Delta k)\sin\theta. \tag{6.13}$$

The first and 3rd fourth terms of this amplitude distribution then reduce to

$$a_{1,4}(x,y) = \left[Ce^{i\delta} - abe^{i\Delta k\,\phi(x,y)}\right] e^{ik\phi(x,y)}. \tag{6.14}$$

Since the wavelength difference between the hologram exposure and the final illumination is arbitrary, it may be chosen small enough that

$$\Delta k\,\phi(x,y) << 2\pi \tag{6.15}$$

for any particular phase variation $\phi(x,y)$. With this choice of Δk, the exponential may be approximated as

$$e^{i\Delta k\,\phi(x,y)} \simeq 1 + i\,\Delta k\,\phi(x,y) \tag{6.16}$$

so that

$$a_{1,4}(x,y) = [C\cos\delta - ab + i(C\sin\delta - ab\,\Delta k\,\phi(x,y))]e^{ik\phi(x,y)} \quad (6.17)$$

a, b, δ, and C may now be chosen to give

$$C\cos\delta - ab = 0, \quad ab = C\cos\delta. \quad (6.18)$$

δ is chosen to make $\sin\delta \gg \cos\delta$ so the resulting image intensity will be

$$I_{1,3}(x,y) \simeq C^2[\sin^2\delta - 2\sin\delta\cos\delta\,\Delta k\,\phi(x,y)] \quad (6.19)$$

The phase object has thus been imaged as an intensity variation with a one-to-one correspondence between image intensity and object phase.

This technique is easy to implement because techniques for holographic subtraction have been developed.[40] It has the additional advantage that the resolution limitations which apply to the differentiation technique may not apply here. The only disadvantage of this technique is that for microscopic work, the resolution problems which arise from coherent speckle become significant. This is the same limitation which applies to any form of holographic microscopy.

Evanescent Readout

One additional technique for imaging of large-variation phase objects relates to surface relief contour phase objects

only. This technique is called evanescent readout. It involves the use of frustrated total internal reflection to read off a relieved surface contour as an amplitude variation across a plane wavefront.

When a plane wave is totally internally reflected from a plane boundary, the amplitude distribution at the surface has two components. One is a traveling wave, which constitutes the reflected beam, and the other is an exponentially decaying field on the opposite side of the boundary. If a refracting or absorbing surface is placed near the outside of this boundary within a few wavelengths of it, a portion of the totally internally reflected light will be absorbed or refracted at this surface so that the amplitude of the reflected beam is reduced. The amount of amplitude reduction is proportional to the separation of the two surfaces.

If a relieved surface contour is placed against the boundary, an amplitude distribution related to this surface contour will be superimposed on the totally internally reflected plane wave. The exact functional relationship between the reflected amplitude distribution and the surface contour depends on the surface composition. However, the relation tends to be exponential. This is useful because the relief height of a photographic emulsion is approximately proportional to the logarithm of the film transmission. Because of this the reflected amplitude distribution will be similar to that which

would result from passing the beam through the film.

This technique may be useful because it allows the input of photographic information to a coherent system. Since the light need not pass through the film,not only is an index matching oil bath not needed, but scattering within the emulsion will not be a problem. Low noise performance may be expected with the additional advantage that large amounts of data may be processed in a short time since an oil bath is not required. This could be particularly valuable for high resolution work such as holographic data storage.

References

1 W. H. Steel, Interferometry (Cambridge University Press, London, 1967).

2 R. L. Lamberts, Thesis--Measurement of Complex Amplitude Transmission (University of Rochester, 1969).

3 Melvin Horman, "An Application of Wavefront Reconstruction to Interferometry," Appl. Opt. 4, 333 (1965).

4 Olaf Bryngdahl, "Shearing Interferometry by Wavefront Reconstruction," J. Opt. Soc. Am. 58, 865-71 (1968).

5 R. E. Brooks, "Phase Visualization Using a Reconstructed Reference Beam," Appl. Opt. 8, 2351-3 (1969).

6 L. H. Tanner, "Some Applications of Holography in Fluid Mechanics," J. Sci. Inst. 43, 81-3 (1966).

7 L. O. Heflinger, R. F. Wuerker, and R. E. Brooks, "Holographic Interferometry," J. Appl. Phys. 37, 642 (1966).

8 B. P. Hildebrand and K. A. Haines, "Multiple-Wavelength and Multiple-Source Holography Applied to Contour Generation," J. Opt. Soc. Am. 57, 155 (1967).

9 J. Zelenka and J. Varner, "A New Method for Generating Depth Contours Holographically," Appl. Opt. 7, 2107 (1968).

10 J. Zelenka and J. Varner, "Multiple Index Holographic Contouring," Appl. Opt. 8, 1431-4 (1969).

11 O. Bryngdahl and A. W. Lohmann, "Interferograms are Image Holograms," J. Opt. Soc. Am. 58, 141 (1968).

12 Olaf Bryngdahl, "Longitudinally Reversed Shearing Interferometry," J. Opt. Soc. Am. 59, 142 (1969).

13 Kazuya Matsumoto and Matsuo Takashima, "Phase Difference Amplification by Nonlinear Holograms," J. Opt. Soc. Am. 60, 30-3 (1970).

[14] R. Bernard and J. C. Gacon, "Frequency Modulation and Spatial Filtering Applied to Photographing of Phase Objects," Nature 222, 664-5 (1969).

[15] G. B. Brandt, "Hologram Moire Interferometry for Transparent Objects," Appl. Opt. 6, 1535-40 (1967).

[16] E. Wolf, "Three Dimensional Structure Determination of Semi-transparent Objects from Holographic Data," Opt. Comm. 1, 153-6 (1969).

[17] William H. Carter, "Computational Reconstruction of Scattering Objects from Holograms," J. Opt. Soc. Am. 60, 306-14 (1970).

[18] Koichi Swata and Ryo Nagata, "Calculation of Three Dimensional Refractive Index Distribution from Interferograms," J. Opt. Soc. Am. 60, 133-5 (1970).

[19] Dandliker and Weiss, "Reconstruction of the Three Dimensional Refractive Index from Scattered Waves," Opt. Commun. 1, 323-8 (1970).

[20] Paul D. Rowley, "Quantitative Interpretation of Three-Dimensional Weakly Refractive Phase Objects Using Holographic Interferometry," J. Opt. Soc. Am. 59, 1496-8 (1969).

[21] John Develis and George Reynolds, Theory and Applications of Holography (Addison-Wesley, Reading, 1967), pp.166-8.

[22] John W. Waddell and Jennie W. Waddell, "Color Schlieren," Res. and Developm. 21, 30-2 (1970).

[23] Serge Lowenthal and Yves Belvaux, "Observations of Phase Objects by Optically Processed Hilbert Transform," Appl. Phys. Let. 11, 49-51 (1967).

[24] Dennis Gabor and George Stroke, "Reconstruction of Phase Objects by Holography," Nature 208, 1159 (1965).

[25] W. G. Alwang, L. A. Cavanaugh, and D. Cain, "Observation of Three-Dimensional Shadowgraphlike Images in Holography of Phase Objects," Appl. Opt. 8, 1256-7 (1969).

[26] A. F. Belozerov, "Production of a Shearing Interferogram and

Schlieren Pictures of an Optical Inhomogeneity From a Singly Exposed Hologram," Optics and Spectroscopy 27, 187-8 (1969).

[27] T. Tsuruta, "Hologram Schlieren and Phase-Contrast Methods," Japan J. Appl. Physics 8, 96-103 (1969).

[28] M. Francon, Progress in Microscopy, (Pergamon Press, Evanston, 1961).

[29] L. C. Martin, The Theory of the Microscope (American Elsevier Publishing Co., Inc., New York, 1966).

[30] A. Bennet, H. Jupink, H. Osterberg, O. Richards, Phase Microscopy (John Wiley and Sons, New York, 1951).

[31] M. Francon, Revue d'Optique (Paris, 1950).

[32] B. O. Payne, "Principles and Applications of Phase Contrast Microscopy," Research and Development 21, 47-50 (1963).

[33] John Develis and George Reynolds, op. cit., pp. 161-2.

[34] Ronald Eguchi and Frederick Carlson, "Coherent Optical Gradient System," Technical Report No. 127 (University of Washington, Department of Electrical Engineering, Seattle, 1968).

[35] J. H. Altman, "Pure Relief Images on Type 649F Plates," Applied Optics 5, 1689 (1966).

[36] J. C. Kent, "Fabrication of Graded Filters for Knife-Edge Replacement in Laser Schlieren Optical Systems," Appl. Opt. 8, 2148-9 (1969).

[37] Bruce Burdick (Eastman Kodak Co.), Private Communication.

[38] C. E. Thomas, "Coherent Optical Noise Suppression," Appl. Opt. 7, 517-22 (1968).

[39] Gary Sommargren (University of Rochester), Private Communication.

[40] K. Bromley, M. A. Monahan, J. F. Bryant, B. J. Thompson, "Holographic Subtraction," Appl. Opt. 10, 174 (1971).

Appendix I

Image of Phase Object Derivative in Integration System

An integration by parts which will be useful throughout this appendix is first calculated

$$\text{Let} \quad u = \int_D^A \frac{\sin \frac{k}{f}(X_5+X_3)X_4}{X_4}\, dX_4 \qquad dv = f'(X_3)dX_3$$

$$du = \frac{k}{f}\int_D^A \cos\frac{k}{f}(X_5+X_3)X_4\, dX_4 \qquad v = f(X_3)$$

$$= + \left.\frac{\sin\frac{k}{f}(X_5+X_3)X_4}{X_5+X_3}\right|_D^A$$

$$= + \left(\frac{\sin\frac{k}{f}(X_5+X_3)A - \sin\frac{k}{f}(X_5+X_3)D}{X_5+X_3}\right)$$

$$= + \frac{kA}{f}\,\mathrm{sinc}\left(\frac{k}{f}(X_5+X_3)A\right) - \frac{kD}{f}\,\mathrm{sinc}\left(\frac{k}{f}(X_5+X_3)D\right)$$

$$\int_{-F}^{F} f'(X_3)dX_3 \int_D^A \frac{\sin\frac{k}{f}(X_5+X_3)X_4}{X_4}\, dX_4 = f(F)\int_D^A \frac{\sin\frac{k}{f}(X_5+F)X_4}{X_4}\, dX_4$$

$$- f(-F)\int_D^A \frac{\sin\frac{k}{f}(X_5-F)X_4}{X_4}\, dX_4 - \frac{k}{f}\int_{-F}^{F} f(X_3)\left[A\,\mathrm{sinc}\frac{k}{f}(X_5+X_3)A - D\,\mathrm{sinc}\frac{k}{f}(X_5+X_3)D\right]$$

$$= f(F)\left[\mathrm{Si}\left(\frac{k}{f}(X_5+F)A\right) - \mathrm{Si}\left(\frac{k}{f}(X_5+F)D\right)\right]$$

$$- f(-F)\left[\mathrm{Si}\left(\frac{k}{f}(X_5-F)A\right) - \mathrm{Si}\left(\frac{k}{f}(X_5-F)D\right)\right]$$

$$- \frac{k}{f}\int_{-F}^{F} f(X_3)\left[A\,\mathrm{sinc}\left(\frac{k}{f}(X_5+X_3)A\right) - D\,\mathrm{sinc}\left(\frac{k}{f}(X_5+X_3)D\right)\right] dX_3$$

Term #1

$$\text{Term \#1} = 2iD\int_{-F}^{F}\frac{X_0}{f}\,dX_3\int_{D}^{A}\frac{\sin\frac{k}{f}(X_5+X_3)X_4}{X_4}\,dX_4$$

$$= \frac{2iDX_0}{f}\Bigg[F\Big\{Si\left(\tfrac{k}{f}(X_5+F)A\right)-Si\left(\tfrac{k}{f}(X_5+F)D\right)$$

$$+Si\left(\tfrac{k}{f}(X_5-F)A\right)-Si\left(\tfrac{k}{f}(X_5-F)D\right)\Big\}$$

$$-\frac{k}{f}\int_{-F}^{F}X_3\left[A\,\mathrm{sinc}\left(\tfrac{k}{f}(X_5+X_3)A\right)-D\,\mathrm{sinc}\left(\tfrac{k}{f}(X_5+X_3)D\right)\right]dX_3\Bigg]$$

$$\int_{-F}^{F}X_3\,\mathrm{sinc}\tfrac{k}{f}(X_5+X_3)A\,dX_3=\int_{-F}^{F}\frac{\sin\frac{k}{f}(X_5+X_3)A}{\frac{k}{f}A}\,dX_3$$

$$-X_5\int_{-F}^{F}\frac{\sin\frac{k}{f}(X_5+X_3)A}{\frac{k}{f}(X_5+X_3)A}\,dX_3$$

$$=-\left(\frac{f}{kA}\right)^2\left[\cos\tfrac{k}{f}(X_5+F)A-\cos\tfrac{k}{f}(X_5-F)A\right]$$

$$-\frac{f}{kA}X_5\left[-Si\left(\tfrac{k}{f}(X_5+F)A\right)-Si\left(\tfrac{k}{f}(X_5-F)A\right)\right]$$

$$\int_{-F}^{F}X_3\,\mathrm{sinc}\tfrac{k}{f}(X_5+X_3)D\,dX_3=-\left(\frac{f}{kD}\right)^2\left[\cos\tfrac{k}{f}(X_5+F)D-\cos\tfrac{k}{f}(X_5-F)D\right]$$

$$-\frac{f}{kD}X_5\left[Si\left(\tfrac{k}{f}(X_5+F)D\right)-Si\left(\tfrac{k}{f}(X_5-F)D\right)\right]$$

$$\text{Term \#1} = \frac{2iDX_0}{f}\Bigg[F\Big\{Si\left(\tfrac{k}{f}(X_5+F)A\right)-Si\left(\tfrac{k}{f}(X_5+F)D\right)$$

$$+Si\left(\tfrac{k}{f}(X_5-F)A\right)-Si\left(\tfrac{k}{f}(X_5-F)D\right)\Big\}$$

$$+\frac{Ak}{f}\left(\frac{f}{kA}\right)^2\left[\cos\tfrac{k}{f}(X_5+F)A-\cos\tfrac{k}{f}(X_5-F)A\right]$$

$$+X_5\left[Si\left(\tfrac{k}{f}(X_5+F)A\right)-Si\left(\tfrac{k}{f}(X_5-F)A\right)\right]$$

$$-\frac{Dk}{f}\left(\frac{f}{kD}\right)^2\left[\cos\tfrac{k}{f}(X_5+F)D-\cos\tfrac{k}{f}(X_5-F)D\right]$$

$$-X_5\left[Si\left(\tfrac{k}{f}(X_5+F)D\right)-Si\left(\tfrac{k}{f}(X_5-F)D\right)\right]\Bigg]$$

Term #2

$$\text{Term \#2} = 2iD\int_{-F}^{F}\Phi_x'(-X_3,-Y_3)\,dX_3\int_{D}^{A}\frac{\sin\frac{k}{f}(X_5+X_3)X_4}{X_4}\,dX_4$$

$$= 2iD\Big[-\Phi(-F,-Y_3)\Big\{Si\Big(\tfrac{k}{f}(X_5+F)A\Big)-Si\Big(\tfrac{k}{f}(X_5+F)D\Big)\Big\}$$

$$+\Phi(F,-Y_3)\Big\{Si\Big(\tfrac{k}{f}(X_5-F)A\Big)-Si\Big(\tfrac{k}{f}(X_5-F)D\Big)\Big\}$$

$$+\frac{k}{f}\int_{-F}^{F}\Phi(-X_3,-Y_3)\Big[A\,\mathrm{sinc}\tfrac{k}{f}(X_5+X_3)A-D\,\mathrm{sinc}\tfrac{k}{f}(X_5+X_3)D\Big]dX_3\Big]$$

Term #3

$$\text{Term \#3} = iB\int_{-F}^{F}\Phi_x'(-X_3,-Y_3)\,dX_3\int_{-D}^{D}e^{i\frac{k}{f}(X_5+X_3)X_4}\,dX_4$$

$$= 2iBD\int_{-F}^{F}\Phi_x'(-X_3,-Y_3)\,\mathrm{sinc}\tfrac{k}{f}(X_5+X_3)\,D\,dX_3$$

Term #4

$$\text{Term \#4} = iB\int_{-F}^{F}\frac{X_0}{f}\,dX_3\int_{-D}^{D}e^{i\frac{k}{f}(X_5+X_3)X_4}\,dX_4$$

$$= \frac{2iBDX_0}{f}\int_{-F}^{F}\frac{\sin\frac{k}{f}(X_5+X_3)D}{\frac{k}{f}(X_5+X_3)D}\,dX_3$$

$$= \frac{2iBX_0}{k}\Big[Si\Big(\tfrac{k}{f}(X_5+F)D\Big)-Si\Big(\tfrac{k}{f}(X_5-F)D\Big)\Big]$$

Appendix II

Point Spread Function of Differentiation System

$A_d(x,y)$ = Point spread function of filtered aperture

$t_d(x',y') = \alpha(X_o - X')$ = Aperture filter amplitude transmittance

X_o = Constant

(x',y') = Aperture coordinates

k = Wave number of illumination

f = Focal length of lenses

(x,y) = Image plane coordinates

A = Aperture half width (square aperture)

$$A_d(x,y) = \int_{-A}^{A} dx' \int_{-A}^{A} dy'\, t_d(x',y')\, e^{i\frac{k}{f}(xx'+yy')} = \alpha \int_{-A}^{A} dx' \int_{-A}^{A} dy' (X_o - X')\, e^{i\frac{k}{f}(xx'+yy')}$$

$$= 2\alpha A \operatorname{sinc}\left(\frac{kAy}{f}\right)\left[X_o \int_{-A}^{A} e^{i\frac{kxx'}{f}} dx' - \int_{-A}^{A} x' e^{i\frac{kxx'}{f}} dx'\right]$$

$$= 2\alpha A \operatorname{sinc}\left(\frac{kAy}{f}\right)\left[2X_o A \operatorname{sinc}\left(\frac{kAx}{f}\right) - \int_{-A}^{A} x' e^{i\frac{kxx'}{f}} dx'\right]$$

The integral may be calculated through integration by parts.

Let $u = x'$ $\qquad dv = e^{i\frac{kxx'}{f}}$

$du = dx'$ $\qquad v = \dfrac{e^{i\frac{kxx'}{f}}}{i\frac{kx}{f}}$

$$\int_{-A}^{A} x' e^{i\frac{kxx'}{f}} dx' = \frac{x'f}{ikx} e^{i\frac{kxx'}{f}}\Big|_{-A}^{A} - \frac{f}{ikx}\int_{-A}^{A} e^{i\frac{kxx'}{f}} dx'$$

$$= \frac{2A^2}{i} \operatorname{cosinc}\left(\frac{kAx}{f}\right) - \frac{2A^2}{i} \frac{\sin\left(\frac{kxA}{f}\right)}{\left(\frac{kxA}{f}\right)^2}$$

$$A_d(x,y) = 4\alpha A^3 \operatorname{sinc}\left(\frac{kAy}{f}\right)\left[\frac{X_o}{A} \operatorname{sinc}\left(\frac{kAx}{f}\right)\right.$$

$$\left. + i\left(\operatorname{cosinc}\left(\frac{kAx}{f}\right) - \frac{\sin\left(\frac{kAx}{f}\right)}{\left(\frac{kAx}{f}\right)^2}\right)\right]$$

Appendix III

Image of Phase Edge in Differentiation System

F = Half width of object

$f_3(X_3)$ = Complex image amplitude

$f_1(X_1)$ = Complex object amplitude

$A_d(x)$ = Differentiation point spread function

For a square aperture, the point spread function is separable, so that a one dimensional treatment will provide the interesting detail.

$$f_3(X_3) = \int_{-F}^{F} f_1(X_1)\, A_d(X_3 + X_1)\, dX_1$$

$$f_3(X_3) = 2\alpha A^2 \int_{-F}^{F} f_1(X_1)\left[\frac{X_0}{A}\,\mathrm{sinc}\left(\frac{k(X_3+X_1)A}{f}\right) + i\left(\mathrm{cosinc}\left(\frac{k(X_3+X_1)A}{f}\right) - \frac{\sin\frac{k(X_3+X_1)A}{f}}{\left(\frac{k(X_3+X_1)A}{f}\right)^2}\right)\right] dX_1$$

I_1 and I_2 may be defined as

$$I_1(X_3) = \int_{-F}^{F} f_1(X_1)\,\mathrm{sinc}\left(\frac{k(X_3+X_1)A}{f}\right) dX_1$$

$$I_2(X_3) = \int_{-F}^{F} f_1(X_1)\left[\mathrm{cosinc}\left(\frac{k(X_3+X_1)A}{f}\right) - \left(\frac{\sin\frac{k(X_3+X_1)A}{f}}{\left(\frac{k(X_3+X_1)A}{f}\right)^2}\right)\right] dX_1$$

so that

$$f_3(X_3) = 2\alpha A\left[X_0 I_1(X_3) + i A I_2(X_3)\right]$$

The object function $f_1(X_1)$ is defined as

$$f_1(X_1) = 1 \qquad X_1 < 0$$
$$= e^{i\frac{kX_1 b}{\Delta}} \qquad 0 \leq X_1 \leq \Delta$$
$$= e^{ikb} \qquad X_1 > \Delta$$

If the function $f_{1F}(X_1)$ is defined as equal to the function $f_1(X_1)$ on the interval $-F \leq X_1 \leq F$ and as zero for all other X_1, the Fourier Transform of $I_1(X_1)$ is determined from

$$\tilde{I}_1(\omega) = \frac{f}{2kA} F_{1F}(-\omega)\, \mathrm{Box}\left(\frac{kA}{f}\right)$$

$$\mathrm{Box}\left(\frac{kA}{f}\right) = 0 \qquad |\omega| > \frac{kA}{f}$$
$$= 1 \qquad |\omega| \leq \frac{kA}{f}$$

$$F_{1F}(\omega) = \int_{-\infty}^{\infty} f_{1F}(X_1)\, e^{i\omega X_1}\, dX_1$$
$$= \int_{-F}^{0} e^{i\omega X_1}\, dX_1 + \int_{0}^{\Delta} e^{i\frac{kbX_1}{\Delta}} e^{i\omega X_1}\, dX_1$$
$$+ e^{ikb} \int_{\Delta}^{F} e^{i\omega X_1}\, dX_1$$
$$= \frac{1}{i\omega} - \frac{e^{-i\omega F}}{i\omega} + \frac{e^{i(\omega + \frac{kb}{\Delta})\Delta}}{i(\omega + \frac{kb}{\Delta})} - \frac{1}{i(\omega + \frac{kb}{\Delta})}$$
$$+ \frac{e^{ikb} e^{i\omega F}}{i\omega} - \frac{e^{ikb} e^{i\omega\Delta}}{i\omega}$$

$$I_1(X_3) = \int_{-\infty}^{\infty} \tilde{I}_1(\omega)\, e^{-i\omega X_3}\, d\omega$$

$$= \frac{f}{2kA} \int_{-\frac{kA}{f}}^{\frac{kA}{f}} \left[-\frac{1}{i\omega}\left(1 - e^{i\omega F}\right) \right.$$

$$+ \frac{1}{i\left(\frac{kb}{\Delta} - \omega\right)} \left(e^{i(kb - \omega\Delta)} - 1\right)$$

$$\left. - \frac{e^{ikb}}{i\omega}\left(e^{-i\omega F} - e^{-i\omega\Delta}\right) \right] e^{-i\omega X_3}\, d\omega$$

The six terms in this integral may be labeled in succession as I_1', I_1'', I_1''', I_1^{IV}, I_1^{V}, and I_1^{VI}, and each calculated separately.

$$I_1' = -\int_{-\frac{kA}{f}}^{\frac{kA}{f}} \frac{e^{-i\omega X_3}}{i\omega}\, d\omega = +i\left[Ci\left(\frac{kAX_3}{f}\right) - Ci\left(-\frac{kAX_3}{f}\right) \right.$$

$$\left. - i\left\{ Si\left(\frac{kAX_3}{f}\right) - Si\left(-\frac{kAX_3}{f}\right) \right\} \right]$$

$$Ci(-z) = Ci(z)$$

$$Si(-z) = -Si(z)$$

$$I_1' = 2\, Si\left(\frac{kAX_3}{f}\right)$$

$$I_1'' = \int_{-\frac{kA}{f}}^{\frac{kA}{f}} \frac{e^{-i\omega(X_3-F)}}{i\omega}\, d\omega = -2\,Si\left(\frac{kA(X_3-F)}{f}\right)$$

The image region of interest may be assumed to be well away from the edge of the field so that

$$Si\left(\frac{kA(X_3-F)}{f}\right) \simeq -\frac{\pi}{2}$$

$$I_1'' \cong \pi$$

$$I_1''' = \int_{-\frac{kA}{f}}^{\frac{kA}{f}} \frac{e^{-i\omega(X_3+\Delta)}}{i\left(\frac{kb}{\Delta}-\omega\right)}\, d\omega = -ie^{-i\frac{kb}{\Delta}(X_3+\Delta)} \int_{\left(\frac{kb}{\Delta}-\frac{kA}{f}\right)(X_3+\Delta)}^{\left(\frac{kb}{\Delta}+\frac{kA}{f}\right)(X_3+\Delta)} \frac{e^{iu}}{u}\, du$$

$$= -ie^{-i\frac{kb}{\Delta}(X_3+\Delta)}\left[Ci\left[k\left(\frac{b}{\Delta}+\frac{A}{f}\right)(X_3+\Delta)\right] - Ci\left[k\left(\frac{b}{\Delta}-\frac{A}{f}\right)(X_3+\Delta)\right] + i\left\{Si\left[k\left(\frac{b}{\Delta}+\frac{A}{f}\right)(X_3+\Delta)\right] - Si\left[k\left(\frac{b}{\Delta}-\frac{A}{f}\right)(X_3+\Delta)\right]\right\}\right]$$

$$I_1^{IV} = -\int_{-\frac{kA}{f}}^{\frac{kA}{f}} \frac{e^{-i\omega X_3}}{i\left(\frac{kb}{\Delta}-\omega\right)}\, d\omega = ie^{-i\frac{kbX_3}{\Delta}}\left[Ci\left[k\left(\frac{b}{\Delta}+\frac{A}{f}\right)X_3\right] - Ci\left[k\left(\frac{b}{\Delta}-\frac{A}{f}\right)X_3\right] + i\left\{Si\left[k\left(\frac{b}{\Delta}+\frac{A}{f}\right)X_3\right] - Si\left[k\left(\frac{b}{\Delta}-\frac{A}{f}\right)X_3\right]\right\}\right]$$

$$I_1^{V} = -\frac{1}{i}\int_{-\frac{kA}{f}}^{\frac{kA}{f}} \frac{e^{-i\omega(F+x_3)}}{\omega}\, d\omega = 2Si\left(\frac{kA(F+x_3)}{f}\right)$$

$$I_1^{V} \cong \pi$$

$$I_1^{VI} = \frac{1}{i}\int_{-\frac{kA}{f}}^{\frac{kA}{f}} \frac{e^{-i\omega(x_3+\Delta)}}{\omega}\, d\omega = -2Si\left(\frac{kA(x_3+\Delta)}{f}\right)$$

$$I_1(x_3) = \frac{f}{2kA}\left[I_1' + I_1'' + I_1''' e^{ikb} + I_1^{IV} + I_1^{V} e^{ikb} + I_1^{VI} e^{ikb}\right]$$

$$I_1(x_3) = \frac{f}{2kA}\left[\pi + 2Si\left(\frac{kAx_3}{f}\right) + e^{ikb}\left(\pi - 2Si\left(\frac{kA(x_3+\Delta)}{f}\right)\right)\right.$$

$$- i e^{-i\frac{kbx_3}{\Delta}}\left\{Ci\left[k\left(\tfrac{b}{\Delta}+\tfrac{A}{f}\right)(x_3+\Delta)\right] - Ci\left[k\left(\tfrac{b}{\Delta}-\tfrac{A}{f}\right)(x_3+\Delta)\right]\right.$$

$$- Ci\left[k\left(\tfrac{b}{\Delta}+\tfrac{A}{f}\right)x_3\right] + Ci\left[k\left(\tfrac{b}{\Delta}-\tfrac{A}{f}\right)x_3\right]$$

$$+ i\left[Si\left[k\left(\tfrac{b}{\Delta}+\tfrac{A}{f}\right)(x_3+\Delta)\right] - Si\left[k\left(\tfrac{b}{\Delta}-\tfrac{A}{f}\right)(x_3+\Delta)\right]\right.$$

$$\left.\left.\left. - Si\left[k\left(\tfrac{b}{\Delta}+\tfrac{A}{f}\right)x_3\right] + Si\left[k\left(\tfrac{b}{\Delta}-\tfrac{A}{f}\right)x_3\right]\right]\right\}\right]$$

$$I_2(X_3) = \int_{-F}^{F} f_1(X_1)\left[\operatorname{cosinc}\left(\frac{k(X_1+X_3)A}{f}\right) - \frac{\sin\left(\frac{k(X_1+X_3)A}{f}\right)}{\left(\frac{k(X_1+X_3)A}{f}\right)^2}\right] dX_1$$

This integral may be calculated through the use of integration by parts.

$$\text{Let} \quad u = f_1(X_1) \qquad dv = \operatorname{cosinc}\left(\frac{k(X_1+X_3)A}{f}\right) - \frac{\sin\left(\frac{k(X_1+X_3)A}{f}\right)}{\left(\frac{k(X_1+X_3)A}{f}\right)^2}$$

$$du = f_1'(X_1) \qquad v = \frac{f}{kA}\operatorname{sinc}\left(\frac{k(X_1+X_3)A}{f}\right)$$

$$I_2(X_3) = \frac{f}{kA} f_1(F)\operatorname{sinc}\left(\frac{k(X_3+F)A}{f}\right)$$

$$-\frac{f}{kA} f_1(-F)\operatorname{sinc}\left(\frac{k(X_3-F)A}{f}\right)$$

$$-\frac{f}{kA}\int_{-F}^{F} f_1'(X_1)\operatorname{sinc}\left(\frac{k(X_1+X_3)A}{f}\right) dX_1$$

The first two terms of this expression have significant value only near the edge of the image field and may be neglected.

$$I_2(X_3) = -\frac{f}{kA}\int_{-F}^{F} f_1'(X_1)\operatorname{sinc}\left(\frac{k(X_1+X_3)A}{f}\right) dX_1$$

The derivative of the edge phase function is the function

$$f_1'(X_1) = 0 \qquad X < 0$$

$$= \frac{ikb}{\Delta} e^{i\frac{kXb}{\Delta}} \qquad 0 \leq X \leq \Delta$$

$$= 0 \qquad X > \Delta$$

$$I_2(X_3) = -\frac{ibf}{\Delta A}\int_0^{\Delta} e^{i\frac{kbX_1}{\Delta}} \operatorname{sinc}\left(\frac{k(X_1+X_3)A}{f}\right) dX_1$$

$$\tilde{I}_2(\omega) = -\frac{ibf^2}{2k\Delta A^2} F_1'(-\omega)\, \mathrm{Box}\left(\frac{kA}{f}\right)$$

$$F_1'(\omega) = \int_0^{\Delta} e^{i\frac{kbX_1}{\Delta}} e^{i\omega X_1} dX_1$$

$$= \frac{e^{i[\omega\Delta + kb]} - 1}{i\left(\omega + \frac{kb}{\Delta}\right)}$$

$$I_2(X_3) = -\frac{bf^2}{2k\Delta A^2}\int_{-\frac{kA}{f}}^{\frac{kA}{f}} \frac{\left(e^{i(kb-\omega\Delta)} - 1\right)e^{-i\omega X_3}}{\left(\frac{kb}{\Delta} - \omega\right)} d\omega$$

Both parts of this integral have already been calculated in the determination of $I_1(X_3)$ so that the final value of $I_2(X_3)$ is

$$I_2(X_3) = -\frac{bf^2}{2k\Delta A^2}\, e^{-i\frac{kbX_3}{\Delta}} \Big[Ci\big[k(\tfrac{b}{\Delta}+\tfrac{A}{f})(X_3+\Delta)\big] - Ci\big[k(\tfrac{b}{\Delta}-\tfrac{A}{f})(X_3+\Delta)\big] - Ci\big[k(\tfrac{b}{\Delta}+\tfrac{A}{f})X_3\big] + Ci\big[k(\tfrac{b}{\Delta}-\tfrac{A}{f})X_3\big] + i\Big\{ Si\big[k(\tfrac{b}{\Delta}+\tfrac{A}{f})(X_3+\Delta)\big] - Si\big[k(\tfrac{b}{\Delta}-\tfrac{A}{f})(X_3+\Delta)\big] - Si\big[k(\tfrac{b}{\Delta}+\tfrac{A}{f})X_3\big] + Si\big[k(\tfrac{b}{\Delta}-\tfrac{A}{f})X_3\big] \Big\} \Big]$$

If these values of $I_1(X_3)$ and $I_2(X_3)$ are substituted in the expression for the actual image amplitude distribution, the result reduces to

$$f_3(X_3) = \frac{\alpha X_0 f}{k}\left(\pi + 2Si\left(\frac{kAX_3}{f}\right)\right) + \frac{\alpha X_0 f}{k} e^{ikb}\left(\pi - 2Si\left(\frac{kA(X_3+\Delta)}{f}\right)\right) - i\alpha\left[\frac{fX_0}{k} + \frac{bf^2}{\Delta k}\right] e^{-i\frac{kbX_3}{\Delta}} \Big[Ci\big[k(\tfrac{b}{\Delta}+\tfrac{A}{f})(X_3+\Delta)\big] - Ci\big[k(\tfrac{b}{\Delta}-\tfrac{A}{f})(X_3+\Delta)\big] - Ci\big[k(\tfrac{b}{\Delta}+\tfrac{A}{f})X_3\big] + Ci\big[k(\tfrac{b}{\Delta}-\tfrac{A}{f})X_3\big] + i\Big\{ Si\big[k(\tfrac{b}{\Delta}+\tfrac{A}{f})(X_3+\Delta)\big] - Si\big[k(\tfrac{b}{\Delta}-\tfrac{A}{f})(X_3+\Delta)\big] - Si\big[k(\tfrac{b}{\Delta}+\tfrac{A}{f})X_3\big] + Si\big[k(\tfrac{b}{\Delta}-\tfrac{A}{f})X_3\big] \Big\} \Big]$$

Appendix IV

Point Spread Function of Integration System

$A_I(x,y)$ = Point spread function of filtered aperture

$$t_I(x',y') = \left\{ \begin{matrix} iB & x' < D \\ \frac{D}{x'} & x' \geq D \end{matrix} \right\} = \text{Aperture filter amplitude transmittance}$$

$$A_I(x,y) = \int_{-A}^{A} dx' \int_{-A}^{A} dy'\, t_I(x',y')\, e^{i\frac{k}{f}(xx'+yy')}$$

$$= 2A\,\text{sinc}\left(\frac{kAy}{f}\right)\left[D\int_{-A}^{-D} \frac{e^{i\frac{kxx'}{f}}}{x'}\,dx' \right.$$

$$\left. + iB\int_{-D}^{D} e^{i\frac{kxx'}{f}}\,dx' + D\int_{D}^{A} \frac{e^{i\frac{kxx'}{f}}}{x'}\,dx' \right]$$

$$= 2A\,\text{sinc}\left(\frac{kAy}{f}\right)\left[D\int_{A}^{D} \frac{e^{-i\frac{kxx'}{f}}}{x'}\,dx' \right.$$

$$\left. + 2iBD\,\text{sinc}\left(\frac{kDx}{f}\right) + D\int_{D}^{A} \frac{e^{i\frac{kxx'}{f}}}{x'}\,dx' \right]$$

$$= 2A\,\text{sinc}\left(\frac{kAy}{f}\right)\left[2iBD\,\text{sinc}\left(\frac{kDx}{f}\right) + 2iD\int_{D}^{A} \frac{\sin\frac{kxx'}{f}}{x'}\,dx' \right]$$

$$A_I(x,y) = 4iAD\,\text{sinc}\left(\frac{kAy}{f}\right)\left[B\,\text{sinc}\left(\frac{kDx}{f}\right) \right.$$

$$\left. + Si\left(\frac{kAx}{f}\right) - Si\left(\frac{kDx}{f}\right) \right]$$

If $B=0$, $A_{It}(x,y) = 4iAD\,\text{sinc}\left(\frac{kAy}{f}\right)\left[Si\left(\frac{kAx}{f}\right) - Si\left(\frac{kDx}{f}\right)\right]$